A STUDY OF STRUCTURES OF NUCLEONS AND NUCLEI IN LOW AND HIGH DENSITY QCD

A THESIS

SUBMITTED TO GAUHATI UNIVERSITY
FOR THE DEGREE OF DOCTOR OF PHILOSOPHY
IN PHYSICS IN THE FACULTY SCIENCE

SUBMITTED BY

Saiful Islam

2010

Dedicated to the loving memories of

Dada and Dida.

Prof. D. K. Choudhury,
Professor,
Department of Physics
Gauhati University
Guwahati – 781014
Assam , INDIA

Ph: 91-361-2570531(O)

Fax: +91-361-2700311

Reference no................ Date..29.09.10......

This is to certify that Mr. Saiful Islam has worked under my supervision for the thesis entitled "**A Study of Structures of Nucleons and Nuclei in Low and High Density QCD**" which is being submitted to the Gauhati University for the degree of Doctor of Philosophy in the faculty of science.

The thesis is Saiful's own work. He has fulfilled all the requirements under the Ph. D. regulations of Gauhati University and to the best of my knowledge, the thesis or part thereof has not been submitted to any other university for any degree or diploma.

D K Choudhury

(Dilip Kumar Choudhury)

Supervisor

PROFESSOR OF PHYSICS
GAUHATI UNIVERSITY

Acknowledgement

I find it difficult to write something in short to acknowledge my research supervisor Professor Dilip Kumar Choudhury whose inspiration, encouragement, guidance and invaluable help led me to follow proper track in the field of High Energy Physics and complete this research work. I consider myself fortunate to have Professor Choudhury as my supervisor and to be a part of his research group. Also, I would like to thank him for introducing me to the High Energy Physics Community of India and abroad.

I am specially greatful to Prof. N. N. Singh, Prof. S. A. S. Ahmed and Prof. D. K. Choudhury (my research supervisor) of the Department of Physics, Gauhati University for teaching me High Energy Physics in my M.Sc. class days. I am highly grateful to all the Heads of the Department for their kind support and good advices during this period. I would like to thank all the faculty members and staff of the department for their kind co-operations.

I am fortunate to have invaluable help and suggetions from Dr. P. K. Sahariah, Sri Pijush K. Dhar, Dr. Atri Deshamukhya, Dr. Abhijit Das, Sri Ranjit Choudhury, Dr. Amal Sarma and I am greatly indebted to them. I am highly grateful to Sabyasachy Roy, Bhaskar, Chabin Thakuria, Akbari, Krishna, Jean, Rupjyoti, Neelakhi and all the research schol-

ars of the Physics Department, Gauhati University, for all kinds of help and suggestions.

I am grateful to the Abdus Salam International Centre for Theoretical Physics - ICTP, Italy for financial support and hospitality in carrying out a fraction of this work there. I am also thankful to Royal Group of Institutions administration for giving me the opportunity for doing the last parts of this work. I express my gratitude to all my colleagues for their good advices and encouragement.

I am indebted to my family members for all kinds of physical and emotional support during this period. Had they not been stood behind me as the source of courage and inspiration, my work would have remained incomplete. Also, I thank all my friends and relatives for their help, support and encouragement during these days.

Saiful Islam

Guwahati-14 Saiful

September, 2010

Table of Contents

List of Tables

List of Figures

Chapter 1

Introduction

The idea that a basic simplicity and regularity govern the apparent complex and diversity of the universe seems to have always been an important aspect of natural philosophy. High energy physics deals with the fundamental building blocks of matter and the nature of the interactions among them. The notion of what constitutes matter in fact is not static but evolves with time, changing in step with technological advances or more precisely with the growth in the power of the sources of energy that become available to the experimenter. It is successively discovered that matter is build up from molecules; that the molecules are composed of atoms; the atoms of electron and nuclei; and the nuclei of protons and neutrons. Extensive researches, since the start of nineteenth century, have been carried out by the scientists to conclude about the ultimate representatives of the matter, i.e. the basic building blocks called the elementary particles or sub-atomic particles [1]. By the end of the nineteenth century, in 1897, J. J. Thomson discovered the electron. In 1932, James Chadwick identified the neutron and Werner Heisenberg suggested that atomic nuclei consist of neutrons and protons [2, 3, 4, 5]. Photon, a quantum of radiation, has been added as a field particle that mediates electromagnetic force between the nucleus and electrons in the atom. Thus atomic picture becomes somewhat clear with electron, neutron, proton and photon as the basic building blocks. Thus, initially, only a few elementary particles were known, viz., electron, proton, neutron, neutrino and photon. However, the study of nuclear forces in accelerators and in cosmic rays led to the discovery of hundreds of new massive and unstable particle states or resonances collectively called hadrons and a few lighter particles called leptons. The electron (e), muon (μ) and the tau (τ) particles along with their associated neutrinos (ν_e, ν_μ, ν_τ) constitute the lepton class of particles which are point-like spin-$\frac{1}{2}$ particles that can interact through electromagnetic and weak forces. The neutrinos being chargeless and massless can interact only through weak forces. The hadron class of particles is subdivided into baryons and mesons. Baryons are massive spin-$\frac{1}{2}$ particles or fermions like proton (p), neutron (n), Λ, Σ, Δ, ... whereas mesons are particles of lower mass and carry integral spin, i.e., they are bosons e.g. pions (π), keons (K), J/ψ, ... The hadrons are found to interact through strong, electromagnetic and weak forces. Apart from the hadrons and the leptons, another class of particles has been constituted by the mediators of the interactions between the hadrons and the leptons. These particles called gauge bosons are the photon (γ) for electromagnetic interactions, the gluons (g) for strong interactions, $W^{\pm}$, Z^0 bosons for weak interactions and the predicted but not yet detected gravitons for gravitational interactions.

1.1 The Quark Model of Hadrons

In the 1960s, the great accumulation of experimental data on hadron resonances showed definite regularities and indicated underlying symmetries. This led Murray Gell-Mann and Zweig in 1964 to independently postulate the quark hypothesis. They proposed that the hadrons are composite objects composed of quarks, which are pointlike, spin-$\frac{1}{2}$ particles carrying fractional electric charges of $+\frac{2}{3}e$ and $-\frac{1}{3}e$. The known properties of hadrons can be accommodated by considering three types or flavours of quarks, namely - up (u)

carrying an electric charge $+\frac{2}{3}e$, down (d) with electric charge $-\frac{1}{3}e$ and strange (s) with electric charge $-\frac{1}{3}e$. The antiquarks have the same magnitude of charges with opposite signs. The carrier of the force between quarks is a field particle called gluon [6, 7, 8]. The baryons are composed of three quarks and the mesons are made of a quark-antiquark pair/pairs. For example: the quark content assigned to the proton and the neutron are $p(uud)$ and $n(udd)$, whereas the quark contents of π^+ and π^- are $\pi^+(u\bar{d})$ and $\pi^-(d\bar{u})$ respectively. The quark model of Gell-Mann and Zweig was proved very successful in explaining the multiplets of baryons and mesons. It predicted a number of baryon and meson resonances which were observed later. With the proliferation of baryons and mesons, the number of quark flavours has gone up to six, namely - up ($u \longrightarrow +\frac{2}{3}e$), down ($u \longrightarrow -\frac{1}{3}e$), charm ($c \longrightarrow +\frac{2}{3}e$), strange ($s \longrightarrow -\frac{1}{3}e$), top ($t \longrightarrow +\frac{2}{3}e$) and bottom ($b \longrightarrow -\frac{1}{3}e$). Each of these quarks and gluon have been experimentally confirmed.

This naive quark model, however, ran into immediate trouble when the composition of the spin $\frac{3}{2}$ baryon Δ^{++} was called for. The properties of this doubly charged baryon is correctly matched by the quark configuration uuu ; whence its spin $\frac{3}{2}$ is obtained by combining three identical u quarks of spin $\frac{1}{2}$ in their ground states. This violates the Pauli exclusion principle. Apart from the spin-statistics problem, this simple quark model is unsatisfactory from other aspects also. Though quark combinations qqq, $\overline{qqq}$ and $q\bar{q}$ reproduce the baryons, antibaryons and meson states, no other possibilities like qq, $qqqq$ etc. or even single quark states have ever been observed.

These problems were overcome by bringing in the concept of colour degree of freedom. The quarks are now assigned a new degree of freedom called colour degree of freedom (a quantum number) which come in three types, namely - red (R), blue (B) and green (G). Each quark can now assume one of the three colour states q_R, q_B or q_G. This takes care of the spin-statistics problem but creates more candidates for each hadron, i.e.

proton may have $u_R u_B d_G$, $u_G u_B d_R$, $u_B u_G d_G$, etc. This impasse was dispelled by imposing the condition that physical quark states must be colourless or colour singlets. This condition disallowed extra quark states like qq or even single quarks from being physically observable since they will possess a net colour.

Thus, according to the quark model, hadrons are made of quarks which are point-like fermions carrying fractional electric charges and a new degree of freedom called colour. Quark combinations must be colour singlets to be physically observable or to have free existence. Baryons are bound states of three quarks qqq, antibaryons of three antiquarks $\overline{qqq}$ and mesons are quark-antiquark pair/pairs $q\bar{q}$ The success of this model lies in explaining the baryon and meson spectroscopy

1.2 Quantum Chromodynamics

Quantum chromodynamics (QCD) is a remarkably successful and rich theory of the strong interactions among quarks derived from the colour gauge symmetry group $SU(3)_C$. The theory provides a dynamical basis for the quark-model description of the hadrons, the strongly interacting particles such as protons and pions that are accessible for direct laboratory study. Interactions among the quarks are mediated by vector force particles called gluons, which themselves experience strong interactions. The nuclear force that binds protons and neutrons together in atomic nuclei emerges from the interactions among quarks and gluons. Just as the photon binds electric charges into atoms, gluons are the binding agents for quarks inside hadrons.

QCD is built in analogy with quantum electrodynamics (QED) [9] wherein there are three colour charges along with the anticolours instead of the positive and negative electric charges in QED. The mediator gluons are bicoloured objects carrying a colour and an anticolour together. Each flavour of quark is a triplet of the colour group $SU(3)_C$ in the fundamental representation and eight types of gluons corresponding to the eight generators of the group. From the field theoretical point of view, QCD is an application of Yang-Mill theory [10] which is a non-abelian gauge field theory and is renormalizable. A key feature of this non-abelian nature of colour interactions is that the gauge bosons of the theory, the gluons, can interact directly with each other. This is in contrast with QED where the photons cannot interact with each other.

It is evident that quark-quark interaction is not solely of electromagnetic origin. The quarks in hadrons are bound far more strongly than is allowed by electromagnetic interactions. The colour degree of freedom, also called colour charge, endows quarks with a new colour field which makes this strong binding possible.

The strong interactions are assumed to be flavour independent and this is supported by the fact that there is no experimental evidence of any flavour dependence of strong force. Also the fact that colour symmetry is an exact gauge symmetry has profound implications. The non-abelian gauge theories possess infra-red singularities that could prevent the liberation of individual quarks and gluons. The direct coupling of gluons, which arise due to the non-abelian nature of QCD, lead to the anti-screening of colour charge analogous to the screening of electric charge in QED. Asymptotically, for very small separations, the strength of the colour fields of interacting quarks is reduced and they approach a state where the quarks behave as essentially free, non-interacting particles. This phenomenon is referred to as asymptotic freedom.

The QCD Lagrangian is constructed along similar lines of QED. It has the form

$$\mathcal{L} = \sum_q \bar{q}_a (i\gamma^\mu D_\mu - m_q)_{ab}\, q_b - \frac{1}{4} F^A_{\mu\nu} F^{A\mu\nu} \tag{1.1}$$

where the covariant derivative is given by

$$(D_\mu)_{ab} = \delta_{ab}\partial_\mu + ig_s\, t^A_{ab}\, G^A_\mu \tag{1.2}$$

and the field strength tensor is given by

$$F^A_{\mu\nu} = p_\mu G^A_\nu - p_\nu G^A_\mu - g_s f^{ABC} G^B_\mu G^C_\nu \tag{1.3}$$

In eq.(1.3), G^A_μ's are the vector fields that represent the gauge particles of QCD, i.e. the gluons, f^{ABC} are the structure constants of SU(3) and g_s is the coupling strength of the quark and gluon field. In the above equations $a, b = 1, 2, 3$ are the colour indices, $\mu, \nu = 0, 1, 2, 3$ are the Lorentz indices and $A, B, C = 1, 2, ...8$ are the indices for the generators of $SU(3)$. The 3×3 matrices t^A are the generators of the fundamental representation of the SU(3) group and they satisfy the commutation relations:

$$\left[t^A, t^B\right] = if^{ABC} t^C. \tag{1.4}$$

There are three elementary vertices of QCD given by the Lagrangian (Eq.(1.1)) : the amplitudes of the first two, i.e., $q\bar{q}g$ and ggg are proportional to the coupling g_s, whereas that of the third, i.e., $gggg$ is proportional to g_s^2. The colour factors can be determined from the properties of the generators by summing over possible colour combinations for final state partons from these elementary vertices of QCD.

1.3 Deep Inelastic Scattering

Deep Inelastic Scattering (DIS) is a process where a high energy lepton (like electron, muon or neutrino) beam is scattered inelastically off a hadron (like proton, neutron or deuteron) target. In this process, the target breaks up and loses its identity completely and massy debris of hadrons along with the scattered lepton is obtained in the final state (Fig.1.1). These experiments provide information on the quark substructure of hadrons. DIS experiments had its beginning in 1968 at SLAC [11] when the first evidence of the substructure of the hadrons was recorded and have since become the testing ground of QCD.

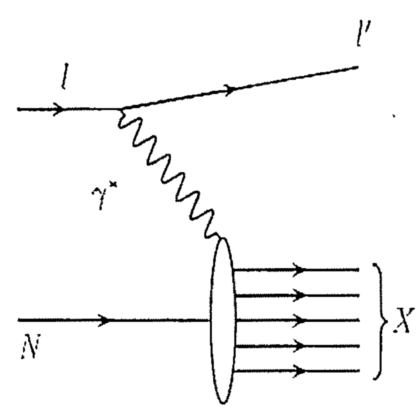

Figure 1.1: Deep inelastic scattering

Kinematically, in the $e\,p \longrightarrow e\,X$ deep inelastic scattering, a high energy electron (lepton) of energy E and four momentum k is scattered inelastically off a proton (hadron) of mass M and four momentum p. The final state consists of the scattered electron with energy E' and four momentum k' and the final hadronic fragmentation products X with an invariant mass W.

The exchanged virtual photon γ^* (vector boson) carries a four-momentum $q = k - k'$. The first component of q is the energy transfer, $\nu = E - E'$. To describe the kinematics of the above process in the laboratory reference frame, the variables introduced [6] are :

- $Q^2 = -q^2$, the negative of the exchanged four-momentum squared,
- $x = \frac{Q^2}{2p\,q} = \frac{Q^2}{2M\nu}$, the Bjorken scaling variable, which describes the fraction of the nucleon momentum carried by the struck quark,
- $W^2 = (p+q)^2$, the invariant mass squared of the virtual-photon nucleon system,
- $y = \frac{p\,q}{p\,k} = \frac{\nu}{E}$, the fraction of the initial lepton energy transferred to the boson.

The expressions for Q^2 and W^2 can be transformed on to $Q^2 = 4EE' sin^2(\theta/2)$ and $W^2 = M^2 + 2M(E - E') + Q^2$ where θ is the scattering angle in the laboratory reference frame (neglecting the mass of the electron). At large values of Q^2, i.e. at small scale distance, DIS probes the constituents of the hadron (i.e. quarks) not the hadron as a whole. At small scale distances, the quarks act as almost free particles and because the interactions are relatively weak at those scales, perturbative QCD (pQCD) techniques can be used in DIS. A typical lower Q^2 limit for which pQCD is applicable, is 1 GeV^2. In DIS, three types of events are distinguished: (*i*) inclusive events, where only the scattered lepton is detected, (*ii*) semi-inclusive events, where apart from the lepton also a hadron is detected, and (*iii*) exclusive events, where all reaction products are identified.

When the virtuality of the photon probe is very low, the photon sees only the total charge and magnetic moment of the hadron and the scattering appears point-like. A photon with higher virtuality can resolve the individual constituents of the hadron's virtual pion cloud and the hadron appears as a composite extended object. At high momentum transfers, the photon (with large virtuality) probes the fine structure of the hadron's charge distribution and sees its elementary constituents. If quarks were non-interacting, no further structure would appear for increasing Q^2 and exact scaling would set in. However, in any renormalizable quantum field theory, we have to introduce a Bose-field (gluon) which mediates the interaction in order to form bound states of quarks, i.e. the observed hadrons. In such a picture, the quark is then always accompanied by a gluon cloud which is probed as the momentum transfer is increased [6, 8, 12].

1.4 The Quark-Parton Model and Parton Distribution Functions

In the quark-parton model (QPM), the proton is described as a composite object, made of partons, i.e., valence quarks (two up and one down quark), sea quarks (pairs of up, down, strange, charm and bottom quark-antiquarks) and the gluons, which serve as the mediating carriers of the strong force binding the quarks within the proton. The cross sections for e-p scattering, which describe the reaction rates, are determined by a set of inelastic structure functions $F_i(x, Q^2)$ $(i = 1, 2)$. These F_i's are the quantities of great interest, as they are the functions that characterise the composite structure of the proton and need to be determined by experiment.

Within the QPM, e-p scattering is described by an incoherent sum of elastic scattering of the exchanged photons (γ) on these partons in the proton. The proton structure functions F_i are directly related to combinations of the so-called parton distribution functions $xq_i(x)$ referred to as PDF's. These PDF's describe the probability that a certain parton i carries a fraction x of the total proton momentum, and thus characterise the proton structure at the parton level. Precise measurements of these F_i's therefore allow a determination of the PDF's.

In the framework of the theory of strong interactions (QCD), the functions $xq_i(x)$ depend also on the reaction scale, and this Q^2-dependence can be accurately described by evolution equations [13]. However, the x-dependencies of the PDF's can only be determined from the experimental data, using elaborated fitting procedures, as performed by various groups. Measurements from a variety of other experiments, such as proton-antiproton scattering or neutrino experiments can also contribute information on the PDF's.

The combined HERA (Hadron Electron Ring Analge) measurements of the e-p DIS reaction rates, so-called reduced cross sections presented as a function of the scaling variable Q^2 for different x-values, are directly proportional to the dominant structure function F_2^p associated to pure photon exchange. Using the QPM picture, the HERA data provide direct sensitivity to the valence quark content of the proton at high-x and to sea quarks and gluons at small-x values. Demonstrating the explicit Q^2-dependence of the structure functions or cross sections not only confirms scaling violations, but also illustrates a very excellent level of precision reached by the HERA experiments which is a remarkable achievement of QCD. The precise data from these experiments allowed the HERA structure function working group to extract the individual parton distribution functions $xq_i(x)$ for the various partons of the proton. At large-x the total proton momentum is equally shared among the three valence quarks $(xu\, xu\, xd)$. However, when considering smaller values of x, i.e., smaller momentum fractions, the sea quarks (xS) and the gluons (xg) increase substantially and become completely dominant [14, 15].

The gluon and quark distribution functions have traditionally been determined simultaneously by fitting experimental data (mainly at small-x) on the proton structure function $F_2^p(x, Q^2)$ measured in deep inelastic e-p scattering. The process starts with an initial Q_0^2, typically in the 1 to 4 GeV^2 range, and individual quark and gluon trial distributions parametrized as functions of x. The distributions are evolved to larger Q^2 using the coupled integral-differential DGLAP equations [16] and the results used to predict the measured quantities. The final distributions are then determined by adjusting the input parameters to obtain a best fit to the data.

1.5 QCD improved parton model

According to the QPM, in a DIS process, the virtual photon of large enough Q^2 can see point-like and free constituents of the nucleon called partons. With the identification of the partons as quarks and also the indirect evidence of the presence of the gluons that escape detection by the DIS probe, one must now accommodate the interactions between quarks and other QCD processes. The incorporation of these QCD processes has significant effect as Q^2 is increased. The interacting quarks will exchange gluons between them and this will imply that the quarks will pretend to have a structure. As Q^2 is increased, the virtual photon probes smaller and smaller distances and what appeared as a single quark at low Q^2 may now radiate a gluon before or after being struck by the virtual photon [6]. Moreover, a gluon constituent in the target can contribute to the DIS process via $\gamma^* g \longrightarrow qq$ pair production.

The inclusion of these QCD processes has two experimentally observable consequences : (1) the scaling property of the structure functions will no longer be exactly true and (2) the outgoing quark will no longer be collinear with the virtual photon.

1.6 Small-x physics

Small-x physics is always being the exciting field of DIS. Important contribution to the interest of the small-x physics came from the puzzling result obtained by HERA at small-x for the proton structure function $F_2^p(x, Q^2)$ which was observed to increase dramatically as x gets smaller and smaller.

The behaviour of the parton distributions of the hadrons in small-x region is of considerable importance both theoretically and phenomenologically. In the small-x region novel effects are expected to emerge. At very small-x region, quarks and gluons radiate soft gluons and thus the number of partons, i.e., quarks and gluons increases rapidly. As the gluon density becomes higher, several effects - like recombination of gluons leading to gluon saturation, shadowing of gluons by each other, collective effects like condensation or super fluidity or formation of local region (known as hot spots) etc. can occur. These may have dominant effect in non-perturbative physics at very small-x. According to QCD, at small-x and at large-Q^2, a nucleon consists predominantly of gluons and sea quarks. Their densities grow rapidly in the limit $x \to 0$ leading to possible spatial overlap and to interactions between the partons. Several DIS experiments have been performed on nuclear targets and various nuclear effects have shown up at small-x. Small-x physics thus represents an interesting area of DIS structure function of hadrons.

1.7 Deuteron structure function b_1^d

Deuteron, a spin-1 object, is described by eight structure functions [17], twice as many as required to describe e-p DIS. The tensor structure function $b_1^d(x, Q^2)$ of the deuteron is the most important one. It does not exist for spin-1/2 targets and vanishes in the absence of nuclear effects, i.e. if the deuteron simply consists of a proton and neutron at rest (a simple system of two particles without strong interactions to form a nucleus) [18, 19].

1.8 High Density Quantum Chromodynamics

Small-x deep inelastic scattering touches on one of the deepest parts of QCD, that of high field strengths and of high quantum occupancy of states, which has become one of the central areas of theoretical study. DIS experiments along with high energy heavy ion collisions are furnishing such crucial experimental inputs for achieving a more complete and deeper understanding of dense matter.

The high parton density regime in DIS (ep, pA and AA collisions) is characterized by small values of the Bjorken variable $x = Q^2/s$ and represents the challenge of studying the interface between the perturbative and nonperturbative QCD, with the peculiar feature that this transition is taken in a kinematical region where the strong coupling constant α_S is small. The DGLAP equations are the main evolution equations in pQCD. For a dense partonic system, where gluon occupation number is very large, the new features of partons inside the nucleon and nuclei leads to new theoretical predictions and experimental findings and the dynamics of these high density partons are accounted by so called the high density quantum chromodynamics (hdQCD) or saturated quantum chromodynamics (sQCD). In the regime of very small-x, the density of gluons and quarks become so high that the cross-section increase infinitely leading to the violation of Unitarity Bound (UB) or Froissart Limit [20, 21]. Hence in this regime, an associated new dynamical effect on partons is expected to stop the further growth of PDF's or the structure functions and hence the total cross-section. The expectation of the transition for the high density regime can be understood considering the physical picture of the deep inelastic scattering In the infinite momentum frame (IMF) the virtual photon with virtuality Q^2 measures the number density of partons having longitudinal momentum fraction x and transverse spatial size $\Delta x_\perp \leq 1/Q$. When Q^2 is large, $\alpha_S(Q^2)$ is small, so that the struck quark can be treated perturbatively. Also, when Q^2 is large the struck quark is small, so that the struck quark can be pictured as being isolated, far away from similar quarks, in the proton. Thus, so long as the parton distributions are not large, the partons in a proton are dilute. However, if the parton distributions get large enough, which happens when x is very small, partons in the proton must begin to overlap. If there is a sufficient amount of parton overlap, then a given parton will not act as a free quantum over its lifetime but will interact strongly with the other partons in the proton, even though α_S may still be in the perturbative regime. In other words, while for large momentum transfer $k_\perp$, the linear evolution equations (DGLAP) predicts that the mechanism $g \longrightarrow gg$ populates the transverse space with a large number of small size gluons per unit of rapidity (the transverse size of a gluon with momentum $k_\perp$ is proportional to $1/k_\perp$), for small $k_\perp$ the produced gluons overlap and fusion processes, $gg \longrightarrow g$, become equally important. In the later process, the rise of the gluon distribution below a typical scale is reduced, restoring the unitarity. That typical scale is energy dependent and is called saturation scale Q_S. The saturation momentum sets the critical transverse size for the unitarization of the cross sections. Therefore, at sufficient small values of x, one enters in the regime of high density QCD, where partons from neighbouring ladders overlap spatially and new dynamical effects associated with the unitarity corrections are expected to stop further growth of the parton densities.

1.9 Higher order corrections

Precision studies of some hadronic processes in the perturbative regime are going to be very important in order to confirm the validity of the mechanism of mass generation in the Standard Model at the new collider, the Large Hadron Collider (LHC). This program involves a rather complex analysis of the Quantum Chromodynamic (QCD) background, with the corresponding radiative corrections taken into account to higher orders.

Studies of these corrections for specific processes have been performed by various groups and the highest level of precession so far achieved for the evolution of PDF's in purturbative QCD is next-to-next-to-leading order (NNLO) in α_s, the QCD coupling constant. The quantification of the impact of these corrections requires the determination of hard scattering of the partonic cross-sections up to order α_s^3, with the matrix of the anomalous dimensions of the DGLAP kernels determined at the same perturbative order. Corrections beyond NNLO, i.e., higher twist corrections, like N^3LO, N^4LO etc., are not available yet in literature. This is because, increasing orders in α_s contain logarithms in Q^2, and order-by-order perturbation theory is not guaranteed to be more accurate there [22].

The global parton analysis of deep inelastic scattering (DIS) and the related hard scattering data are generally performed at next-to leading order (NLO). Presently the next-to leading order is the standard approximation for most of the important processes in QCD. Analysing DIS at NNLO is important to investigate the processes using the most precise available data. The corresponding one- and two-loop splitting functions have been known for a long time. The NNLO corrections should be included in order to arrive at quantitatively reliable predictions for hard processes occurring at present and future high-energy colliders. Recently much effort has been invested in computing NNLO QCD corrections to a wide variety of partonic processes and therefore it is needed to generate parton distributions also at NNLO, so that the theory can be applied in a consistent manner.

The higher order corrections to the evolution of PDF's is an immense field of work for researchers and of great interest for their useful applications in quantitative and reliable predictions of hard processes at present and future colliders. Such corrections are indirectly related to the predictions for $W^{\pm}$ and Z^0 production at LHC and Tevatron.

1.10 Methods of solutions of DGLAP equations

There are different methods of solutions of DGLAP equations out of which frequently reffered ones are :

- Laguerre Polynomial method [23, 24, 25],
- Mellin transformation method [26, 27, 25],

- Brute force method [28, 29, 30, 25],
- Jacobi evolution method [31, 32, 33, 34, 35],
- Semi analytical method [36, 37],
- Matrix based approach [38, 36],
- Taylor expansion approach [39, 40, 41],
- Method of characteristics [42, 43],
- Lagrange's auxiliary method [44, 45].

We use the last two methods in the present work which have been outlined below.

1.10.1 Method of characteristics:

The method of characteristics [42, 43] is an important technique for solving initial value problems of first order partial differential equation (PDE). In this method, the coordinates (x, t) are transferred to an appropriate new set of coordinates (S, τ) called characteristic coordinates so that the PDE reduces to ordinary differential equation (ODE) with respect to any one of the new variables. Thus the problem of solution of PDE reduces to that of ODE. This ODE can now be solved by standard methods. The last step is to plug in the values of S and τ in terms of x and t with the help of coordinate transformation equations to obtain the desired solution.

1.10.2 Lagrange's auxiliary method:

Lagrange's auxiliary method [44, 46, 47, 48] is used to solve first order linear differential equation. It is based on the following theorem :

The general solution of the linear partial differential equation

$$Pp + Qq = R \tag{1.5}$$

is

$$F(u, v) = 0 \tag{1.6}$$

where F is an arbitrary function and $u(x, y, z) = c_1$ and $v(x, y, z) = c_2$ form a solution of the equations

$$\frac{dx}{P} = \frac{dy}{Q} = \frac{dz}{R} \tag{1.7}$$

Here, P, Q and R are given functions of x, y, z (which donot involve p or q). p and q denote $\partial z/\partial x$ and $\partial z/\partial y$ respectively.

1.11 Some Important Research Centres and Experiments

1.11.1 SLAC (Stanford Linear Accelerator Centre)

SLAC is a high-energy physics and synchrotron radiation research centre established in 1962 at Stanford University in Menlo Park, California, USA. It houses now the longest linear accelerator (linac) of the world – a machine of 3.2 km long that accelerates electrons up to energies of 50 GeV. In 1966 a new machine, designed to reach 20 GeV was completed. In 1968 experiments at SLAC found the first direct evidence for further structure (i.e., quarks) of protons and neutrons. In 1972, an electron-positron collider called SPEAR (Stanford Positron-Electron Asymmetric Rings) producing collisions at energies of 2.5 GeV per beam was constructed. In 1974 SPEAR was upgraded to reach 4.0 GeV per beam. A new type of quark, known as charm, and a new heavy lepton called the tau were discovered using SPEAR. SPEAR was followed by a larger, higher-energy colliding-beam machine, the PEP (Positron-Electron Project), which began operation in 1980 and took electron-positron collisions to a total energy of 36 GeV.

1.11.2 FNAL (Fermi National Accelerator Laboratory)

FNAL, also called fermilab, centre for particle-physics research is located at Batavia, Il-lions in USA. The major components of Fermilab are two large particle accelerators called proton synchrotrons, configured in the form of a ring with a circumference of 6.3 km. The first, which went into operation in 1972, is capable of accelerating particles to 400 billion electron volts. The second, called the Tevatron, is installed below the first and uses more powerful superconducting magnets; it can accelerate particles to 1 trillion electron volts. The older instrument, operating at lower energy levels, now is used as an injector for the Tevatron. The high-energy beams of particles (notably muons and neutrinos) produced at the laboratory, have been used to study the structure of protons in terms of their most fundamental components, the quarks. In 1972 a team of scientists at Fermilab isolated the bottom quark and its associated antiquark. In 1977, the upsilon meson was discovered, which revealed the existence of the bottom quark and its accompanying antiquark. The existence of the top quark predicted by the standard model was established at Fermilab in March 1994.

1.11.3 DESY (Deutsches Elektronen-Synchrotron)

DESY, the largest centre for particle-physics research located in Hamburg, Germany was founded in 1959. The construction of an electron synchrotron to generate an energy level of 7.4 billion electron-volts was completed in 1964. Ten years later, the Double Ring Storage Facility (DORIS) was completed which is capable of colliding beams of electrons and positrons at 3.5 GeV per beam. In 1978 its power was upgraded to 5 GeV per beam. A larger collider capable of reaching 19 GeV per beam, the Positron-Electron Tandem Ring Accelerator (PETRA), began operation in 1978. Experiments with PETRA in the following year gave the first direct evidence of the existence of gluons.

The Hadron Electron Ring Anlage (HERA) capable of colliding electrons and protons was completed in 1992. HERA consists of two rings in a single tunnel with a circumference of 6.3 km, one ring accelerates electrons to 27.6 GeV and the other protons to 920 GeV. One of the main physics goals of the HERA experiments was the detailed investigation of the proton substructure up to the highest attainable energies. HERA follows the tradition of the Rutherford Scattering Experiments and uses point-like leptons to probe the substructure of the composite object proton. Unlike in earlier fixed target experiments, colliding beams (electrons at 27.6 GeV and protons up to 920 GeV) produced centre-of-mass energies up to 319 GeV, extending the available kinematic regions by orders of magnitude. After successful operation for over a decade (1992 - 2007), the HERA collider was finally shut down on 1.7.2007.

The HERA experiments have produced a wealth of results of highest scientific interest. It has already allowed to push the knowledge about the parton momentum distributions in the proton to an unprecedented high precision. Among others, an unexpected substantial increase of gluons at low momentum fractions was observed. Overall, the theory describes the features of inelastic electron-proton scattering very well in all details, which can be considered as a great success of the theory of electroweak and strong interactions. Besides studies of the proton structure, detailed investigations of the theory of strong interactions (QCD), heavy quark physics, searches for phenomena beyond the standard model and many others have been performed. Analyses of the accumulated data still continues, and further results will continue to emerge in the future. These results are of imminent relevance for the physics studies at LHC.

1.11.4 CERN (Conseil Europeen pour la Recherche Nucleaire)

CERN is an international scientific organization for collaborative research in sub-nuclear physics (high-energy, or particle physics) located at Geneva, Switzerland. The activation of a 600-mega volt synchrocyclotron in 1957 enabled CERN physicists to observe the decay of a pion, into an electron and a neutrino. The event was instrumental in the development of the theory of weak interaction. The laboratory grew steadily, activating the particle accelerator known as the Proton Synchrotron (PS; 1959), which used strong focusing of particle beams; the Intersecting Storage Rings (ISR; 1971), enabling head-on collisions between protons; and the Super Proton Synchrotron (SPS; 1976), with a 7 kilometre circumference. With the addition of an Antiproton Accumulator Ring, the SPS was converted into a proton-antiproton collider in 1981 and the system led to the discovery of the $W^{\pm}$ and Z^0 particles in 1983. In 2000, the Large Electron-Positron collider (LEP), a particle accelerator was installed at CERN in an underground tunnel of 27 km in circumference. LEP was used to counter-rotate accelerated electrons and positrons in a narrow evacuated tube at velocities close to that of light, making a complete round about 11000 times per second.

More recently, CERN has installed the Large Hadron collider (LHC) - the world's largest and highest energy particle accelerator and hadron collider. Six detectors have been constructed at the LHC. The CMS (Compact Muon Solenoid) is an experimental setup for particle physics experiment at high energies. Its aim is to record the Universe's tiniest constituents. The ATLAS (A Toroidal LHC Apparatus) is an experimental setup for particle physics experiment at high energies. Its aim is to search for new discoveries in the head-on collisions of protons of extraordinarily high energy. It will provide informations on the fundamental forces that have shaped our universe since the beginning of time, unification of fundamental forces, the origin of mass, extra dimensions of space and evidence for dark matter candidates in the universe. The ALICE (A Large Ion Collider Experiment) is an experimental setup for heavy-ion collider experiment to exploit the unique physics potential of nucleus-nucleus interactions at LHC energies. Its aim is to study the physics of strongly interacting matter at extreme energy densities, where the formation of a new phase of matter, the quark-gluon plasma, is expected. The existence of such a phase and its properties are key issues in QCD. LHCb (Large Hadron Collider beauty) is an experiment set up to explore what happened after the Big Bang that allowed matter to survive and build the Universe we inhabit today.

The LHC has delivered its first high-energy collisions on 29th march 2010 where two proton beams collide at 3.5 TeV energy per beam, 7 TeV total energy. Many different particles are created in the proton collisions delivered by the LHC and the task of the detectors is to recognize them by measuring their mass, their charge and a few other properties. Physicists are currently using the signals coming from known particles to verify that their detectors are working as expected. After mastering operation with nominal bunch intensities, in June 2010, the number of nominal intensity bunches injected into the machine has been carefully increased. This achievement has allowed the LHC experiments to record more than 250 nb^{-1} of integrated luminosity. This represents a rich harvest of data whose analysis being continued.

With successive improvements, LHC is now operating with the highest stored beam energy of any collider. Improvements of set-up and conditions will be continued and the new data will give us an unprecedented tool to understand the universe we live in.

Parton distribution functions (PDF) are the vital tools for reliable predictions for new physics signals and their background cross sections at the LHC. Since QCD does not predict the parton content of the proton, the PDF parameters are determined by fit to data from experimental observables in various processes using the DGLAP evolution equation. Recently PDF's also provide uncertainties which take into account experimental errors and their correlations. Since the LHC kinematic region is much broader than currently explored, we will have the unique opportunity to test QCD at very high-Q^2 and small-x, where predictions are extremely important for precise measurements and new physics searches at the LHC.

1.11.5 BNL (Brookhaven National Laboratory)

Brookhaven National Laboratory is located at Upton, New York. The setup of Relativistic Heavy Ion Collider (RHIC) is a heavy-ion collider used to collide ions at relativistic speeds.

RHIC is the first machine in the world capable of colliding heavy ions, which are atoms which have had their outer cloud of electrons removed. RHIC primarily uses ions of gold, one of the heaviest common elements, because its nucleus is densely packed with particles. p-p, d-Au, Cu-Cu collisions are also studied in RHIC. The RHIC double storage ring is itself hexagonally shaped with curved edges in which stored particles are deflected by superconducting magnets. The six interaction points are at the middle of the six relatively straight sections, where the two rings cross, allowing the particles to collide. Four detectors – STAR, PHENIX, PHOBOS, and BRAHMS – help physicists to analyse RHIC particle collisions. These detectors electronically record the results of collisions, seeking insight into what happens when quarks are liberated from their atomic nuclei.

Analyses of RHIC data have established that collisions of gold ions produce sufficiently high temperature (about 4 trillion degree Celsius) and pressure so that the protons and neutrons melt and, for a brief instant, liberates their constituent quarks and gluons in the form of quarks-gluon plasma. Just after the collision, thousands more particles form as the area cools off. Each of these particles provides a clue as to what occurred inside the collision zone.

All protons and neutrons are made up of three quarks, along with the gluons that bind them together. Theory holds that for a brief time at the beginning of the universe there were no protons and neutrons, only free quarks and gluons. However, as the universe expanded and cooled, the quarks and gluons bound together and, for the next 13 billion years, remained virtually inseparable. RHIC is the first instrument humans have built that can take us back in time to see how matter behaved at the start of the universe.

Another collider eRHIC, also known as spin-dependent electron-hadron collider was designed based on the RHIC hadron rings. The main goal of the eRHIC is to explore the physics at small-x, and the physics of colour-glass condensate in electron-hadron collisions.

Unlike the LHC, RHIC is able to accelerate spin polarized protons, which would leave RHIC as the world's highest energy accelerator for studying spin-polarized proton structure.

1.12 Aim and Plan of the present work

The present work (Thesis) devotes mainly to the higher order effects in structure functions and some aspects in high density QCD. The analysis is based on DGLAP evolutions equations which are the basic tools to study the underlying dynamics of quarks and gluons.

We have planned our work as follows :

Chapter-1 contains general introduction relevant to the present work. We have gone through them in short in the previous sections.

In chapter-2, we solve DGLAP equations in leading order (LO) by using method of characteristics and obtain an analytical form of gluon distribution function at small-x without any *ad-hoc* assumption of factorizability of x and $t(=\ln\frac{Q^2}{\Lambda^2})$ dependence of the gluon distribution function $G(x,t)$.

In chapter-3 , we solve DGLAP equations for both the singlet structure and non-singlet structure functions in NLO at small-x by using Lagrange's auxiliary method and obtain expressions for proton, neutron and deuteron structure functions in NLO and analyse NMC experiment data.

In chapter-4 , we solve DGLAP equations for both the singlet structure and non-singlet structure functions in NNLO at small-x by using Lagrange's auxiliary method and obtain expressions for proton, neutron and deuteron structure functions in NNLO and analyse NMC experiment data.

In chapter-5 , we obtain the expression of the tensor structure function $b_1^d(x,Q^2)$ of the deuteron in NLO and NNLO using the solutions of DGLAP equations for the singlet structure function $F_2^S(x,Q^2)$ obtained in chapters 3 & 4, and analyse HERMES experiment data.

Chapter-6 deals with a quantitative study of the gluon-gluon interaction probability $k_{G_N}(x,t)$ using currently available forms of gluon distributions. We analyse how the gluon-gluon interaction probability $k_{G_N}(x,t)$ and $k_{G_A}(x,t)$ in nucleon and nuclei very with rapidity $y=\ln(1/x)$, mass number of nuclei A and the running coupling constant $\alpha_S(t)$.

Finally, chapter-7 contains a summary of the results obtained in the previous chapters and future scope of the present work.

Chapter 2

The gluon distribution function in the leading order (LO)

2.1 Introduction

Dokshitzer, Gribov, Lipatov, Altarelli, Parisi (DGLAP) evolution equations [49, 50, 51, 52, 53] are the basic tools to study the underlying dynamics of quarks and gluons. Several approximate and numerical solutions of DGLAP evolution equations are available in literature [54, 55, 56, 57], but their exact analytical solutions are not known [58, 59]. Because these evolution equations are partial differential equations (PDE), their ordinary solutions are not unique solutions, rather a range of solutions. These solutions were selected as the simplest ones with a single boundary condition on the non-perturbative x-distribution of the structure function at some $Q^2 = Q_0^2$. However, the complete solution of DGLAP equations with two differential variables generally needs two boundary conditions [60], one at $x \to 0, t \to \infty$ limit of double asymptotic scaling and the other at any fixed $Q^2 = Q_0^2$. Moreover, they are based on an *ad-hoc* assumption of factorizability of x and $t(= \ln \frac{Q^2}{\Lambda^2})$

dependence of the gluon momentum distribution $G(x,t)$. These limitations can be over come by the use of Method of Characteristics [42, 43].

In the present chapter, we solve DGLAP equations in leading order (LO) by using method of characteristics and obtain an analytical form of gluon distribution function at small-x which is free from the above mentioned limitations and in good agreement with exact results and data.

2.2 Formalism

DGLAP equations for gluon distribution have the standard form [49, 50, 51, 52, 53] in LO :

$$\frac{\partial G(x,t)}{\partial t} - \frac{\alpha_s(t)}{2\pi} I_1^G(x,t) = 0 \tag{2.1}$$

where,

$$\begin{aligned} I_1^G(x,t) &= 6\left\{\frac{11}{12} - \frac{N_f}{18} + \ln(1-x)\right\} G(x,t) + 6\int_x^1 \frac{zG(\frac{x}{z},t) - G(x,t)}{1-x} dz \\ &+6\int_x^1 \left\{z(1-z) + \frac{(1-z)}{z}\right\} G(\frac{x}{z},t) + \frac{4}{3}\int_x^1 \frac{1+(1-z)^2}{z} \\ &\times F_2^S(\frac{x}{z},t) \end{aligned} \tag{2.2}$$

with, $t = \ln(\frac{Q^2}{\Lambda^2})$, $\alpha_S(t) = \frac{4\pi}{\beta_0}$, $\beta_0 = 11 - \frac{2}{3}N_f$, N_f being the number of flavours. Introducing the variable $u = 1 - z$, we note that [61, 62, 63] :

$$\frac{x}{z} = \frac{x}{1-u} = x\sum_{l=0}^{\infty} u^l = x + x\sum_{l=1}^{\infty} u^l \tag{2.3}$$

Since $x < z < 1$ so $0 < u < 1 - x$; hence the series is convergent for $|u| < 1$ and we can use Taylor's expansion of $F_2^S(\frac{x}{z},t)$ and $G(\frac{x}{z},t)$ in approximated form [39, 40, 41] at small-x as :

$$F_2^S(\frac{x}{z},t) \approx F_2^S(x,t) + x\sum_{l=1}^{\infty} u^l \frac{\partial F_2^S(x,t)}{\partial x} \tag{2.4}$$

$$G(\frac{x}{z},t) \approx G(x,t) + x\sum_{l=1}^{\infty} u^l \frac{\partial G(x,t)}{\partial x} \tag{2.5}$$

where terms containing x^2 and higher powers of x are neglected at small-x. Using eq.(2.4) and (2.5) in eq.(2.2) and performing the integrations w.r.t. z, eq.(2.1) can be written in the form :

$$t\frac{\partial G(x,t)}{\partial t} = P(x)G(x,t) + Q(x)\frac{\partial G(x,t)}{\partial x} + R(x)F_2^S(x,t) + S(x)\frac{\partial F_2^S(x,t)}{\partial x} \tag{2.6}$$

where, at small-x,

$$P(x) = \frac{12}{\beta_0}\left\{\ln(\frac{1}{x}) + 2x - \frac{N_f}{18} - \frac{11}{12}\right\} \tag{2.7a}$$

$$Q(x) = \frac{11}{\beta_0}x \tag{2.7b}$$

$$R(x) = \frac{12}{\beta_0}x \tag{2.7c}$$

$$S(x) = \frac{16}{\beta_0}x \tag{2.7d}$$

A reasonable approximate relationship between $F_2^S(x,t)$ and $G(x,t)$, representing the relative strength of gluon to singlet distribution, can be taken as [56, 63, 64]

$$F_2^S(x,t) = kG(x,t) \tag{2.8}$$

where k is a suitable function of x or may be a constant. For simplicity and well adaptation to method of characteristics, k is considered here as a constant with $0 <$

$k < 1$, since gluon distribution is always higher than singlet distributions at any Q^2 at small-x.

Using this relationship (2.8) in eq.(2.6),

$$J(x)\frac{\partial G(x,t)}{\partial x} - t\frac{\partial G(x,t)}{\partial t} + H(x)G(x,t) = 0 \tag{2.9}$$

where,

$$H(x) = P(x) + kR(x) \tag{2.10a}$$

$$J(x) = Q(x) + kS(x) \tag{2.10b}$$

Equation (2.9) is a first order PDE, which can be solved by Method of Characteristics.

To use method of characteristics, let us introduce two variables S and τ as follows:

$$\frac{dt}{dS} = -t \tag{2.11}$$

$$\frac{dx}{dS} = J(x) \tag{2.12}$$

Use of eqs.(2.11) and (2.12) in eq.(2.9) gives,

$$\frac{dG}{dS} + U(S,\tau)G(S,\tau) = 0 \tag{2.13}$$

Thus the PDE (2.9) in (x,t) reduces to the ODE (2.13) in new coordinates (S,τ).

Here,

$$
\begin{aligned}
U(S,\tau) &= H(x) \\
&= P(x) + kR(x) \\
&= \frac{12}{\beta_0}\left\{(2+k)x + \ln\left(\frac{1}{x}\right) - \frac{N_f}{18} - \frac{11}{12}\right\}
\end{aligned} \tag{2.14}
$$

To obtain transformation equations between (S,τ) and (x,t), we have to solve eq.(2.11) and (2.12).

Integrating eq.(2.11),

$$\ln t = -S + C_1 \tag{2.15}$$

Using the boundary condition, at $S = 0,\ t = t_0$ and $x = \tau$, we obtain,

$$C_1 = \ln t_0 \tag{2.16}$$

Using eq.(2.16) in (2.15), we get the transformation equation between S and t as,

$$S = \ln\left(\frac{t_0}{t}\right) \tag{2.17}$$

Again, eq.(2.12) can be expressed as,

$$
\begin{aligned}
\frac{dx}{dS} &= J(x) \\
&= Q(x) + kS(x) \\
&= \frac{1}{\beta_0}(11+16k)x
\end{aligned} \tag{2.18}
$$

Integrating eq.(2.18),

$$\ln x = \frac{1}{\beta_0}(11+16k)S + C_2 \tag{2.19}$$

Using the same boundary condition, we obtain,

$$C_2 = \ln \tau \tag{2.20}$$

Using eq.(2.20) in (2.19) and simplifying, we get the transformation equation between τ and x as,

$$\tau = x\left(\frac{t}{t_0}\right)^{\frac{1}{\beta_0}(11+16k)} \tag{2.21}$$

Thus, equations (2.17) and (2.21) are the set of transformation equations between (S,τ) and (x,t) .

Equation (2.14) can be expressed in terms of S and τ explicitly as :

$$\begin{aligned} U(S,\tau) &= \frac{1}{\beta_0}\Big[(24+12k)\tau\exp\left\{\frac{(11+16k)S}{\beta_0}\right\} \\ &\quad -12\left\{\frac{(11+16k)S}{\beta_0}+\ln\tau\right\}-\frac{2}{3}N_f-11\Big] \end{aligned} \tag{2.22}$$

Use of eq.(2.22) in eq.(2.13) gives,

$$\begin{aligned} \frac{dG(S,\tau)}{G(S,\tau)} &= -\frac{1}{\beta_0}\Big[(24+12k)\tau\exp\left\{\frac{(11+16k)S}{\beta_0}\right\} \\ &\quad -12\left\{\frac{(11+16k)S}{\beta_0}+\ln\tau\right\}-\frac{2}{3}N_f-11\Big]ds \end{aligned} \tag{2.23}$$

Integrating eq.(2.23),

$$\begin{aligned} \ln G(S,\tau) &= -\frac{(24+12k)}{(11+16k)}\tau\exp\left\{\frac{(11+16k)S}{\beta_0}\right\}+\frac{6}{\beta_0^2}(11+16k)S^2 \\ &\quad +\frac{12}{\beta_0}\ln\tau\times S+\frac{1}{\beta_0}(\frac{2}{3}N_f+11)S+C \end{aligned} \tag{2.24}$$

Using the boundary condition; when $S = 0$, $G(S,\tau) = G(\tau)$, we obtain,

$$C = \ln G(\tau) + \frac{(24+12k)}{(11+16k)}\tau \tag{2.25}$$

Using eq.(2.25) in (2.24),

$$\begin{aligned} G(S,\tau) &= G(\tau)\times \exp\left[\frac{(24+12k)}{(11+16k)}\tau - \frac{(24+12k)}{(11+16k)}\tau \exp\left\{\frac{(11+16k)S}{\beta_0}\right\}\right. \\ &\left. +\frac{6}{\beta_0^2}(11+16k)S^2 + \frac{12}{\beta_0}\ln\tau\times S + \frac{1}{\beta_0}(\frac{2}{3}N_f+11)S\right] \end{aligned} \tag{2.26}$$

Now transforming eq.(2.26) back to the original variables (x, t) with the help of transformation eq.(2.17) and (2.21), we get,

$$\begin{aligned} G(x,t) &= G(\tau)\times \exp\left[\frac{(24+12k)}{(11+16k)}x\left(\frac{t}{t_0}\right)^{\frac{1}{\beta_0}(11+16k)}\right. \\ &+\frac{(66+96k)}{\beta_0^2}\left\{\ln\left(\frac{t_0}{t}\right)\right\}^2 + \ln\left\{x\left(\frac{t}{t_0}\right)^{\frac{1}{\beta_0}(11+16k)}\right\}\ln\left(\frac{t_0}{t}\right)^{\frac{12}{\beta_0}} \\ &\left.+\ln\left(\frac{t_0}{t}\right)^{\frac{1}{\beta_0}(\frac{2}{3}N_f+11)} - \frac{(24+12k)}{(11+16k)}x\right] \end{aligned} \tag{2.27}$$

where $G(S,\tau) = G(\tau)$ is the input function obtained from the boundary condition, at $S = 0, t = t_0$ with τ given by eq.(2.21).

Equation (2.27) represents solution of DGLAP equation for gluon in LO. This result is different from eq.(36) of Ref. [62] given by,

$$G(x,t) = G(\tau)x^{-\{1-(t_0/t)^{12/\beta_0}\}}\left(\frac{t_0}{t}\right)^{2N_f/3\beta_0} exp\left[-\frac{11}{12}\left\{1-\left(\frac{t_0}{t}\right)^{12/\beta_0}\right\}\right] \tag{2.28}$$

with,

$$\tau = \left[\left(-\ln\frac{1}{x}+\frac{11}{12}\left(\frac{t_0}{t}\right)\right)^{12/\beta_0} - \frac{11}{12}\right] \tag{2.29}$$

which was obtained by using the same method but neglecting the singlet structure function $F_2^S(x,t)$ from the DGLAP equation for gluons in LO. We have included the contribution of the singlet structure function $F_2^S(x,t)$ in our formalism.

Standard DLLA (double leading logarithmic approximation) result for gluon distribution [65] is given by

$$G^{DLLA}(x,t) = G(x,t_0) \times \exp\left[\left\{\frac{48}{\beta_0}\ln\left(\frac{t}{t_0}\right)\ln\left(\frac{1}{x}\right)\right\}^{0.5}\right] \tag{2.30}$$

provided the gluon distribution is not singular at $t = t_0$. We compare our result with this standard DLLA result for gluon distribution.

The expressions for the gluon number density and energy density in Froissart saturation region can also be obtained using the present formalism. Using the relationship (2.8), the gluon number density and energy density in Froissart saturation model [66] are given by

$$\begin{aligned} N_F(x,t) &= \frac{xg(x,t)}{\frac{4}{3}\pi R_N^3} = \frac{G(x,t)}{\frac{4}{3}\pi R_N^3} = \frac{1.0}{\frac{4}{3}\pi R_N^3 k}\frac{1-x}{1+\frac{4m^2x^2}{Q^2}} \\ &\times\left\{A+\beta\mathrm{Log}\left[x_0\frac{1-x}{x}\left(1+\frac{m^2}{Q^2}\frac{x}{1-x}\right)\right]^2\right\} \end{aligned} \tag{2.31}$$

$$\begin{aligned} \epsilon_F(x,t) &= \frac{xg(x,t)xE_p}{\frac{4}{3}\pi R_N^3} = \frac{xe_p}{\frac{4}{3}\pi R_N^3 k}\frac{1-x}{1+\frac{4m^2x^2}{Q^2}} \\ &\times\left\{A+\beta\mathrm{Log}\left[x_0\frac{1-x}{x}\left(1+\frac{m^2}{Q^2}\frac{x}{1-x}\right)\right]^2\right\} \end{aligned} \tag{2.32}$$

and that for the solution (2.27) are given by

$$
\begin{aligned}
N(x,t) &= \frac{xg(x,t)}{\frac{4}{3}\pi R_N^3} = \frac{G(x,t)}{\frac{4}{3}\pi R_N^3} = \frac{G(\tau)}{\frac{4}{3}\pi R_N^3}\exp\left[\frac{(24+12k)}{(11+16k)}x\left(\frac{t}{t_0}\right)^{\frac{1}{\beta_0}(11+16k)}\right. \\
&+\frac{(66+96k)}{\beta_0^2}\left\{\ln\left(\frac{t_0}{t}\right)\right\}^2+\ln\left\{x\left(\frac{t}{t_0}\right)^{\frac{1}{\beta_0}(11+16k)}\right\} \\
&\left.\times\ln\left(\frac{t_0}{t}\right)^{\frac{12}{\beta_0}}+\ln\left(\frac{t_0}{t}\right)^{\frac{1}{\beta_0}\left(\frac{2}{3}N_f+11\right)}-\frac{(24+12k)}{(11+16k)}x\right]
\end{aligned}
\tag{2.33}
$$

$$
\begin{aligned}
\epsilon(x,t) &= \frac{xg(x,t)xE_p}{\frac{4}{3}\pi R_N^3} = \frac{xe_p}{\frac{4}{3}\pi R_N^3 k}G(\tau)\exp\left[\frac{(24+12k)}{(11+16k)}x\left(\frac{t}{t_0}\right)^{\frac{1}{\beta_0}(11+16k)}\right. \\
&+\frac{(66+96k)}{\beta_0^2}\left\{\ln\left(\frac{t_0}{t}\right)\right\}^2+\ln\left\{x\left(\frac{t}{t_0}\right)^{\frac{1}{\beta_0}(11+16k)}\right\} \\
&\left.\times\ln\left(\frac{t_0}{t}\right)^{\frac{12}{\beta_0}}+\ln\left(\frac{t_0}{t}\right)^{\frac{1}{\beta_0}\left(\frac{2}{3}N_f+11\right)}-\frac{(24+12k)}{(11+16k)}x\right]
\end{aligned}
\tag{2.34}
$$

where $x = \frac{E_q}{E_p}$ and R_N is size of the target (nucleon/nucleus) [67]. Here, E_p is the energy of the target proton and E_q is the energy of the stuck quark.

2.3 Results and Discussion

We compare our predicted result with MRST2001LO exact results and with the parametrized experimental data from H12000 at different Q^2 values for x-range $10^{-5} < x < 10^{-1}$. A comparison is also made with standard DLLA result (eq.(2.30)). For quantitative analysis, we have used MRST2001LO input [57] and considered $Q_0^2 = 4\ Gev^2$, QCD cut-off parameter $\Lambda = 220\ Mev$ and $N_f = 4$ [68]. The Dependence of our prediction on the values of the arbitrary constant k has been observed and it is found that the predicted result is almost independent of k at $k \leq 10^{-2}$.

Figure 2.1 (a-d) represent the predicted gluon distribution $G(x,t)$ against x at fixed Q^2. Comparison is made with MRST2001LO exact results at different $Q^2 = 8, 9, 10$, and 11 Gev^2 for the same x-range $10^{-5} < x < 10^{-1}$ and $k = 0.01$ and a good agreement is obtained. Figure 2.2 (a-f) represent the same at $Q^2 = 6, 7, 12, 15$ and $20, 50$ Gev^2. It is seen that disagreement increases at lower Q^2 as well as at higher Q^2 values. Figure 2.3 (a-d) represents dependence of the predicted gluon distribution $G(x,t)$ on the values of the arbitrary constant k. The acceptable range of k is found to be $0 < k < 10^{-1}$. The best fit value of k is found to be $k = 0.0916$. It is also observed that the predicted result is almost independent of k at $k \leq 10^{-2}$. Figure 2.4 (a-b) represent predicted gluon distribution $G(x,t)$ and comparison with MRST2001LO exact results, data from H1 2000 and with standard DLLA result at $Q^2 = 9$ and 10 Gev^2 for the same x-range $10^{-5} < x < 10^{-1}$ and $k = 0.01$. Comparison shows more suitability of our predicted result over the standard DLLA result.

The analysis on gluon number and energy density shows that both the models (eq.2.31-2.32 and eq.2.33-2.34) predict increase in gluon number density as well as the gluon energy density with decrease in x (fig.2.5 and 2.6). Here, we have used $R_N = 5\ GeV^{-2}$ [67]. As an illustration, at $x = 0.0001$, the gluon number densities of are $1.06 \times 10^4\ fm^{-3}$ & $2.63 \times 10^5\ fm^{-3}$ and energy densities are $4.87 \times 10^5\ GeVfm^{-3}$& $1.21 \times 10^7\ GeVfm^{-3}$ in the two models respectively. These quantities at small-x correspond to partons (gluons) in the central rapidity region ($y = 0$) as the rapidity is defined as $y = \frac{1}{2}log\left(\frac{E+P_L}{E-P_L}\right)$, where E and P_L are the energy and longitudinal momentum of the parton [69]. The faster rise of number density and energy density of gluons predicted by the solution (2.33) and (2.34) indicates that the solution (2.27) of DGLAP equations for gluons do not conform to Froissart bound. The comparison of gluon number and energy density with data is not possible at this moment as proper data is not yet available.

2.4 Conclusion

In this chapter, we have applied method of characteristics to solve DGLAP equation for gluon distribution without any *ad-hoc* assumption of factorizability of x and t dependence of the gluon distribution function $G(x, t)$. A good agreement of our predicted result with MRST2001LO exact results and H1 data within moderate x- and Q^2-range is obtained.

The application of method of characteristics in perturbative quantum chromodynamics (pQCD), specially in DGLAP equations, is relatively new. Although it has got considerable phenomenological success [62, 41, 70, 71, 48] in solving DGLAP equations in leading order (LO), in the process of solution of DGLAP equations in NLO and NNLO, the method becomes very complicated and it goes almost out of mathematical control. Hence we search for a new method to solve higher order equations and find Lagrange's auxiliary method [44, 45] as a viable effective alternative with considerable phenomenological success in more recent times [47, 46, 72, 73].

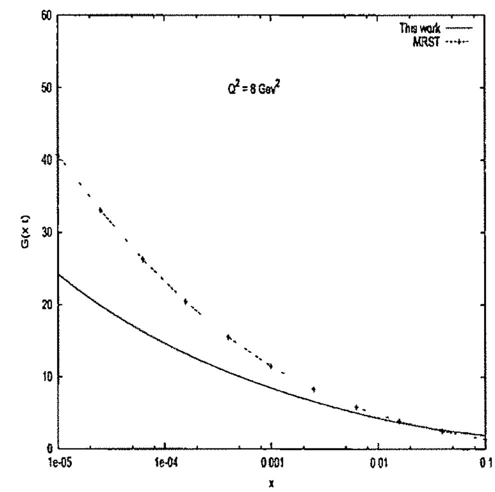
This work
MRST
$Q^2 = 8$ Gev^2
G(x t)
x
1e-05
1e-04
0.001
0.01
0.1
0
10
20
30
40
50
60

(a)

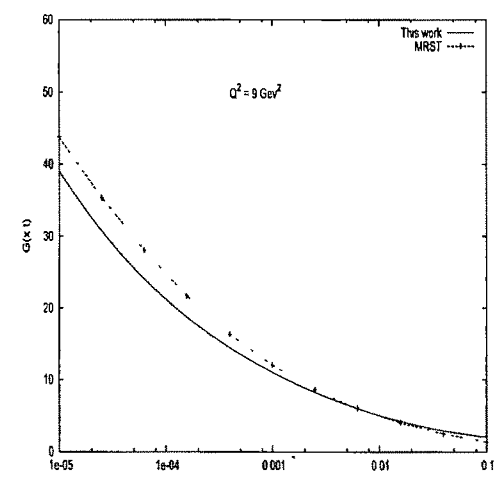
This work
MRST
$Q^2 = 9$ Gev^2
G(x t)
x
1e-05
1e-04
0.001
0.01
0.1
0
10
20
30
40
50
60

(b)

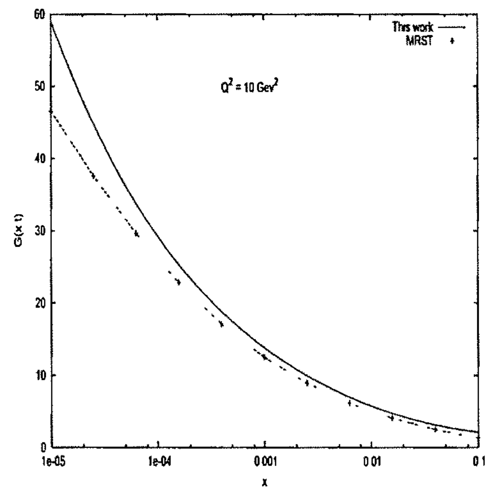

(c)

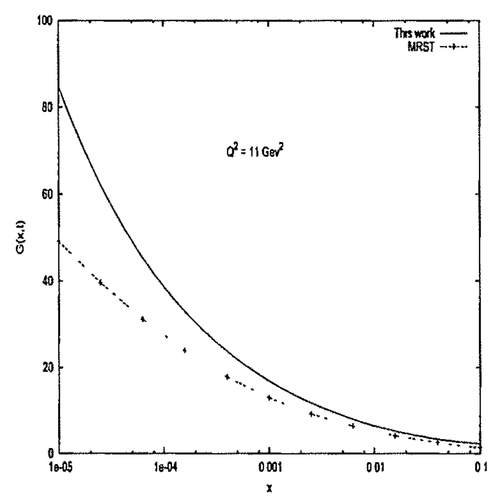

(d)

Figure 2.1: (a-d). Gluon distribution from our predicted result and its comparison with MRST2001LO exact results at different $Q^2 = 8, 9, 10$, and 11 Gev^2.

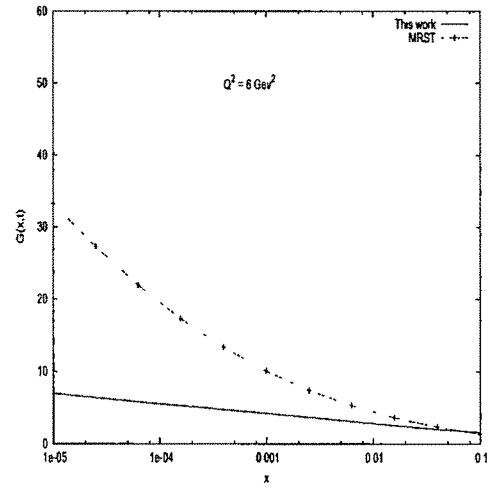
This work
MRST
$Q^2 = 6\ Gev^2$
60
50
40
30
20
10
0
G(x,t)
1e-05
1e-04
0.001
0.01
0.1
x

(a)

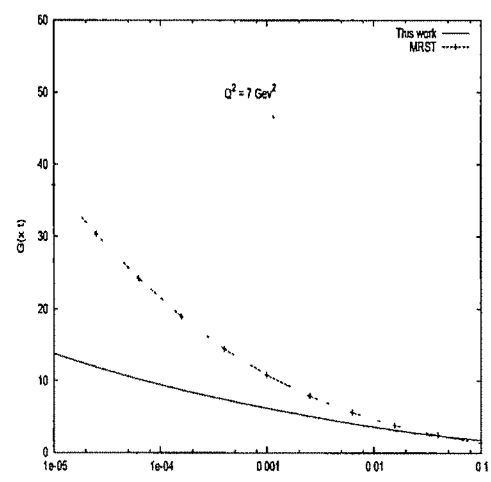
This work
MRST
$Q^2 = 7\ Gev^2$
60
50
40
30
20
10
0
G(x,t)
1e-05
1e-04
0.001
0.01
0.1
x

(b)

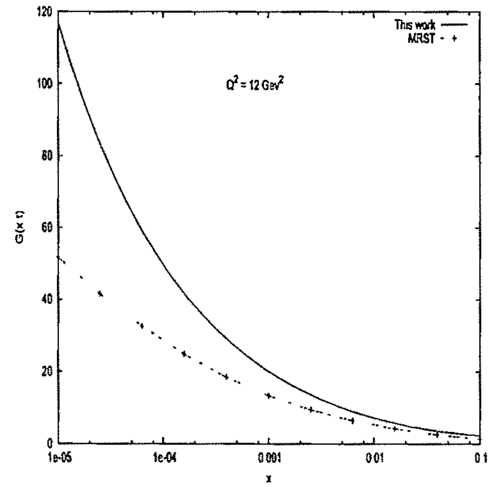
This work
MRST
$Q^2 = 12\ Gev^2$
120
100
80
60
40
20
0
G(x t)
1e-05
1e-04
0.001
0.01
0.1
x

(c)

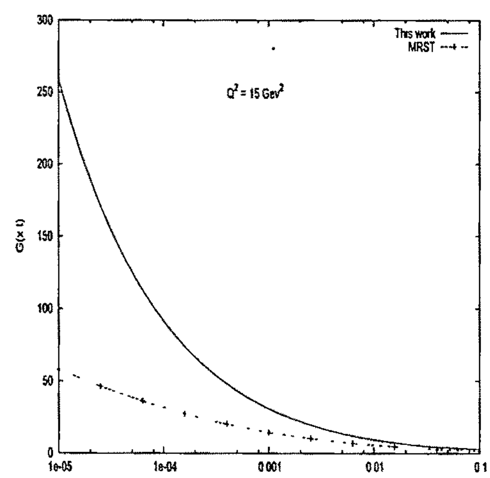
This work
MRST
$Q^2 = 15\ Gev^2$
300
250
200
150
100
50
0
G(x t)
1e-05
1e-04
0.001
0.01
0.1
x

(d)

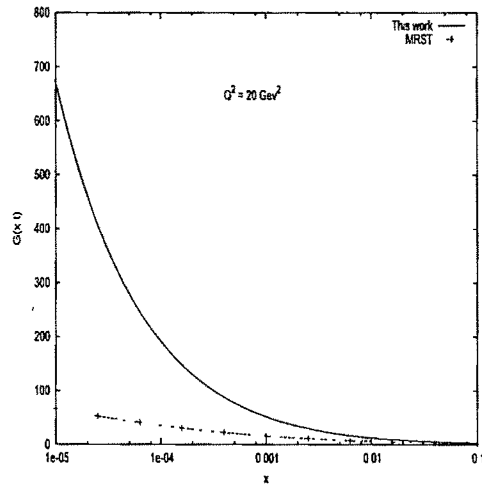

(e)

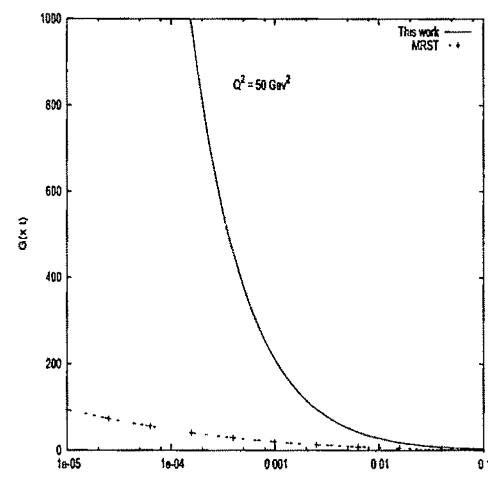

(f)

Figure 2.2: (a-f). Gluon distribution from our predicted result and its comparison with MRST2001LO exact results at different $Q^2 = 6, 7, 12, 15$ and $20, 50$ Gev^2.

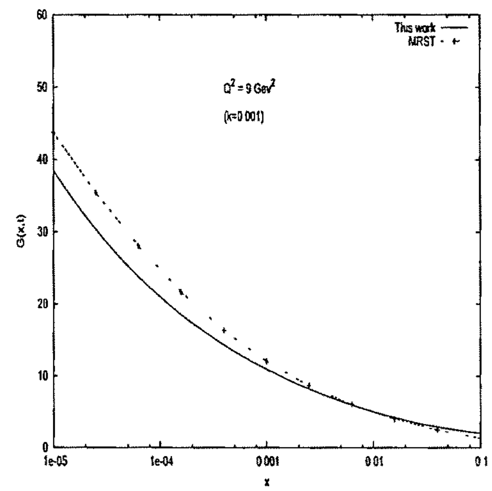
This work
MRST
$Q^2 = 9$ Gev^2
(k=0 001)
G(x,t)
x
0
10
20
30
40
50
60
1e-05
1e-04
0 001
0 01
0 1

(a)

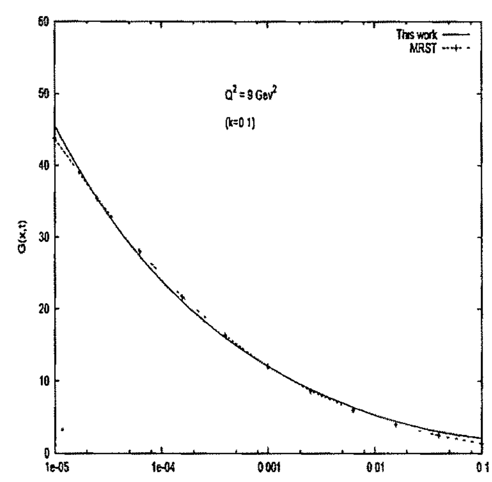
This work
MRST
$Q^2 = 9$ Gev^2
(k=0 1)
G(x,t)
x
0
10
20
30
40
50
60
1e-05
1e-04
0 001
0 01
0 1

(b)

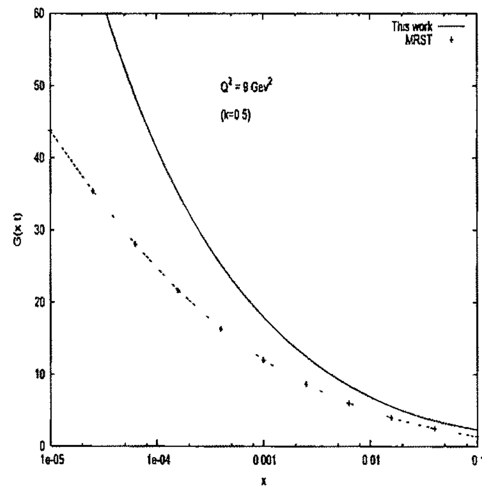

(c)

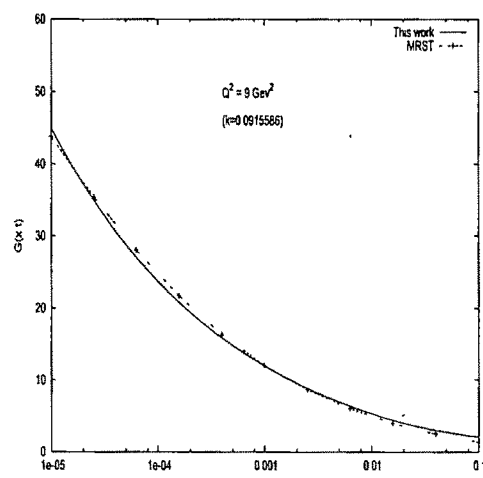

(d)

Figure 2.3: (a-d). Dependence of the predicted gluon distribution on the values of the arbitrary constant k. The best fit value of k is found to be $k = 0.0916$ at $Q^2 = 9Gev^2$.

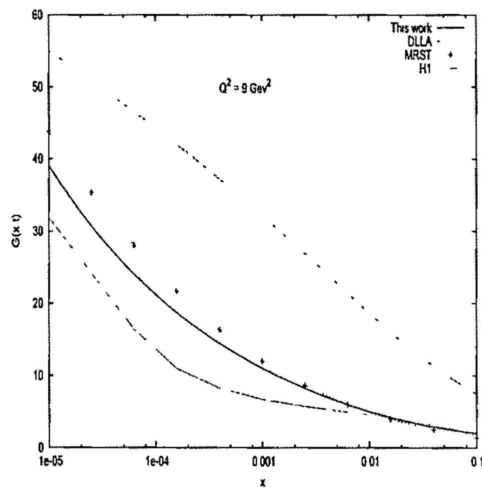

(a)

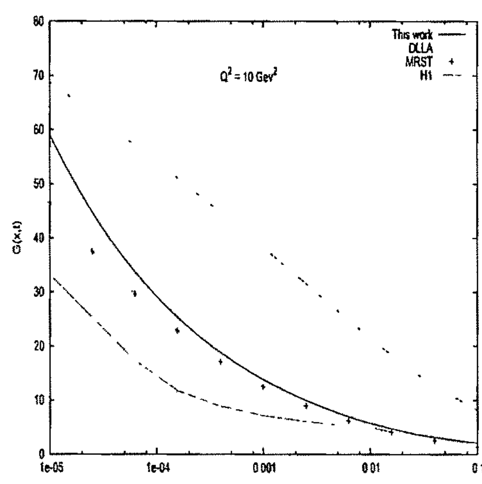

(b)

Figure 2.4: (a-b). Predicted gluon distribution and its comparison with MRST2001LO exact results, with data from H1 and with standard DLLA result.

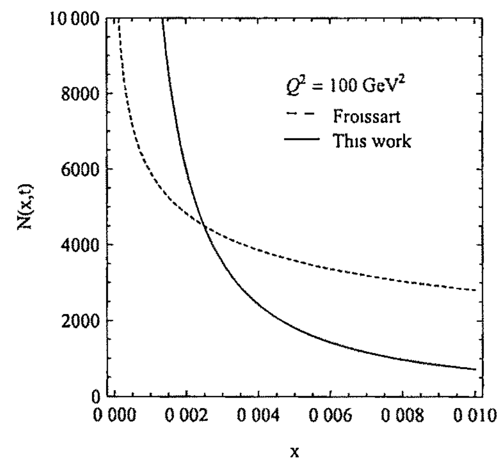

Figure 2.5: Variation of gluon number density with x.

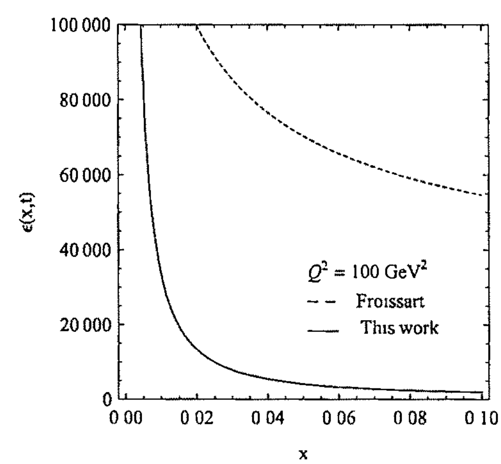

Figure 2.6: Variation of gluon energy density with x.

Chapter 3

The proton, neutron and deuteron structure functions in the next-to-leading order (NLO)

3.1 Introduction

The precision of the contemporary experimental data demands that atleast NLO, and preferably NNLO DGLAP evolution should be used in comparison between QCD theory and experiment.

In this chapter, we have solved DGLAP equations for both the singlet structure and non-singlet structure functions in NLO at small-x by using Lagrange's auxiliary method and obtain expressions for proton, neutron and deuteron structure functions in NLO and analyse NMC experiment data [74]. Because of the complexity mentioned in section 2.4, we switch over to Lagrange's auxiliary method [44, 45] to solve DGLAP equations in higher orders. We have adapted the method from Ref. [46, 47] which was originally used to study non-singlet structure function in DIS neutrino scattering.

3.2 Formalism

DGLAP equations for singlet and non-singlet structure functions in NLO have the standard form [53, 75, 76] :

$$\frac{\partial F_2^S(x,t)}{\partial t} - \frac{\alpha_s(t)}{2\pi} I_1^S(x,t) - \left(\frac{\alpha_s(t)}{2\pi}\right)^2 I_2^S(x,t) = 0 \tag{3.1}$$

and

$$\frac{\partial F_2^{NS}(x,t)}{\partial t} - \frac{\alpha_s(t)}{2\pi} I_1^{NS}(x,t) - \left(\frac{\alpha_s(t)}{2\pi}\right)^2 I_2^{NS}(x,t) = 0 \tag{3.2}$$

where,

$$\begin{aligned} I_1^S(x,t) &= \left[\frac{2}{3}\{3+4\ln(1-x)\}F_2^S(x,t)\right] + \frac{4}{3}\int_x^1 \frac{dz}{1-z}[(1+z^2) \\ &\times F_2^S(\frac{x}{z},t) - 2F_2^S(x,t)] + N_f\int_x^1 z^2 + (1-z)^2 G(\frac{x}{z},t) \end{aligned} \tag{3.3}$$

$$\begin{aligned} I_2^S(x,t) &= (x-1)F_2^S(x,t)\int_0^1 f(z)dz + \int_x^1 f(z)F_2^S(\frac{x}{z},t)dz \\ &+ \int_x^1 F_{qq}^S(z)F_2^S(\frac{x}{z},t)dz + \int_x^1 F_{qg}^S(z)G(\frac{x}{z},t)dz \end{aligned} \tag{3.4}$$

and

$$I_1^{NS}(x,t) = \frac{4}{3}\int_x^1 \frac{dz}{1-z}\left[(1+z^2)F_2^{NS}(\frac{x}{z},t) - 2F_2^{NS}(x,t)\right] \tag{3.5}$$

$$I_2^{NS}(x,t) = (x-1)F_2^{NS}(x,t)\int_0^1 f(z)dz + \int_x^1 f(z)F_2^{NS}(\frac{x}{z},t)dz \tag{3.6}$$

The explicit forms of higher order kernels in NLO are [75, 77, 78],

$$
\begin{aligned}
f(z) &= C_F^2[P_F(z) - P_A(z)] + \frac{1}{2}C_F C_A[P_G(z) + P_A(z)] \\
&+ C_F T_R N_f P_{N_f}(z)
\end{aligned}
\tag{3.7}
$$

$$
F^S_{qq}(z) = 2C_F T_R N_f F_{qq}(z) \tag{3.8}
$$

$$
F^S_{qg}(z) = C_F T_R N_f F^1_{qg}(z) + C_G T_R F^2_{qg}(z) \tag{3.9}
$$

$$
\begin{aligned}
P_F(z) &= -\frac{2(1+z^2)}{(1-z)} ln(z) ln(1-z) - \left(\frac{3}{1-z} + 2z\right) ln(z) \\
&- \frac{1}{2}(1+z) ln(z) + \frac{40}{3}(1-z)
\end{aligned}
\tag{3.10}
$$

$$
\begin{aligned}
P_G(z) &= \frac{(1+z^2)}{(1-z)}\left(ln^2(z) + \frac{11}{3} ln(z) + \frac{67}{9} - \frac{\pi^2}{3}\right) \\
&- 2(1+z) ln(z) + \frac{40}{3}(1-z)
\end{aligned}
\tag{3.11}
$$

$$
P_{N_f}(z) = \frac{2}{3}\left[\frac{(1+z^2)}{(1-z)}\left(-ln(z) - \frac{5}{3}\right) - 2(1-z)\right] \tag{3.12}
$$

$$
\begin{aligned}
P_A(z) &= \frac{2(1+z^2)}{(1-z)} \int_{(\frac{z}{1+z})}^{(\frac{1}{1+z})} \frac{dk}{k} ln\left(\frac{1-k}{k}\right) \\
&+ 2(1+z) ln(z) + 4(1-z)
\end{aligned}
\tag{3.13}
$$

$$F_{qq}(z) = \frac{20}{9z} - 2 + 6z - \frac{56}{9}z^2 + \left(1 + 5z + \frac{8}{3}z^2\right) ln(z) \\ -(1+z)ln^2(z) \tag{3.14}$$

$$F^1_{qg}(z) = 4 - 9z - (1-4z)ln(z) - (1-2z)ln^2(z) + 4ln(1-z) \\ + \left\{2ln^2\left(\frac{1-z}{z}\right) - 4ln\left(\frac{1-z}{z}\right) - \frac{2}{3}\pi^2 + 10\right\} P^1_{qg}(z) \tag{3.15}$$

$$F^2_{qg}(z) = \frac{182}{9} + \frac{14}{9}z + \frac{40}{9z} + \left(z - \frac{38}{3}\right) ln(z) - 4ln(1-z) \\ -(2+8z)ln^2(z) + \left\{ - ln^2(z) + \frac{44}{3}ln(z) - 2ln^2(1-z) \right. \\ \left. +2ln(1-z) + \frac{z^2}{3} - \frac{218}{9}\right\} P^1_{qg}(z) \\ +2P^1_{qg}(-z)\int_{\left(\frac{z}{1+z}\right)}^{\left(\frac{1}{1+z}\right)} \frac{dz}{z} ln\left(\frac{1-z}{z}\right) \tag{3.16}$$

$$P^1_{qg}(z) = z^2 + (1-z)^2 \tag{3.17}$$

$$A(z) = C_F^2 A_1(z) + C_F C_G A_2(z) + C_F T_R N_F A_3(z) \tag{3.18}$$

$$A_1(z) = -\frac{5}{2} - \frac{7}{2}z + \left(2 + \frac{7}{2}z\right) ln(z) + \left(-1 + \frac{1}{2}z\right) ln^2(z) - 2zln(1-z) \\ +\{ - 3ln(1-z) - ln^2(1-z)\} \frac{1 + (1-z)^2}{z} \tag{3.19}$$

$$
\begin{aligned}
A_2(z) &= -\frac{28}{9} - \frac{65}{18}z + \frac{44}{9}z^2 + \left(-12 - 5z - \frac{8}{3}z^2\right) ln(z) + (4+z)ln^2(z) \\
&+2zln(1-z) + \Big\{ -2ln(z)ln(1-z) + \frac{1}{2}ln^2(z) + \frac{11}{3}ln(1-z) \\
&+ln^2(1-z) + \frac{1}{6}\pi^2 + \frac{1}{2}\Big\}\frac{1+(1-z)^2}{z} \\
&-\frac{1+(1-z)^2}{z}\int_{\left(\frac{z}{1+z}\right)}^{\left(\frac{1}{1+z}\right)} \frac{dz}{z} ln\left(\frac{1-z}{z}\right)
\end{aligned} \tag{3.20}
$$

$$
A_3(z) = -\frac{4}{3}z - \left\{\frac{20}{9} + \frac{4}{3}ln(1-z)\right\}\frac{1+(1-z)^2}{z} \tag{3.21}
$$

with $C_A = C_G = 3$, $L_0 = ln(x)$ and $L_1 = ln(1-x)$. The strong coupling constant $\alpha_s(t)$ is related to the β-function by the relation

$$
\beta(\alpha_s) = \frac{\partial \alpha_s(t)}{\partial \ln Q^2} = -\frac{\beta_0}{4\pi}\alpha_s^2 - \frac{\beta_1}{16\pi^2}\alpha_s^3 - \frac{\beta_2}{64\pi^3}\alpha_s^4 + \ldots\ldots \tag{3.22}
$$

where,

$$
\beta_0 = \frac{11}{3}N_C - \frac{4}{3}T_f \tag{3.23a}
$$

$$
\beta_1 = \frac{34}{3}N_C^2 - \frac{10}{3}N_C N_f - 2C_F N_f \tag{3.23b}
$$

$$
\beta_2 = \frac{2857}{54}N_C^3 + 2C_F^2 T_f - \frac{205}{9}C_F N_C T_f + \frac{44}{9}C_F T_f^2 + \frac{158}{27}N_C T_f^2 \tag{3.23c}
$$

are the one-loop, two-loop and three-loop corrections to the QCD β-function. We set $N_C = 3, C_F = \frac{N_C^2-1}{2N_C} = \frac{4}{3}$ and $T_f = \frac{1}{2}N_f$ with

$$\frac{\alpha(t)}{2\pi} = \frac{2}{\beta_0 t}\left[1 - \frac{\beta_1}{\beta_0^2}\frac{ln(t)}{t} + \frac{1}{\beta_0^3 t}\left\{\frac{\beta_1^2}{\beta_0}(ln^2(t) - ln(t) - 1) + \beta_2\right\} + O\left(\frac{1}{t^3}\right)\right] \tag{3.24}$$

The results used here are from direct x-space evolutions [40, 79, 80, 81].

Now introducing the variable $u = 1 - z$, we note that [61, 62, 63] :

$$\frac{x}{z} = \frac{x}{1-u} = x\sum_{l=0}^{\infty} u^l = x + x\sum_{l=1}^{\infty} u^l \tag{3.25}$$

Since $x < z < 1$, so $0 < u < 1 - x$; hence the series is convergent for $|u| < 1$ and we can use Taylor's expansion of $F_2^S(\frac{x}{z}, t)$ and $F_2^{NS}(\frac{x}{z}, t)$ in approximated form [39, 41, 40] at small-x as :

$$F_2^{S,NS}(\frac{x}{z}, t) \approx F_2^{S,NS}(x,t) + x\sum_{l=1}^{\infty} u^l \frac{\partial F_2^{S,NS}(x,t)}{\partial x} \tag{3.26}$$

where terms containing x^2 and higher powers of x are neglected at small-x.

A reasonable approximate relationship between $F_2^S(x,t)$ and $G(x,t)$, representing the relative strength of gluon to singlet distribution, can be taken as [56, 63, 64]

$$G(x,t) = k' F_2^S(x,t) \tag{3.27}$$

where k' is a suitable function of x or may be a constant. For simplicity, k' is considered as a constant with $k' > 1$, since gluon distribution is always higher than singlet distributions at any Q^2 at small-x. Considering all these, eqns.(3.1) and (3.2) take the forms :

$$\frac{\partial F_2^S(x,t)}{\partial t} - \frac{\alpha_s(t)}{2\pi}\left[A_1^S(x)F_2^S(x,t) + A_2^S(x)\frac{\partial F_2^S(x,t)}{\partial x}\right] - \left(\frac{\alpha_s(t)}{2\pi}\right)^2\left[B_1^S(x)F_2^S(x,t) + B_2^S(x)\frac{\partial F_2^S(x,t)}{\partial x}\right] = 0 \qquad (3.28)$$

and

$$\frac{\partial F_2^{NS}(x,t)}{\partial t} - \frac{\alpha_s(t)}{2\pi}\left[A_1^{NS}(x)F_2^{NS}(x,t) + A_2^{NS}(x)\frac{\partial F_2^{NS}(x,t)}{\partial x}\right] - \left(\frac{\alpha_s(t)}{2\pi}\right)^2\left[B_1^{NS}(x)F_2^{NS}(x,t) + B_2^{NS}(x)\frac{\partial F_2^{NS}(x,t)}{\partial x}\right] = 0 \qquad (3.29)$$

where,

$$A_1^S(x) = \frac{2}{3}\{3 + 4ln(1-x)\} + \frac{4}{3}\int_x^1 \frac{z^2-1}{1-z}dz + N_f\int_x^1 \left\{z^2 + (1-z)^2\right\}dz \qquad (3.30)$$

$$A_2^S(x) = \frac{4}{3}\int_x^1 x\sum_{l=1}^{\infty} u^l \frac{dz}{1-z} + N_f\int_x^1 k'\sum_{l=1}^{\infty} u^l\left\{z^2 + (1-z)^2\right\}dz \qquad (3.31)$$

$$B_1^S(x) = (1-x)\int_0^1 f(z)dz + \int_x^1 f(z)dz + \int_x^1 F_{qq}^S(z)dz + \int_x^1 k'F_{qg}^S(z)dz \qquad (3.32)$$

$$B_2^S(x) = \int_x^1 x\sum_{l=1}^{\infty} u^l f(z)dz + \int_x^1 x\sum_{l=1}^{\infty} u^l F_{qq}^S(z)dz + \int_x^1 xk'\sum_{l=1}^{\infty} u^l F_2^S(z)dz \qquad (3.33)$$

and,

$$A_1^{NS}(x) = 2x + x^2 + 4ln(1-x) \quad (3.34)$$

$$A_2^{NS}(x) = x - x^3 - 2xln(x) \quad (3.35)$$

$$B_1^{NS}(x) = x\int_0^1 f(z)dz - \int_0^x f(z)dz + \frac{4}{3}^{NS} N_f \int_x^1 F_{qq}(z)dz \quad (3.36)$$

$$B_2^{NS}(x) = x\int_x^1 \left[f(z) + \frac{4}{3}N_f F_{qg}^S(z)\right]\frac{1-z}{z}dz \quad (3.37)$$

Eq.(3.28) and (3.29) can be written in the forms,

$$\frac{\partial F_2^S(x,t)}{\partial t} + L^S(x,t)\frac{\partial F_2^S(x,t)}{\partial x} = M^S(x,t)F_2^S(x,t) \quad (3.38)$$

$$\frac{\partial F_2^{NS}(x,t)}{\partial t} + L^{NS}(x,t)\frac{\partial F_2^S(x,t)}{\partial x} = M^{NS}(x,t)F_2^{NS}(x,t) \quad (3.39)$$

where,

$$L^{S,NS}(x,t) = \frac{2}{\beta_0 t}\left\{1 - \frac{\beta_1}{\beta_0^2}\frac{ln(t)}{t}\right\}(A_2 + T_0 B_2) \quad (3.40)$$

$$M^{S,NS}(x,t) = \frac{2}{\beta_0 t}\left\{1 - \frac{\beta_1}{\beta_0^2}\frac{ln(t)}{t}\right\}(A_1 + T_0 B_1) \quad (3.41)$$

with, $T(t) = \frac{\alpha_s(t)}{2\pi}$, where $T^2(t)$ is linearised through the ansatz : $T^2(t) = T_0 T(t)$, where T_0 is a suitable numerical parameter [47, 82, 40].

The general solution of eq.(3.38) or (3.39), which is frequently referred to as Lagrange's equation [44, 45], is obtained from the solutions of the equation

$$\frac{dx}{L^{S,NS}(x,t)} = \frac{dt}{1} = \frac{dF_2^{S,NS}(x,t)}{M^{S,NS}(x,t)F_2^{S,NS}(x,t)} \tag{3.42}$$

The general solution of eq.(3.38) or eq.(3.39) in NLO is given by

$$F(U_{NLO}^{S,NS}, V_{NLO}^{S,NS}) = 0 \tag{3.43}$$

where, $F(U_{NLO}^{S,NS}, V_{NLO}^{S,NS})$ is an arbitrary function. $U_{NLO}^{S,NS}(x, t, F_2^{S,NS}) = C_1$ and $V_{NLO}^{S,NS}(x, t, F_2^{S,NS}) = C_2$ are two independent solutions of eq.(3.42). Solving eq.(3.42), we obtain,

$$U_{NLO}^{S,NS}(x,t,F_2^{S,NS}) = t^{\left(1+\frac{b}{t}\right)} e^{\left(\frac{b}{t}\right)} \times exp\left\{\frac{N^{S,NS}(x)}{a}\right\} \tag{3.44}$$

$$V_{NLO}^{S,NS}(x,t,F_2^{S,NS}) = F_{2\,NLO}^{S,NS}(x,t) \times exp\left\{N'^{S,NS}(x)\right\} \tag{3.45}$$

where,

$$N^{S,NS}(x) = \int \frac{dx}{A_2^{S,NS}(x) + T_0 B_2^{S,NS}(x)} \tag{3.46}$$

$$N'^{S,NS}(x) = \int \frac{A_1^{S,NS}(x) + T_0 B_1^{S,NS}(x)}{A_2^{S,NS}(x) + T_0 B_2^{S,NS}(x)} dx \tag{3.47}$$

and $a = \frac{2}{\beta_0}$, $b = \frac{\beta_1}{\beta_0^2}$. (Solution of $\frac{dx}{L^{S,NS}(x,t)} = \frac{dt}{1}$ yields eq.(3.44) and that of $\frac{dt}{1} = \frac{dF_2^{S,NS}(x,t)}{M^{S,NS}(x,t)F_2^{S,NS}(x,t)}$ yields eq.(3.45)).

The most general form of eq.(3.43) is given by [46, 47],

$$V_{NLO}^{S,NS} = \alpha\left(U_{NLO}^{S,NS}\right)^{m} + \beta \tag{3.48}$$

where α and β are two arbitrary constants and m is a real positive function of x and t which is to be determined through experimental parametrizations.

From equations (3.44), (3.45) and (3.48),

$$\begin{aligned} F_{2NLO}^{S}(x,t) &= \frac{1}{exp\{N'^{S}(x)\}}\Big[\alpha t^{m(1+\frac{b}{t})} e^{m(\frac{b}{t})} \\ &\quad \times exp\left\{\frac{m}{a}N^{S}(x)\right\} + \beta\Big] \end{aligned} \tag{3.49}$$

Using the initial condition [46, 47, 83, 84],

$$F_2^S(x,t)\big|_{x=1} = 0 \tag{3.50}$$

at any t for all order, we obtain,

$$\beta = -\alpha t^{m(1+\frac{b}{t})} e^{m(\frac{b}{t})} \times exp\left\{\frac{m}{a}N^{S}(1)\right\} \tag{3.51}$$

Using eq.(3.51) in (3.49),

$$\begin{aligned} F_{2NLO}^{S}(x,t) &= \frac{1}{exp\{N'^{S}(x)\}}\alpha t^{m(1+\frac{b}{t})} e^{m(\frac{b}{t})} \\ &\quad \times\left[exp\left\{\frac{1}{a}N^{S}(x)\right\} - exp\left\{\frac{1}{a}N^{S}(1)\right\}\right] \end{aligned} \tag{3.52}$$

Defining the input $F^S_{2NLO}(x,t_0)$ as,

$$F^S_{2NLO}(x,t_0) = \frac{1}{exp\{N'^S(x)\}}\alpha t_0^{m\left(1+\frac{b}{t_0}\right)} e^{m\left(\frac{b}{t_0}\right)} \times\left[exp\left\{\frac{1}{a}N^S(x)\right\} - exp\left\{\frac{1}{a}N^S(1)\right\}\right] \quad (3.53)$$

we finally get,

$$F^S_{2NLO}(x,t) = F^S_{2NLO}(x,t_0)\left\{\frac{t^{m\left(1+\frac{b}{t}\right)}}{t_0^{m\left(1+\frac{b}{t_0}\right)}}\right\}\times e^{mb\left(\frac{1}{t}-\frac{1}{t_0}\right)} \quad (3.54)$$

Proceeding exactly in the similar way for the non-singlet case, one can find,

$$F^{NS}_{2NLO}(x,t) = F^{NS}_{2NLO}(x,t_0)\left\{\frac{t^{m\left(1+\frac{b}{t}\right)}}{t_0^{m\left(1+\frac{b}{t_0}\right)}}\right\}\times e^{mb\left(\frac{1}{t}-\frac{1}{t_0}\right)} \quad (3.55)$$

Equations (3.54) and (3.55) represent the solutions for singlet and non-singlet structure functions in NLO which are more general than that of Ref. [40].

The proton, neutron and deuteron spin-independent structure functions, in terms of singlet and non-singlet structure functions can be given by [53]

$$F^p_2(x,t) = \frac{5}{18}F^S_2(x,t) + \frac{3}{18}F^{NS}_2(x,t) \quad (3.56)$$

$$F^n_2(x,t) = \frac{5}{18}F^S_2(x,t) - \frac{3}{18}F^{NS}_2(x,t) \quad (3.57)$$

$$F^d_2(x,t) = \frac{5}{9}F^S_2(x,t) \quad (3.58)$$

Use of equations (3.54) and (3.55) in equations (3.56), (3.57) and (3.58) give,

$$F^{p}_{2NLO}(x,t) = \left\{\frac{5}{18}F^{S}_{2NLO}(x,t_0) + \frac{3}{18}F^{NS}_{2NLO}(x,t_0)\right\}\left\{\frac{t^{m\left(1+\frac{b}{t}\right)}}{t_0^{m\left(1+\frac{b}{t_0}\right)}}\right\} \times e^{mb\left(\frac{1}{t}-\frac{1}{t_0}\right)} \quad (3.59)$$

$$F^{n}_{2NLO}(x,t) = \left\{\frac{5}{18}F^{S}_{2NLO}(x,t_0) - \frac{3}{18}F^{NS}_{2NLO}(x,t_0)\right\}\left\{\frac{t^{m\left(1+\frac{b}{t}\right)}}{t_0^{m\left(1+\frac{b}{t_0}\right)}}\right\} \times e^{mb\left(\frac{1}{t}-\frac{1}{t_0}\right)} \quad (3.60)$$

$$F^{d}_{2NLO}(x,t) = \frac{5}{9}F^{S}_{2NLO}(x,t_0)\left\{\frac{t^{m\left(1+\frac{b}{t}\right)}}{t_0^{m\left(1+\frac{b}{t_0}\right)}}\right\} \times e^{mb\left(\frac{1}{t}-\frac{1}{t_0}\right)} \quad (3.61)$$

Equations (3.59), (3.60) and (3.61) are our predicted results for proton, neutron and deuteron structure functions in NLO.

3.3 Results and Discussion

We compare our predicted results for $F_2^p(x,t)$, $F_2^n(x,t)$ and $F_2^d(x,t)$ with NMC experiment data [74]. For quantitative analysis, we use MRST 2004 NLO inputs [57, 85] for $F_2^S(x,t_0)$ and $F_2^{NS}(x,t_0)$ with $Q_0^2 = 1\ GeV^2$, $N_f = 4$ and $\Lambda = 0.323\ GeV$ for NLO.

Figure 3.1 (a-d) represent variation of $F_2^p(x,t)$ in NLO with Q^2 at four different representative x-bins : $x = 0.0175, 0.025, 0.035, 0.050$. The figures represent best fit graphs. The vertical error bars represent statistical uncertainties. Figure 3.2 (a-d) represent the same both for best fit values of m for this work and $m = 1$ for previous works [40, 83, 84]. Figure 3.3 represent variation of $F_2^n(x,t)$ in NLO with Q^2 at $x = 0.050$. Figure 3.4 (a-d) represent variation of $F_2^d(x,t)$ in NLO with Q^2 at the representative x-bins : $x = 0.0175, 0.025, 0.035, 0.050$. In NLO, the best fit values of m for $F_2^p(x,t)$ are found to be $m = 0.575, 0.689, 0.508, 0.528$ in the said x-bins. Similarly, $m = 0.512$ for $F_2^n(x,t)$ and $m = 0.430, 0.543, 0.469, 0.443$ for $F_2^d(x,t)$ in the respective x-bins. A good agreement of our predicted result with NMC experiment data within moderate x and Q^2-range is obtained.

However, in Ref. [47] , eqns.(3.50) and (3.57) were used to study the non-singlet structure function $xF_3(x,t)$ using CCFR data (neutrino) where the exponent m were found to have x dependence and was parametrized by an interpolating function

$$H_{expt}^{NLO}(x) = 0.412 - 4.51x + 0.913(1-x)$$

for both large and small-x. For small-x, it is positive while for large-x, it is negative.

Table 3.1: Values of $H_{NLO}(x)$ at a few representative x-values.

x	$H_{NLO}(x)$
0.0175	0.337
0.025	0.320
0.035	0.298
0.050	0.264

The numerical values of $H(x)$ given in table-3.1 do not conform to the exponent obtained in our analysis. It implies that such function might be process dependent. However the estimated values of the exponent m is invariably positive in conformity with the expectation [46, 47] for small-x.

3.4 Conclusion

We have incorporated the Next-to-Leading order (NLO) effects to the proton, neutron and deuteron structure function $F_2^p(x,t)$, $F_2^n(x,t)$ and $F_2^d(x,t)$ in the more general approach [46, 47, 72, 73] as shown in eq.(3.48). The analysis indicates that m as defined in eq.(3.48) deviates significantly from unity and has x-dependence. Unlike the previous works [40, 83, 84], the present general approach reported in Ref. [46, 47, 71, 72] can well accommodate such features of the experiment.

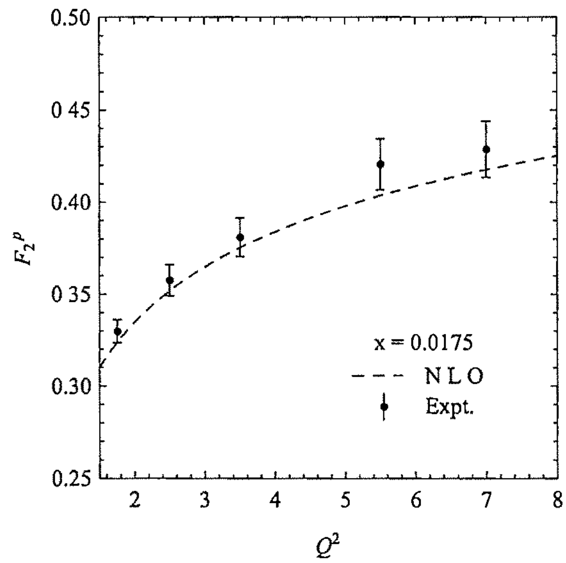
0.50
0 45
0.40
0 35
0.30
0.25
$F_2{}^p$
2
3
4
5
6
7
8
Q^2
x = 0.0175
N L O
Expt.

(a)

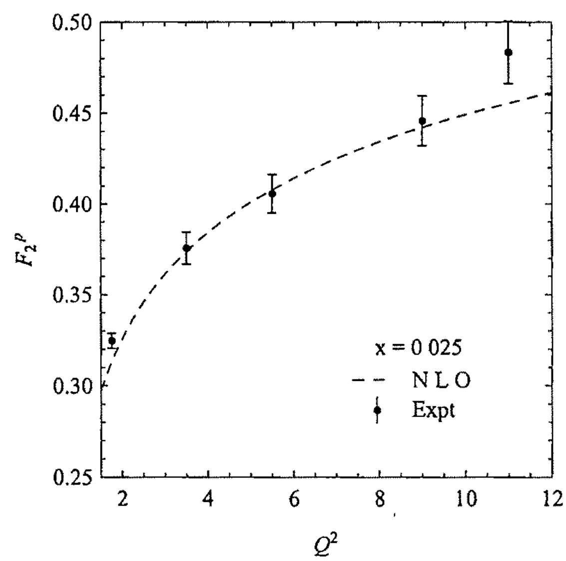
0.50
0.45
0.40
0.35
0.30
0.25
$F_2{}^p$
2
4
6
8
10
12
Q^2
x = 0 025
N L O
Expt

(b)

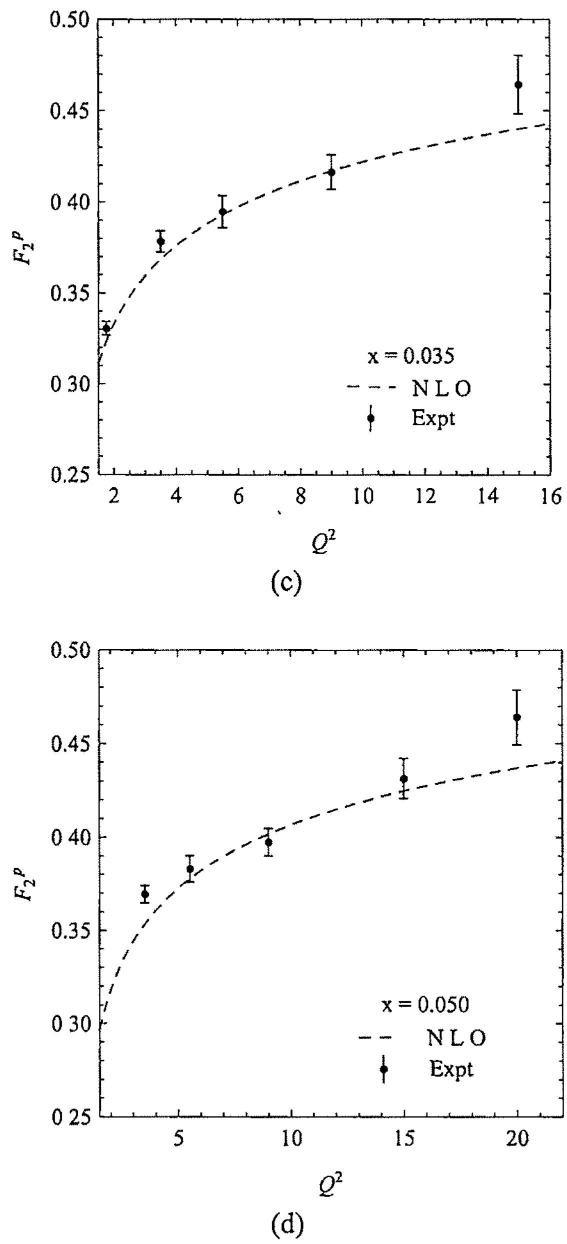

Figure 3.1: (a-d). Proton structure function $F_2^p(x,t)$ in NLO and its comparison with NMC experiment data.

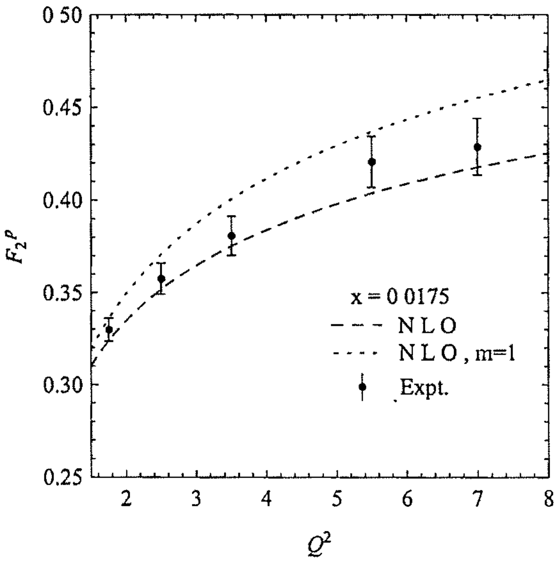

(a)

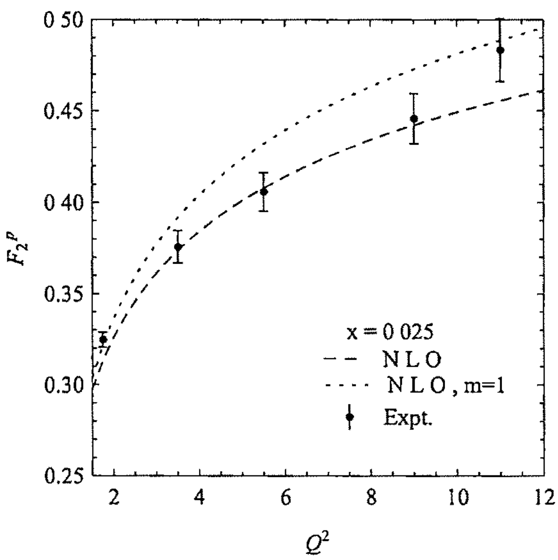

(b)

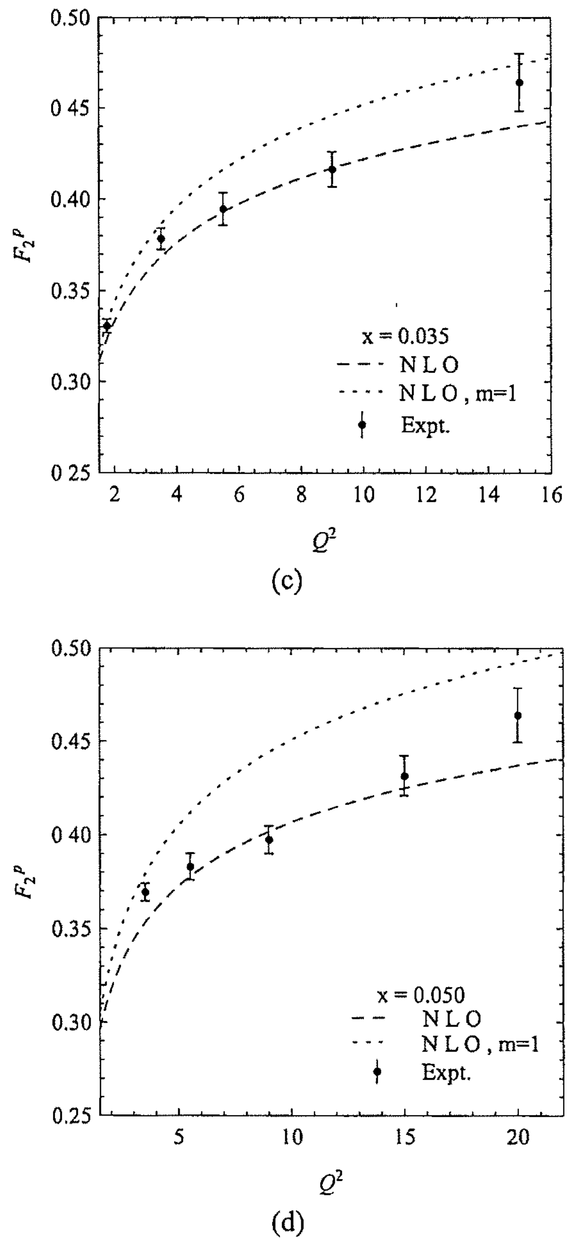

Figure 3.2: (a-d). Proton structure function $F_2^p(x,t)$ (best fit and $m = 1$) in NLO and its comparison with NMC experiment data.

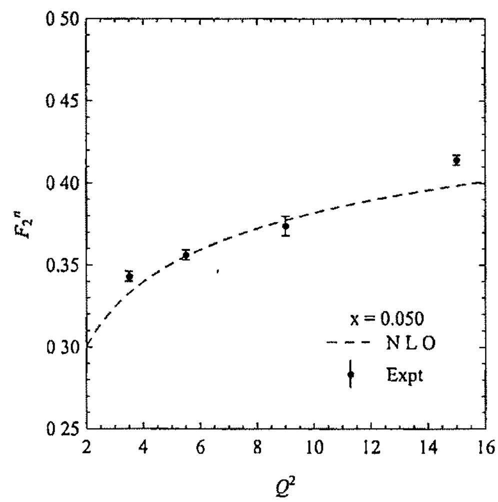

Figure 3.3: Neutron structure function $F_2^n(x, t)$ in NLO and its comparison with NMC experiment data.

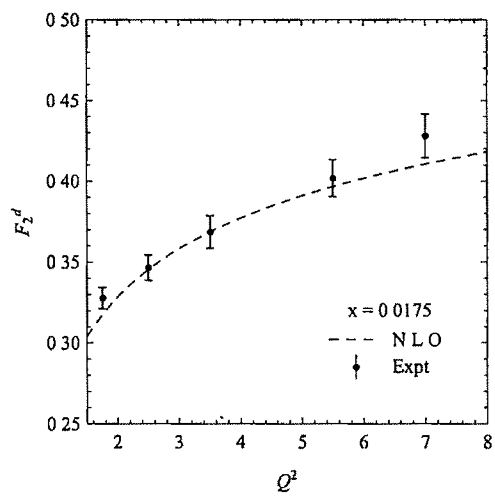
0 50
0 45
0 40
0 35
0 30
0 25
F_2^d
2 3 4 5 6 7 8
Q^2
x = 0 0175
NLO
Expt

(a)

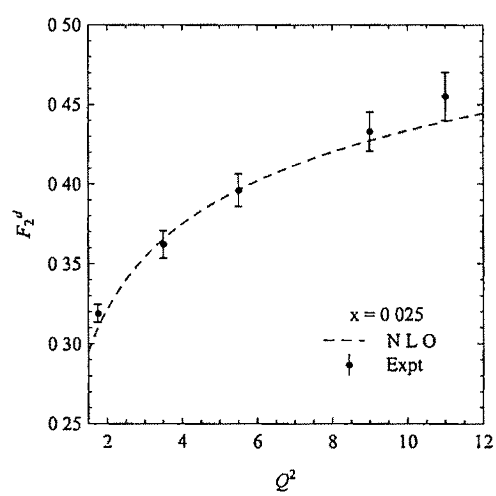
0 50
0 45
0 40
0 35
0 30
0 25
F_2^d
2 4 6 8 10 12
Q^2
x = 0 025
NLO
Expt

(b)

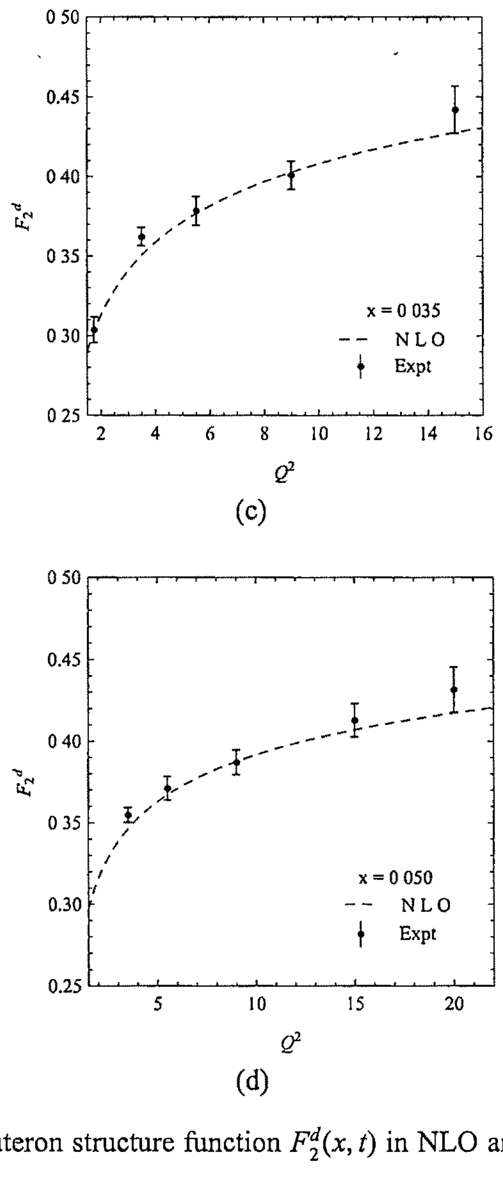

Figure 3.4: (a-d). Deuteron structure function $F_2^d(x,t)$ in NLO and its comparison with NMC experiment data.

Chapter 4

The proton, neutron and deuteron structure functions in the next-to-next-to-leading order (NNLO)

4.1 Introduction

In chapter 3, we solved DGLAP equations for both the singlet structure and the non-singlet structure functions in NLO and obtain expressions for proton, neutron and deuteron structure functions corrected upto NLO. The NNLO corrections should be included in order to arrive at quantitatively reliable predictions for hard processes at present and future high energy colliders. Recently, the three loop splitting functions are introduced with a good phenomenological success [79, 80, 86, 87, 88, 89]

In this chapter, we solve DGLAP equations for both the singlet structure and non-singlet structure functions in NNLO at small-x by using Lagrange's auxiliary method pursued in Ref. [46, 47, 72, 73] and obtain expressions for proton, neutron and deuteron structure functions corrected upto order NNLO and analyse NMC experiment data [74].

4.2 Formalism

DGLAP equations for singlet and non-singlet structure functions in NNLO have the standard form [79, 80, 86, 87, 88, 89] :

$$\frac{\partial F_2^S(x,t)}{\partial t} - \frac{\alpha_s(t)}{2\pi} I_1^S(x,t) - \left(\frac{\alpha_s(t)}{2\pi}\right)^2 I_2^S(x,t) - \left(\frac{\alpha_s(t)}{2\pi}\right)^3 I_3^S(x,t) = 0 \tag{4.1}$$

and

$$\frac{\partial F_2^{NS}(x,t)}{\partial t} - \frac{\alpha_s(t)}{2\pi} I_1^{NS}(x,t) - \left(\frac{\alpha_s(t)}{2\pi}\right)^2 I_2^{NS}(x,t) - \left(\frac{\alpha_s(t)}{2\pi}\right)^3 I_3^{NS}(x,t) = 0 \tag{4.2}$$

where,

$$I_3^S(x,t) = \int_x^1 \frac{dz}{z}\left[P_{qq}(z) F_2^S(\frac{x}{z},t) + P_{qg}(z) G(\frac{x}{z},t)\right] \tag{4.3}$$

$$I_3^{NS}(x,t) = \int_x^1 \frac{dz}{z}\left[P_{NS}^{(2)}(x) F_2^{NS}(\frac{x}{z},t)\right] \tag{4.4}$$

The explicit forms of higher order kernels in NNLO are [79, 80, 81]

$$P_{qq}(z) = P_{NS}^2(z) + P_{PS}^2(z) \tag{4.5}$$

$$\begin{aligned} P_{NS}^{(2)}(z) = {} & N_f\Big\{\big(L_1(-163.9x^{-1} - 7.208x) + 151.49 + 44.51 \\ & -43.12x^2 + 4.82x^3\big)(1-x) + L_0L_1(-173.1 + 46.18L_0) \\ & +178.04L_0 + 6.892L_0^2 + \frac{40}{27}(L_0^4 - 2L_0^3)\Big\} \end{aligned} \tag{4.6}$$

$$
\begin{aligned}
P_{PS}^{(2)}(z) \cong\ & (1-z)\Big\{N_f\Big(-5.926L_1^3 - 9.75L_1^2 - 72.11L_1 + 177.4 \\
& +392.9z - 101.4z^2 - 57.04L_0L_1 - 661.6L_0 + 131.4L_0^2 \\
& -\frac{400}{9}L_0^3 + \frac{160}{27}L_0^4 - 506.0z^{-1} - \frac{3584}{27}z^{-1}L_0\Big) \\
& +N_f^2\Big(1.778L_1^2 + 5.944L_1 + 100.1 - 125.2z \\
& +49.26z^2 - 12.59z^3 - 1.889L_0L_1 + 61.75L_0 \\
& +17.89L_0^2 + \frac{32}{27}L_0^3 + \frac{256}{81}z^{-1}\Big)\Big\}
\end{aligned}
\tag{4.7}
$$

$$
\begin{aligned}
P_{qg}(z) \cong\ & N_f\Big\{\frac{100}{27}L_1^4 - \frac{70}{9}L_1^3 - 120.5L_1^2 + 104.42L_1 + 2522 - 3316z \\
& +2126z^2 + L_0L_1(1823 - 25.22L_0) - 252.5zL_0^3 + 424.9L_0 \\
& +881.5L_0^2 - \frac{44}{3}L_0^3 + \frac{536}{27}L_0^4 - 1268.3z^{-1} - \frac{896}{3}z^{-1}L_0\Big\} \\
& +N_f^2\Big\{\frac{20}{27}L_1^3 + \frac{200}{27}L_1^2 - 5.496L_1 - 252.0 + 158.0z + 145.4z^2 \\
& -139.28z^3 - 98.07L_0^3 + 11.70L_0^3 - L_0L_1(53.09 + 80.616L_0) \\
& -254.0L_0 - 90.80L_0^2 - \frac{336}{27}L_0^3 + \frac{16}{9}L_0^4 + \frac{1112}{243}z^{-1}\Big\}
\end{aligned}
\tag{4.8}
$$

other terms being introduced in chapter 3. The results used here are from direct x-space evolutions [79, 80, 81, 40].

Approaching in a similar way as in case of equations (3.27), (3.28) and (3.29) of chapter 3, eq.(4.1) and (4.2) take the forms :

$$
\begin{aligned}
\frac{\partial F_2^S(x,t)}{\partial t} - \frac{\alpha_s(t)}{2\pi}\left[A_1^S(x)F_2^S(x,t) + A_2^S(x)\frac{\partial F_2^S(x,t)}{\partial x}\right] & \\
-\left(\frac{\alpha_s(t)}{2\pi}\right)^2\left[B_1^S(x)F_2^S(x,t) + B_2^S(x)\frac{\partial F_2^S(x,t)}{\partial x}\right] & \\
-\left(\frac{\alpha_s(t)}{2\pi}\right)^3\left[C_1^S(x)F_2^S(x,t) + C_2^S(x)\frac{\partial F_2^S(x,t)}{\partial x}\right] &= 0
\end{aligned}
\tag{4.9}
$$

and

$$\frac{\partial F_2^{NS}(x,t)}{\partial t} - \frac{\alpha_s(t)}{2\pi}\left[A_1^{NS}(x)F_2^{NS}(x,t) + A_2^{NS}(x)\frac{\partial F_2^{NS}(x,t)}{\partial x}\right]$$
$$-\left(\frac{\alpha_s(t)}{2\pi}\right)^2\left[B_1^{NS}(x)F_2^{NS}(x,t) + B_2^{NS}(x)\frac{\partial F_2^{NS}(x,t)}{\partial x}\right]$$
$$-\left(\frac{\alpha_s(t)}{2\pi}\right)^3\left[C_1^{NS}(x)F_2^{NS}(x,t) + C_2^{NS}(x)\frac{\partial F_2^{NS}(x,t)}{\partial x}\right] = 0 \qquad (4.10)$$

where,

$$A_1^S(x) = \frac{2}{3}\{3 + 4ln(1-x)\} + \frac{4}{3}\int_x^1 \frac{z^2-1}{1-z}dz + N_f\int_x^1\left\{z^2 + (1-z)^2\right\}dz \qquad (4.11)$$

$$A_2^S(x) = \frac{4}{3}\int_x^1 x\sum_{l=1}^{\infty}u^l\frac{dz}{1-z} + N_f\int_x^1 k'\sum_{l=1}^{\infty}u^l\left\{z^2 + (1-z)^2\right\}dz \qquad (4.12)$$

$$B_1^S(x) = (1-x)\int_0^1 f(z)dz + \int_x^1 f(z)dz + \int_x^1 F_{qq}^S(z)dz + \int_x^1 k'F_{qg}^S(z)dz \qquad (4.13)$$

$$B_2^S(x) = \int_x^1 x\sum_{l=1}^{\infty}u^l f(z)dz + \int_x^1 x\sum_{l=1}^{\infty}u^l F_{qq}^S(z)dz + \int_x^1 xk'\sum_{l=1}^{\infty}u^l F_2^S(z)dz \qquad (4.14)$$

$$C_1^S(x) = \int_x^1 P_{qq}(z)\frac{dz}{z} + \int_x^1 k' P_{qg}(z)\frac{dz}{z} \tag{4.15}$$

$$C_2^S(x) = \int_x^1 x\sum_{l=1}^{\infty} u^l P_{qq}(z)\frac{dz}{z} + \int_x^1 k' x\sum_{l=1}^{\infty} u^l P_{qg}(z)\frac{dz}{z} \tag{4.16}$$

and,

$$A_1^{NS}(x) = 2x + x^2 + 4ln(1-x) \tag{4.17}$$

$$A_2^{NS}(x) = x - x^3 - 2xln(x) \tag{4.18}$$

$$B_1^{NS}(x) = x\int_0^1 f(z)dz - \int_0^x f(z)dz + \frac{4}{3}^{NS} N_f \int_x^1 F_{qq}(z)dz \tag{4.19}$$

$$B_2^{NS}(x) = x\int_x^1 \left[f(z) + \frac{4}{3}N_f F_{qg}^S(z)\right]\frac{1-z}{z}dz \tag{4.20}$$

$$\begin{aligned} C_1^{NS}(x) = N_f \int_0^{1-x} \frac{dz}{1-z}\Big[& \{ln(z)(-163.9(1-z)^{-1} - 7.208(1-z)) \\ & +151.49 + 44.51(1-z) - 43.12(1-z)^2 + 4.82(1-z)^3\}z \\ & +\{ln(z)ln(1-z)(-173.1 + 46.18ln(1-z)) + 178.04ln(1-z) \\ & +6.892ln^2(1-z) + \frac{40}{27}\left(ln^4(1-z) - 2ln^3(1-z)\right)\}\Big] \end{aligned} \tag{4.21}$$

$$
\begin{aligned}
C_2^{NS}(x) &= N_f\int_0^{1-x}\frac{xdz}{(1-z)^2}\Big[\{ln(z)(-163.9(1-z)^{-1}-7.208(1-z)) \\
&+151.49+44.51(1-z)-43.12(1-z)^2+4.82(1-z)^3\}z \\
&+\{ln(z)ln(1-z)(-173.1+46.18ln(1-z))+178.04ln(1-z) \\
&+6.892ln^2(1-z)+\frac{40}{27}\left(ln^4(1-z)-2ln^3(1-z)\right)\}\Big] \qquad (4.22)
\end{aligned}
$$

Eq.(4.9) and (4.10) can be written in the forms,

$$\frac{\partial F_2^S(x,t)}{\partial t}+L^S(x,t)\frac{\partial F_2^S(x,t)}{\partial x} = M^S(x,t)F_2^S(x,t) \qquad (4.23)$$

$$\frac{\partial F_2^{NS}(x,t)}{\partial t}+L^{NS}(x,t)\frac{\partial F_2^S(x,t)}{\partial x} = M^{NS}(x,t)F_2^{NS}(x,t) \qquad (4.24)$$

where,

$$
\begin{aligned}
L^{S,NS}(x,t) &= \frac{2}{\beta_0 t}\left[1-\frac{\beta_1}{\beta_0^2}\frac{ln(t)}{t}+\frac{1}{\beta_0^3 t}\left\{\frac{\beta_1^2}{\beta_0}(ln^2(t)-ln(t)-1)+\beta_2)\right\}\right] \\
&\times(A_2+T_0B_2+T_1C_2) \qquad (4.25)
\end{aligned}
$$

$$
\begin{aligned}
M^{S,NS}(x,t) &= \frac{2}{\beta_0 t}\left[1-\frac{\beta_1}{\beta_0^2}\frac{ln(t)}{t}+\frac{1}{\beta_0^3 t}\left\{\frac{\beta_1^2}{\beta_0}(ln^2(t)-ln(t)-1)+\beta_2)\right\}\right] \\
&\times(A_1+T_0B_1+T_1C_1) \qquad (4.26)
\end{aligned}
$$

with, $T(t)=\frac{\alpha_s(t)}{2\pi}$, where $T^2(t)$ and $T^3(t)$ are linearised through the ansatz : $T^2(t)=T_0T(t)$ and $T^3(t)=T_1T(t)$, where T_0 and T_1 are two suitable numerical parameters [47, 82, 40].

The general solution of eq.(4.23) or (4.24), which is frequently referred to as Lagrange's equation [44, 45], is obtained from the solutions of the equation

$$\frac{dx}{L^{S,NS}(x,t)} = \frac{dt}{1} = \frac{dF_2^{S,NS}(x,t)}{M^{S,NS}(x,t)F_2^{S,NS}(x,t)} \tag{4.27}$$

The general solution of eq.(4.23) or eq.(4.24) in NNLO is given by

$$F(U_{NNLO}^{S,NS}, V_{NNLO}^{S,NS}) = 0 \tag{4.28}$$

where, $F(U_{NNLO}^{S,NS}, V_{NNLO}^{S,NS})$ is an arbitrary function. $U_{NNLO}^{S,NS}(x,t,F_2^{S,NS}) = C_1$ and $V_{NNLO}^{S,NS}$ $(x,t,F_2^{S,NS}) = C_2$ are two independent solutions of eq.(4.27). Solving eq.(4.27), we obtain

$$U_{NNLO}^{S,NS}(x,t,F_2^{S,NS}) = t^{\left(1+\frac{3b^2+b}{t}\right)} e^{\left(\frac{4b^2+b^2\ln^2(t)+b-c}{t}\right)} \times exp\left\{\frac{1}{a}N^{S,NS}(x)\right\} \tag{4.29}$$

$$V_{NNLO}^{S,NS}(x,t,F_2^{S,NS}) = F_2^{S,NS}(x,t) \times exp\left\{N'^{S,NS}(x)\right\} \tag{4.30}$$

where,

$$N^{S,NS}(x) = \int \frac{dx}{A_2^{S,NS}(x) + T_0 B_2^{S,NS}(x) + T_1 C_2^{S,NS}(x)} \tag{4.31}$$

$$N'^{S,NS}(x) = \int \frac{A_1^{S,NS}(x) + T_0 B_1^{S,NS}(x) + T_1 C_1^{S,NS}(x)}{A_2^{S,NS}(x) + T_0 B_2^{S,NS}(x) + T_1 C_2^{S,NS}(x)} dx \tag{4.32}$$

and $c = \frac{\beta_2}{\beta_0^3}$; a & b being introduced in sec. 3.2.

The most general form of eq.(4.28) is given by [46, 47],

$$V^{S,NS}_{NNLO} = \alpha \left(U^{S,NS}_{NNLO}\right)^{n} + \beta \tag{4.33}$$

where α and β are two arbitrary constants and n is a real positive function of x and t which is to be determined through experimental parametrizations.

From equations (4.29), (4.30) and (4.33), for the singlet case,

$$\begin{aligned} F^{S}_{2NNLO}(x,t) &= \frac{1}{exp\left\{N'^{S}(x)\right\}}\left[\alpha t^{n\left(1+\frac{3b^2+b}{t}\right)} e^{n\left(\frac{4b^2+b^2 ln^2(t)+b-c}{t}\right)} \right. \\ &\quad \left. \times exp\left\{\frac{1}{a}N^{S}(x)\right\} + \beta\right] \end{aligned} \tag{4.34}$$

Using the initial condition [46, 47, 83, 84],

$$F^{S}_{2}(x,t)\Big|_{x=1} = 0 \tag{4.35}$$

at any t for all order, we obtain,

$$\beta = -\alpha t^{n\left(1+\frac{3b^2+b}{t}\right)} e^{n\left(\frac{4b^2+b^2 ln^2(t)+b-c}{t}\right)} \times exp\left\{\frac{1}{a}N^{S}(1)\right\} \tag{4.36}$$

Using eq.(4.36) in (4.34),

$$\begin{aligned} F^{S}_{2NNLO}(x,t) &= \frac{1}{exp\left\{N'^{S}(x)\right\}}\alpha t^{n\left(1+\frac{3b^2+b}{t}\right)} e^{n\left(\frac{4b^2+b^2 ln^2(t)+b-c}{t}\right)} \\ &\quad \times\left[exp\left\{\frac{1}{a}N^{S}(x)\right\} - exp\left\{\frac{1}{a}N^{S}(1)\right\}\right] \end{aligned} \tag{4.37}$$

Defining the input $F^S_{2NNLO}(x, t_0)$ as,

$$
\begin{aligned}
F^S_{2NNLO}(x, t_0) &= \frac{1}{exp\left\{N'^S(x)\right\}} \alpha t_0^{n\left(1+\frac{3b^2+b}{t_0}\right)} e^{n\left(\frac{4b^2+b^2 ln^2(t)+b-c}{t_0}\right)} \\
&\quad \times \left[exp\left\{\frac{1}{a} N^S(x)\right\} - exp\left\{\frac{1}{a} N^S(1)\right\} \right]
\end{aligned}
\tag{4.38}
$$

we finally get,

$$
\begin{aligned}
F^S_{2NNLO}(x, t) &= F^S_{2NNLO}(x, t_0) \left\{ \frac{t^{n\left(1+\frac{3b^2+b}{t}\right)}}{t_0^{n\left(1+\frac{3b^2+b}{t_0}\right)}} \right\} \\
&\quad \times e^{n\left\{b^2\left(\frac{ln^2(t)}{t} - \frac{ln^2(t_0)}{t_0}\right) + \left(4b^2+b-c\right)\left(\frac{1}{t}-\frac{1}{t_0}\right)\right\}}
\end{aligned}
\tag{4.39}
$$

Proceeding exactly in the similar way for the non-singlet case, we find,

$$
\begin{aligned}
F^{NS}_{2NNLO}(x, t) &= F^{NS}_{2NNLO}(x, t_0) \left\{ \frac{t^{n\left(1+\frac{3b^2+b}{t}\right)}}{t_0^{n\left(1+\frac{3b^2+b}{t_0}\right)}} \right\} \\
&\quad \times e^{n\left\{b^2\left(\frac{ln^2(t)}{t} - \frac{ln^2(t_0)}{t_0}\right) + \left(4b^2+b-c\right)\left(\frac{1}{t}-\frac{1}{t_0}\right)\right\}}
\end{aligned}
\tag{4.40}
$$

Equations (4.39) and (4.40) represent the solutions for singlet and non-singlet structure functions in NNLO which are more general than that in Ref. [40].

The proton, neutron and deuteron spin-independent structure functions in terms of singlet and non-singlet structure functions can be given by [53]

$$F_2^p(x,t) = \frac{5}{18}F_2^S(x,t) + \frac{3}{18}F_2^{NS}(x,t) \tag{4.41}$$

$$F_2^n(x,t) = \frac{5}{18}F_2^S(x,t) - \frac{3}{18}F_2^{NS}(x,t) \tag{4.42}$$

$$F_2^d(x,t) = \frac{5}{9}F_2^S(x,t) \tag{4.43}$$

Use of equations (4.39) and (4.40) in equations (4.41), (4.42) and (4.43) give

$$F^p_{2NNLO}(x,t) = \left\{\frac{5}{18}F^S_{2NNLO}(x,t_0) + \frac{3}{18}F^{NS}_{2NNLO}(x,t_0)\right\}\left\{\frac{t^{n\left(1+\frac{3b^2+b}{t}\right)}}{t_0^{n\left(1+\frac{3b^2+b}{t_0}\right)}}\right\} \times e^{n\left\{b^2\left(\frac{ln^2(t)}{t}-\frac{ln^2(t_0)}{t_0}\right)+(4b^2+b-c)\left(\frac{1}{t}-\frac{1}{t_0}\right)\right\}} \tag{4.44}$$

$$F^n_{2NNLO}(x,t) = \left\{\frac{5}{18}F^S_{2NNLO}(x,t_0) - \frac{3}{18}F^{NS}_{2NNLO}(x,t_0)\right\}\left\{\frac{t^{n\left(1+\frac{3b^2+b}{t}\right)}}{t_0^{n\left(1+\frac{3b^2+b}{t_0}\right)}}\right\} \times e^{n\left\{b^2\left(\frac{ln^2(t)}{t}-\frac{ln^2(t_0)}{t_0}\right)+(4b^2+b-c)\left(\frac{1}{t}-\frac{1}{t_0}\right)\right\}} \tag{4.45}$$

$$F^d_{2NNLO}(x,t) = \left\{\frac{5}{9}F^S_{2NNLO}(x,t_0)\right\}\left\{\frac{t^{n\left(1+\frac{3b^2+b}{t}\right)}}{t_0^{n\left(1+\frac{3b^2+b}{t_0}\right)}}\right\} \times e^{n\left\{b^2\left(\frac{ln^2(t)}{t}-\frac{ln^2(t_0)}{t_0}\right)+(4b^2+b-c)\left(\frac{1}{t}-\frac{1}{t_0}\right)\right\}} \tag{4.46}$$

Equations (4.44), (4.45) and (4.46) are our predicted results for proton, neutron and deuteron structure functions in NNLO.

The structure function for helium nucleus can also be studied with the present formalism. If helium nucleus is considered to be made up of free nucleons (a system of 2 protons and 2 neutrons) as in case of deuteron, then its structure function can be written as

$$\begin{aligned} F_2^{He_2^4}(x,t) &= 2\left(F_2^p(x,t)+F_2^n(x,t)\right) \\ &= 2\times\frac{5}{9}F_2^S(x,t) \\ &= 2\times F_2^d(x,t) \end{aligned} \tag{4.47}$$

4.3 Results and Discussion

We compare our predicted results for $F_2^p(x,t)$, $F_2^n(x,t)$ and $F_2^d(x,t)$ with NMC experiment data [74]. For quantitative analysis, we use MRST 2006 NNLO inputs [57, 85, 90] for $F_2^S(x,t_0)$ and $F_2^{NS}(x,t_0)$ with $Q_0^2 = 1\ GeV^2$, $N_f = 4$ and $\Lambda = 0.235\ GeV$ for NNLO.

Figure 4.1 (a-d) represent variation of $F_2^p(x,t)$ in NNLO with Q^2 at four different representative x-bins : $x = 0.0175, 0.025, 0.035, 0.050$. Figure 4.2 represent variation of $F_2^n(x,t)$ in NNLO with Q^2 at $x = 0.050$. Figure 4.3 (a-d) represent variation of $F_2^d(x,t)$ in NNLO with Q^2 at the representative x-bins : $x = 0.0175, 0.025, 0.035, 0.050$. The figures represent best fit graphs. The vertical error bars represent statistical uncertainties. In NNLO, the best fit values of n for $F_2^p(x,t)$ are found to be $n = 0.501, 0.605, 0.461, 0.541$ in the said x-bins. Similarly, $n = 0.536$ for $F_2^n(x,t)$ and $n = 0.393, 0.458, 0.410, 0.407$ for $F_2^d(x,t)$ in the respective x-bins. A good agreement of our predicted result with NMC experiment data within moderate x and Q^2-range is obtained. As in chapter 3 , it also conform to the expectation [46, 47] that the exponent n should be positive for small-x. Finally, figure 4.4 (a-i) represent a comparison of NLO and NNLO effects of $F_2^p(x,t)$, $F_2^n(x,t)$ and $F_2^d(x,t)$.

Fig.4.5 shows variation of $F_2^{He_2^4}(x,t)$ with Q^2 and its comparison with NMC experimental data [91]. The disagreement of the predicted results with NMC experimental data is due to the over simplified assumption for the helium structure function $F_2^{He_2^4}(x,t)$ (eq.4.47). It falls short of incorporating binding energy effects of nucleons in the nucleus.

The overall analysis shows that NNLO curves are steeper than NLO ones which is in conformity with theoretical expectation [92]. It also indicates preference of NNLO over NLO when compared with data.

4.4 Conclusion

We have incorporated the NNLO effects to the proton, neutron and deuteron structure function $F_2^p(x,t)$, $F_2^n(x,t)$ and $F_2^d(x,t)$ in the more general approach [47, 46, 72, 73] shown in eq.(4.33). The analysis indicates that n as defined in eq.(4.33) deviates significantly from unity and has x-dependence. As noted in chapter 3, unlike the previous works [83, 84, 40], the present general approach reported in Ref. [46, 47, 72, 71] can well accommodate such features of the experiment.

We have demonstrated that NNLO analysis is more suitable than LO and NLO analysis. From the theoretical point of view, our analysis has found new insight into the preferred choice of approximate method of solutions. We have found that once the DGLAP equation is transformed into partial differential equations in two variables x and t (eq.2.9: LO; eqs.3.28-3.29: NLO; eqs.4.9-4.10 :NNLO), the general Lagrange's method [44, 45] is the best choice to represent data more accurately than the special Lagrange's method used earlier [46, 47].

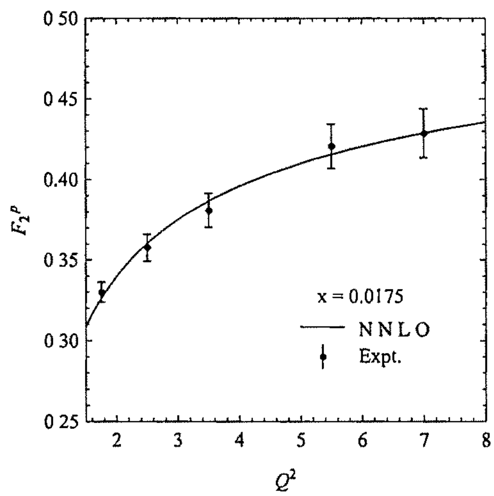

0 50
0 45
0.40
0 35
0 30
0 25
2
3
4
5
6
7
8
F_2^p
Q^2
x = 0.0175
NNLO
Expt.

(a)

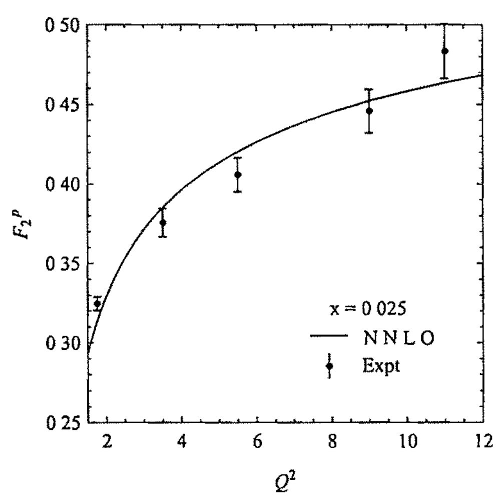

0 50
0 45
0 40
0 35
0 30
0 25
2
4
6
8
10
12
F_2^p
Q^2
x = 0 025
NNLO
Expt

(b)

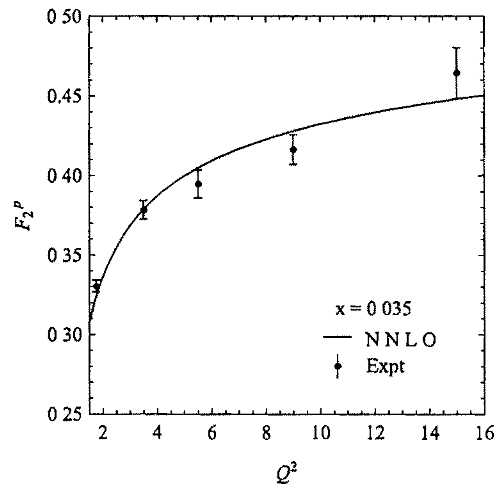

(c)

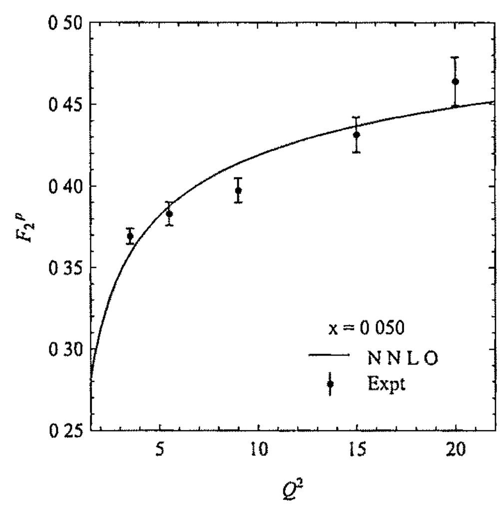

(d)

Figure 4.1: (a-d). Proton structure function $F_2^p(x,t)$ in NNLO and its comparison with NMC experiment data.

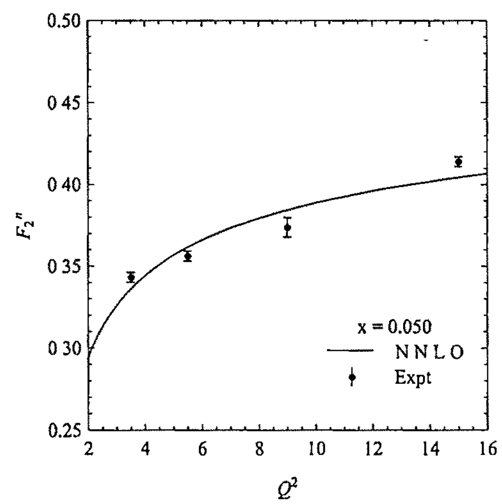

Figure 4.2: Neutron structure function $F_2^n(x, t)$ in NNLO and its comparison with NMC experiment data.

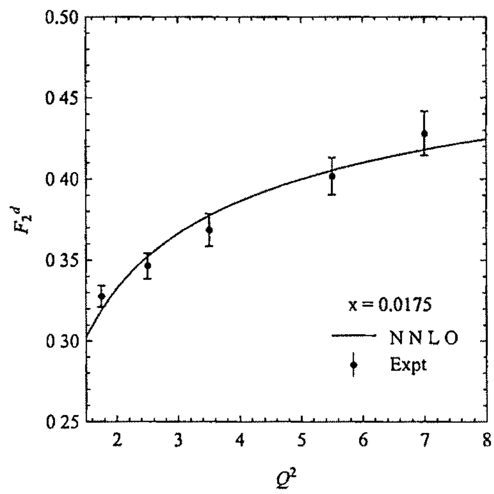
0.50
0 45
0 40
0 35
0 30
0 25
2 3 4 5 6 7 8
F_2^d
Q^2
x = 0.0175
NNLO
Expt

(a)

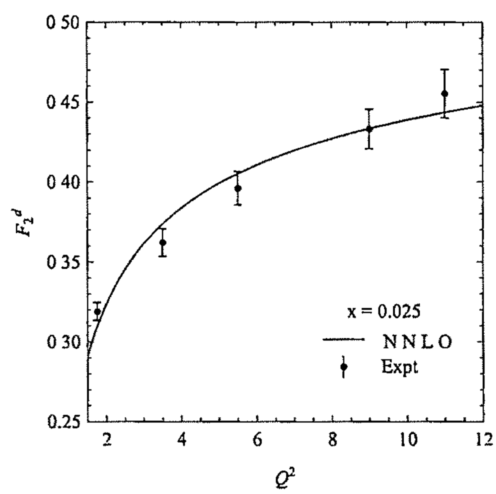
0 50
0 45
0 40
0 35
0 30
0.25
2 4 6 8 10 12
F_2^d
Q^2
x = 0.025
NNLO
Expt

(b)

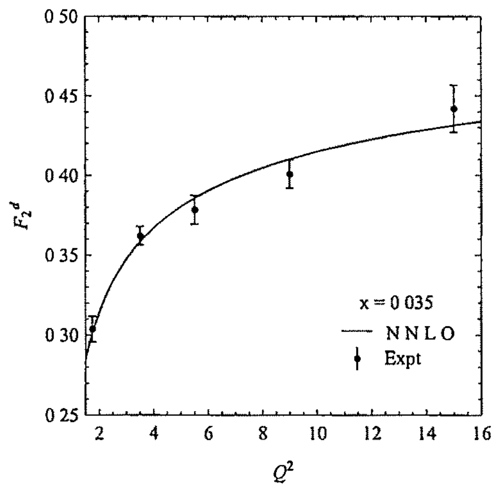

(c)

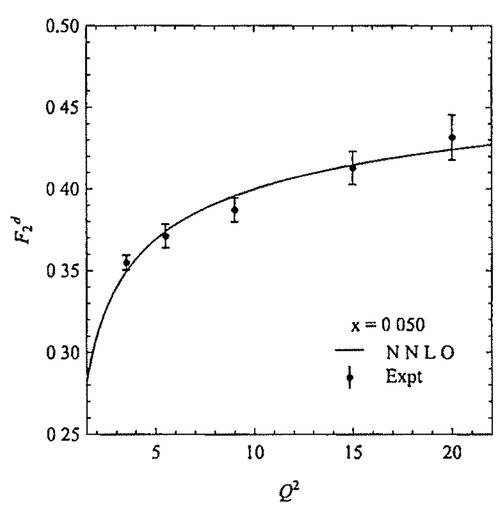

(d)

Figure 4.3: (a-d). Deuteron structure function $F_2^d(x, t)$ in NNLO and its comparison with NMC experiment data.

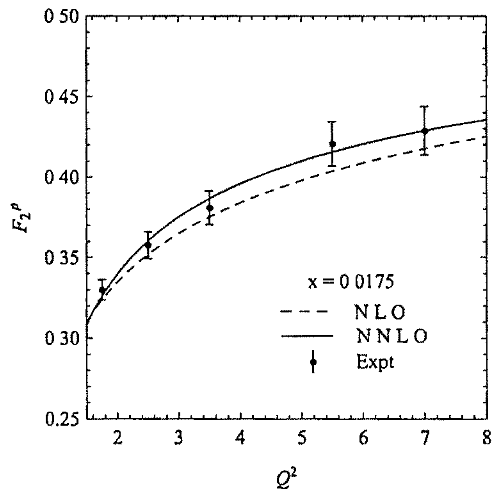

(a)

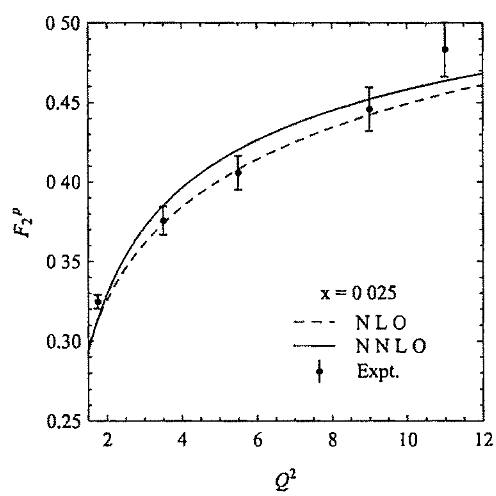

(b)

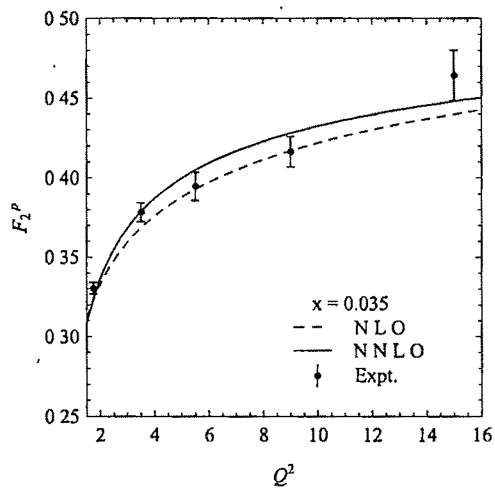
0 50
0 45
0 40
0 35
0 30
0 25
F_2^p
2 4 6 8 10 12 14 16
Q^2
x = 0.035
NLO
NNLO
Expt.

(c)

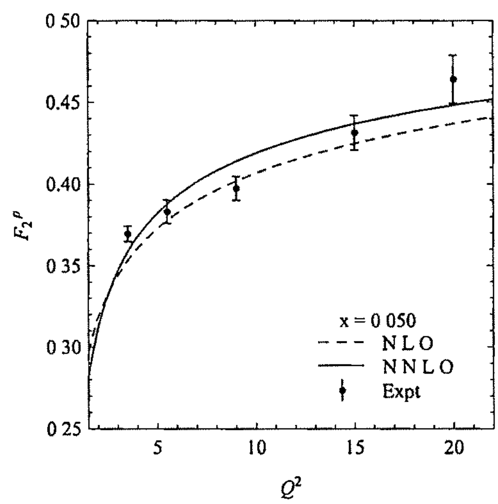
0 50
0.45
0.40
0 35
0 30
0 25
F_2^p
5 10 15 20
Q^2
x = 0 050
NLO
NNLO
Expt

(d)

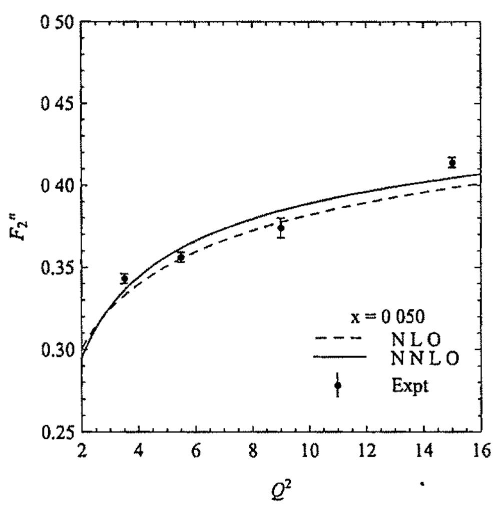
0 50
0 45
0 40
0.35
0.30
0.25
F_2^n
2
4
6
8
10
12
14
16
Q^2
x = 0 050
NLO
NNLO
Expt

(e)

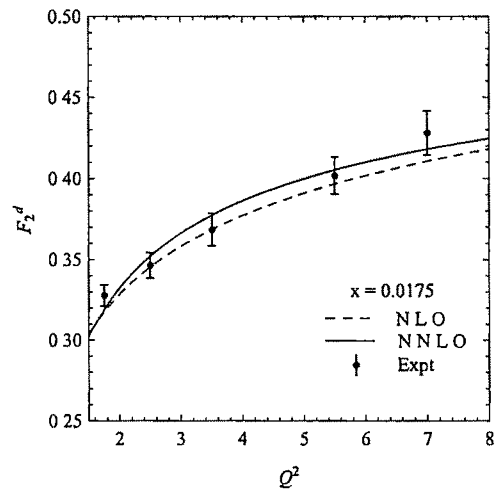

(f)

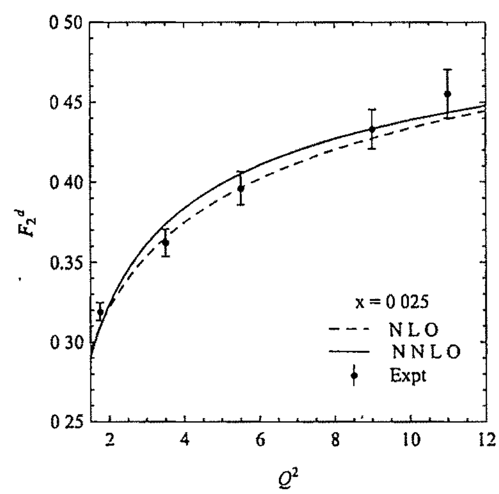

(g)

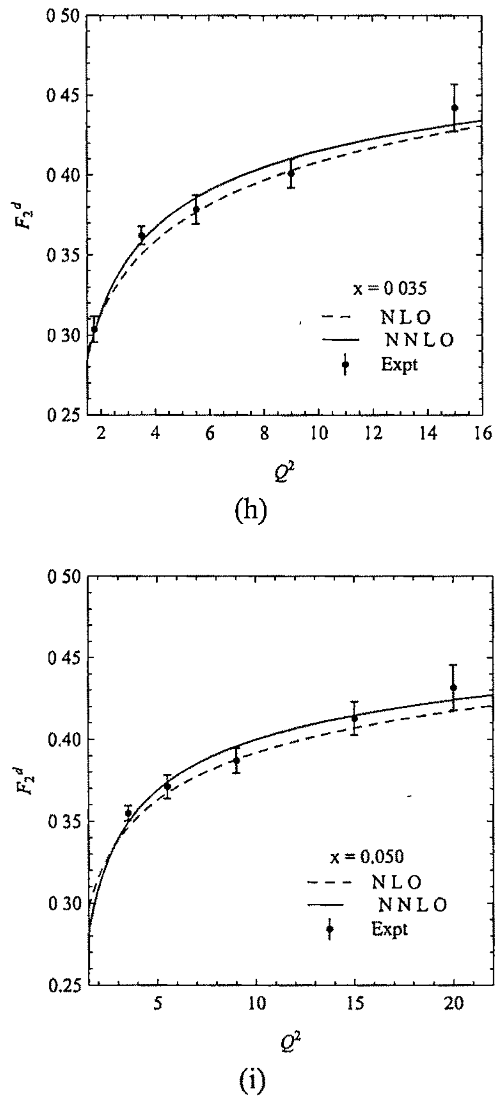

Figure 4.4: (a-i). Comparison of NLO and NNLO effects of $F_2^p(x,t)$, $F_2^n(x,t)$ and $F_2^d(x,t)$.

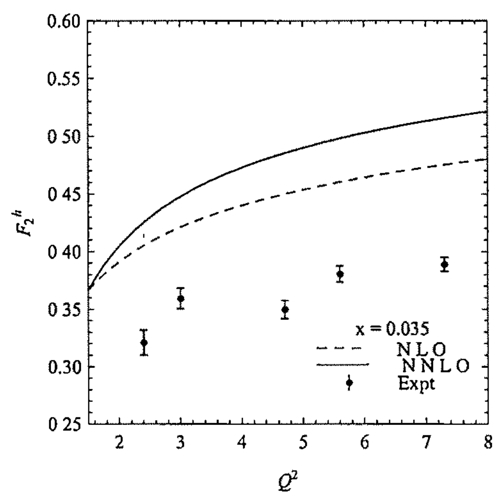

Figure 4.5: Comparison of NLO and NNLO effects of $F_2^{He_2^4}(x,t)$.

Chapter 5

The tensor structure function b_1^d of the deuteron in NLO and NNLO

5.1 Introduction

In chapters 3 and chapter 4 , we have solved DGLAP equations for the singlet structure function $F_2^S(x, Q^2)$ in NLO and NNLO at small-x by using Lagranges auxiliary method adopted in Ref. [46, 47]. In this chapter, we use these solutions in the expression of the tensor structure function $b_1^d(x, Q^2)$ of the deuteron and analyse HERMES experiment data.

5.2 Formalism

The expression of the tensor structure function $b_1^d(x, Q^2)$ of the deuteron within the Quark-Parton Model (QPM) is given by,

$$b_1^d = \frac{1}{2}\sum_q e_q^2[2q_\uparrow^0 - (q_\downarrow^1 + q_\downarrow^{-1})] \tag{5.1}$$

where $q_\uparrow^m$ ($q_\downarrow^m$) is the number density of quarks with spin-up (down) along the z-axis in a hadron (nucleus) with helicity m moving with infinite momentum along the z-axis. Reflection symmetry implies that $q_\uparrow^m = q_\downarrow^{-m}$. The sums run over quark and antiquark flavors q with a charge e_q in units of the elementary charge e. Both structure functions and quark number densities depend on the Bjorken variable x and the square of the four-momentum transfer $-Q^2$ by the virtual photon.

The tensor structure function b_1^d describes the difference in the quark distributions between the helicity-0, $q^0 = (q_\uparrow^0 + q_\downarrow^0) = 2q_\uparrow^0$, and the averaged non-zero helicity, $q^1 = (q_\uparrow^1 + q_\downarrow^1) = (q_\uparrow^1 + q_\downarrow^{-1})$, states of the deuteron [17, 93, 94]. Because b_1^d depends only on the spin averaged quark distributions $b_1^d = \frac{1}{2}\sum_q e_q^2[q^0 - q^1]$, its measurement does not require a polarized beam.

The deuteron, being a weakly bound state of spin-$1/2$ nucleons, b_1^d was initially predicted to be negligible at least at moderate and large-x [95, 96] following *e-d* DIS as single scattering. It was usually ignored in the extraction of polarization-dependent neutron structure functions g_1^n derived from deuteron and proton data which is in general not *a priori* justified [18]. Later, it was realised that b_1^d could raise to values which significantly differ from zero as $x \to 0$, and its magnitude could reach about 1% of the unpolarized structure function F_1^d, due to the same mechanism that leads to well-known effect of nuclear shadowing in unpolarized scattering [97]. This feature is described by coherent double-scattering models [98, 99, 100, 101, 102, 19].

The tensor structure function $b_1^d(x, Q^2)$ of the deuteron is extracted from the tensor asymmetry factor A_{ZZ}^d using the relations [103, 98],

$$b_1^d(x, Q^2) = -\frac{3}{2}A_{ZZ}^d F_1^d(x, Q^2) \tag{5.2}$$

$$F_1^d(x, Q^2) = \frac{(1 + \frac{Q^2}{\nu^2})}{2x(1 + R)} F_2^d(x, Q^2) \tag{5.3}$$

No contribution from the hitherto unmeasured double spin-flip structure function Δ [104] is considered here, being kinematically suppressed for a longitudinally polarized target [105]. Here, $R = \sigma_L/\sigma_T$ is the ratio of longitudinal to transverse photo-absorption cross section [103] and $\nu = Q^2/2Mx$ is the virtual-photon energy. The polarisation-averaged (unpolarized) structure functions $F_1^d(x, Q^2)$ and $F_2^d(x, Q^2)$ of the deuteron describes the quark distributions averaged over the target spin states.

The structure function $F_2^d(x, Q^2)$ is related to the proton structure function $F_2^p(x, Q^2)$ and the neutron structure function $F_2^n(x, Q^2)$ by the relation

$$\begin{aligned} F_2^d(x, Q^2) &= \frac{1}{2}F_2^p(x, Q^2)\left\{1 + \frac{F_2^n(x, Q^2)}{F_2^p(x, Q^2)}\right\} \\ &= \frac{1}{2}\left\{F_2^p(x, Q^2) + F_2^n(x, Q^2)\right\} \end{aligned} \tag{5.4}$$

Experimentally, $F_2^d(x, Q^2)$ is calculated using the parametrizations of the precisely measured $F_2^p(x, Q^2)$ and the $F_2^n(x, Q^2)/F_2^p(x, Q^2)$ ratio [106, 107].

Also, $F_2^p(x, Q^2)$ and $F_2^n(x, Q^2)$ can be expressed in terms of the singlet and non-singlet structure functions $F_2^S(x, Q^2)$ and $F_2^{NS}(x, Q^2)$ as [53]

$$F_2^p(x, Q^2) = \frac{5}{18} F_2^S(x, Q^2) + \frac{5}{18} F_2^{NS}(x, Q^2) \tag{5.5}$$

$$F_2^n(x, Q^2) = \frac{5}{18} F_2^S(x, Q^2) - \frac{3}{18} F_2^{NS}(x, Q^2) \tag{5.6}$$

Using eqns.(5.5) & (5.6) in eq.(5.4),

$$F_2^d(x, Q^2) = \frac{5}{18} F_2^S(x, Q^2) \tag{5.7}$$

Using eqns.(5.7) & (5.3) in eq.(5.2),

$$b_1^d(x, Q^2) = -\frac{5}{24} A_{ZZ}^d \frac{(1 + \frac{Q^2}{\nu^2})}{2x(1+R)} F_2^S(x, Q^2) \tag{5.8}$$

The solutions of DGLAP equations for the singlet structure function $F_2^S(x, Q^2)$ in NLO and NNLO at small-x (obtained in chapter 3 and 4) have the form

$$F_{2NLO}^S(x, t) = F_{2NLO}^S(x, t_0) \left\{ \frac{t^{m\left(1+\frac{b}{t}\right)}}{t_0^{m\left(1+\frac{b}{t_0}\right)}} \right\} \times e^{mb\left(\frac{1}{t}-\frac{1}{t_0}\right)} \tag{5.9}$$

and

$$F_{2NNLO}^S(x, t) = F_{2NNLO}^S(x, t_0) \left\{ \frac{t^{n\left(1+\frac{3b^2+b}{t}\right)}}{t_0^{n\left(1+\frac{3b^2+b}{t_0}\right)}} \right\} \times e^{n\left\{b^2\left(\frac{ln^2(t)}{t}-\frac{ln^2(t_0)}{t_0}\right)+\left(4b^2+b-c\right)\left(\frac{1}{t}-\frac{1}{t_0}\right)\right\}} \tag{5.10}$$

Using eqns.(5.9) & (5.10) in eq.(5.8), we obtain,

$$\begin{aligned} b_1^d(x,t) &= -\frac{5}{24}A_{ZZ}^d\frac{(1+\frac{e^t\Lambda^2}{\nu^2})}{2x(1+R)}F_{2NLO}^S(x,t_0)\left\{\frac{t^{m\left(1+\frac{b}{t}\right)}}{t_0^{m\left(1+\frac{b}{t_0}\right)}}\right\} \\ &\quad \times e^{mb\left(\frac{1}{t}-\frac{1}{t_0}\right)} \end{aligned} \tag{5.11}$$

and

$$\begin{aligned} b_1^d(x,t) &= -\frac{5}{24}A_{ZZ}^d\frac{(1+\frac{e^t\Lambda^2}{\nu^2})}{2x(1+R)}F_{2NNLO}^S(x,t_0)\left\{\frac{t^{n\left(1+\frac{3b^2+b}{t}\right)}}{t_0^{n\left(1+\frac{3b^2+b}{t_0}\right)}}\right\}. \\ &\quad \times e^{n\left\{b^2\left(\frac{ln^2(t)}{t}-\frac{ln^2(t_0)}{t_0}\right)+\left(4b^2+b-c\right)\left(\frac{1}{t}-\frac{1}{t_0}\right)\right\}} \end{aligned} \tag{5.12}$$

where, $t = \ln\left(\frac{Q^2}{\Lambda^2}\right)$, $b = \frac{\beta_1}{\beta_0^2}$, $c = \frac{\beta_2}{\beta_0^3}$ and β_0, β_1, β_2 are QCD β-functions introduced in chapter 3.

Equations(5.11) & (5.12) are the expressions for $b_1^d(x,t)$ in NLO and NNLO.

5.3 Results and Discussion

HERMES [18] has provided the first measurement of the deuteron tensor structure function b_1^d in the kinematic range $0.01 < x < 0.45$ and $0.5\ GeV^2 < Q^2 < 5\ GeV^2$. For quantitative analysis of b_1^d using eq.(5.11) and eq.(5.12), we use MRST 2004 NLO and MRST 2006 NNLO inputs [57, 85, 90] for the input distributions $F_2^S(x,t_0)$ with $Q_0^2 = 1\ GeV^2$, $N_f = 4$ and $\Lambda = 0.323\ GeV$, $0.235\ GeV$ for NLO and NNLO respectively. The value of R is taken 0.18 (SLAC) [108].

For comparison of b_1^d with HERMES experiment data [18], we have considered the x-range $0.032 < x < 0.248$ at the average $Q^2 = 2.037\ GeV^2$, to exclude two extreme data points: ($x = 0.012$, $Q^2 = 0.5\ GeV^2$) and ($x = 0.012$, $Q^2 = 0.5\ GeV^2$); the first one being at a very low Q^2 (less than Q_0^2) and the second one being at a large-x. This x-range of the experimental data points is not sufficiently small and hence the best fit value of m and n are found to be negative. Also we have considered the HERMES experiment average asymmetry $A_{ZZ}^{d(ex)} = 0.0074$ and a theoretical asymmetry $A_{ZZ}^{d(th)} = b_1^d / F_1^d = 0.01$ obtained by J. Edelmann, G. Piller and W. Weise in Ref. [98] following the Glauber-Gribov multiple scattering theory for coherent double scattering of the e-d process.

The figures (5.1 - 5.4) represent the behaviour of the tensor structure function $b_1^d(x, t)$ with x. Fig. 5.1 represents the variation of $b_1^d(x, t)$ with x in NLO and NNLO for experimental asymmetry $A_{ZZ}^{d(ex)} = 0.0074$ and the best fit values $m = -1.061$ & $n = -1.025$. Estimated negative values of the exponent m and n presumably suggest that the x-range used in HERMES experiment do not correspond to sufficiently small-x region where such exponents are to be positive [46, 47]. Fig. 5.2 represents the same for theoretical asymmetry $A_{ZZ}^{d(th)} = 0.01$. Fig. 5.3 represents the variation $b_1^d(x, t)$ with x in NLO for $A_{ZZ}^{d(ex)} = 0.0074$ & $A_{ZZ}^{d(th)} = 0.01$. Fig. 5.4 represents the same in NNLO.

The analysis shows that NNLO curves are more sensitive to the experimental data and also than the NLO curves at smaller-x specially, which is an expected general feature of higher order effects. Also, the analysis shows that both the experimental and theoretical asymmetries predict similar behaviour; the theoretical asymmetry showing slightly lesser b_1^d values at smaller-x values. The curves are in good agreement with the HERMES data.

The violation of the QPM sum rule [109, 110, 111, 112] for b_1^d is a signature of the mechanism that leads to the well known effect of nuclear shadowing in unpolarized scattering. We have calculated the first moment of b_1^d at NLO and NNLO using eqns.(5.11)

& (5.12) and obtain non-zero values:

$$\int_{x\to 0}^{x=1} b_1^d(x,t)dx\Big|_{Q^2=fixed}^{NLO,NNLO} \neq 0$$

The integrand has a singularity at $x = 0$ and hence we have considered the lower limit as $x \to 0$. For example, in the x-limits $[10^{-10}, 1]$, at $Q^2 = 2.037\ GeV^2$, the integral give values 1.523×10^{-2} and 1.223×10^{-2} at NLO and NNLO respectively. Similarly, in the x-range of our analysis, $[0.02, 0.30]$, at $Q^2 = 2.037\ GeV^2$, the integral give values 0.0139×10^{-2} and 0.0174×10^{-2} at NLO and NNLO respectively. These calculations show that our results in eqns.(5.11) & (5.12) also imply a violation of QPM sum rule.

5.4 Conclusion

The asymmetry factor A_{ZZ}^d present in the expressions (5.11) and (5.12) for b_1^d includes the polarization-dependent part while the polarization-averaged contribution comes through the unpolarized singlet structure function F_2^S. The b_1^d measurement can be used to reduce the systematic uncertainty on the measurement of the polarized neutron structure function g_1^d.

The analysis predicts that b_1^d is non-vanishing, found to raise with decreasing x and also QPM sum rule is found to be violated. This can be interpreted to originate from the mechanism that leads to nuclear shadowing in unpolarized scattering which has been established in recent experiments at FNAL [113, 114] and CERN [115, 116]. Also the predicted behaviour of b_1^d is in good agreement with the experiment within the limits of uncertainties.

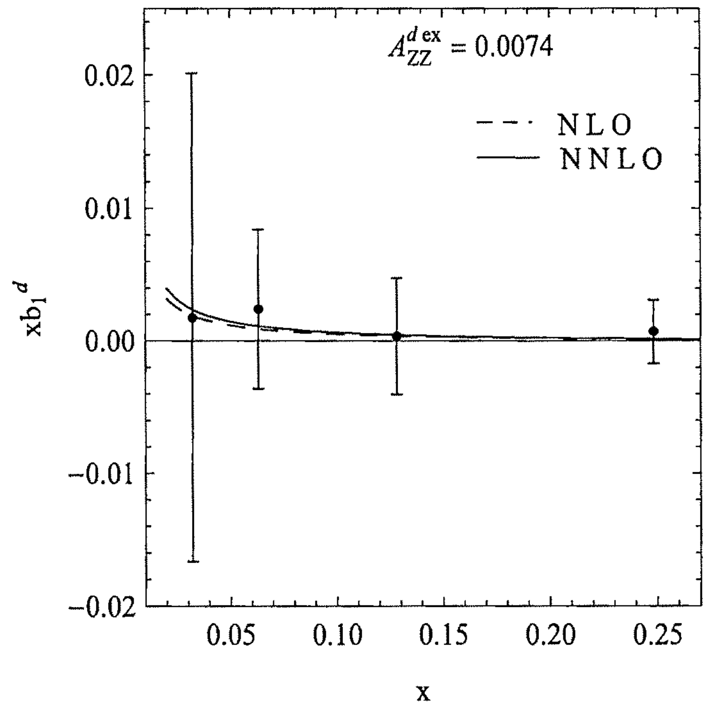

Figure 5.1: Variation of tensor structure function $b_1^d(x,t)$ of the deuteron with x in NLO and NNLO for experimental asymmetry $A_{ZZ}^{d(ex)} = 0.0074$ and its comparison with HERMES experiment data.

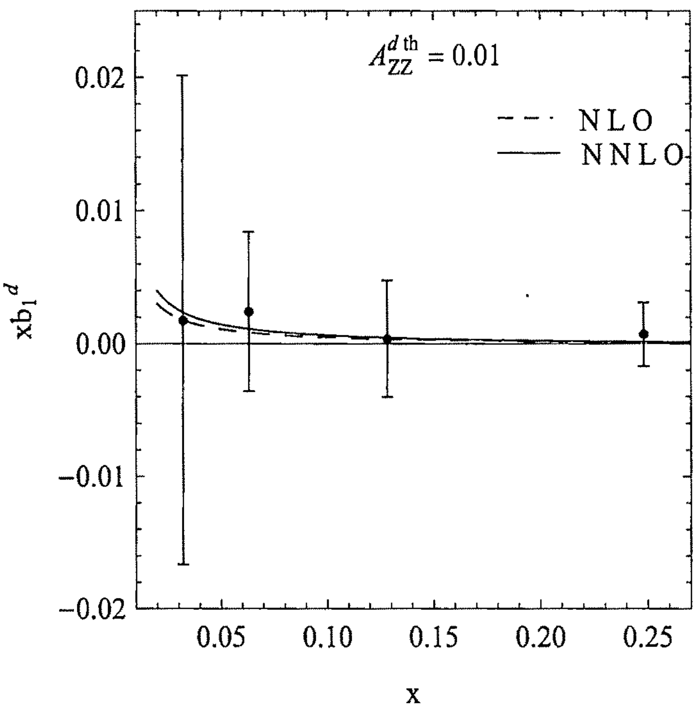

Figure 5.2: Variation of tensor structure function $b_1^d(x,t)$ of the deuteron with x in NLO and NNLO for theoretical asymmetry $A_{ZZ}^{d(th)} = 0.01$ and its comparison with HERMES experiment data.

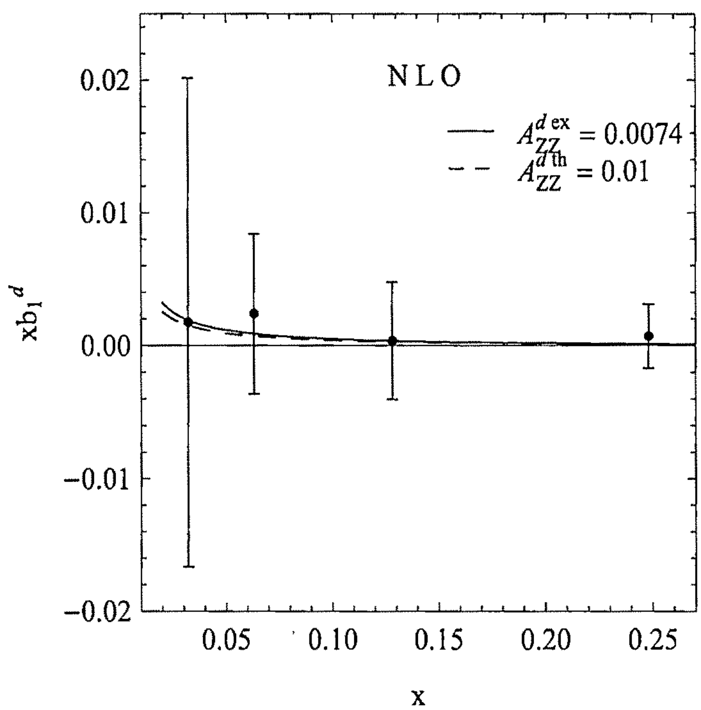

Figure 5.3: Variation of tensor structure function $b_1^d(x,t)$ of the deuteron with x in NLO for $A_{ZZ}^{d(ex)} = 0.0074$ & $A_{ZZ}^{d(th)} = 0.01$ and its comparison with HERMES experiment data.

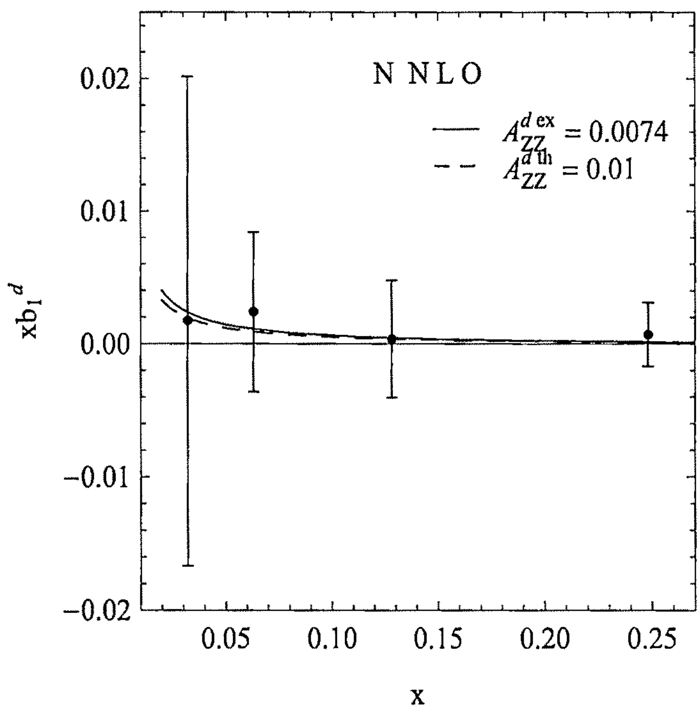

Figure 5.4: Variation of tensor structure function $b_1^d(x,t)$ of the deuteron with x in NNLO for $A_{ZZ}^{d(ex)} = 0.0074$ & $A_{ZZ}^{d(th)} = 0.01$ and its comparison with HERMES experiment data.

Chapter 6

The gluon-gluon interaction probability and high density QCD

6.1 Introduction

QCD at high parton density i.e. hdQCD deals both with fundamental theoretical issues, such as unitarity of strong interactions at high energies, and with the challenge of describing experimental data coming at present from RHIC and LHC and expected exciting physics of forthcoming experiments. Over the past few years much theoretical effort has been devoted towards the understanding of the growth of the total scattering cross sections with energy [21].

The picture of the small-x gluon distribution in a nucleon and large nuclei is similar, but not exactly same. Saturation or a maximum field strength comes about when many gluons are available to occupy the same region of phase space in a wave function. In a large nucleus the source producing those gluons is the large number of valence quarks. In a proton, the similar phenomena can occur at extremely small values of x, where the large rapidity $y = \ln(1/x)$, available for gluon evolution can lead to high gluon number densities. There is some evidence for it at low-Q^2 and small-x structure function data at HERA [117].

While at small-x valence quarks are of little importance and the behaviour of the sea is expected to follow that of the gluon distribution, which is not an observable quantity, is badly determined and represents one of the largest uncertainties in computation of cross sections both for moderate and large scales Q^2 [118]. In this situation and while waiting for new experimental data to come from lepton-ion, p-A or A-A colliders, the guidance from different theoretical models is of uttermost importance to perform safe extrapolations from the region where experimental data exist to those interesting for LHC studies [119] or physics beyond standard model.

With this aim, the present chapter deals with a quantitative study of probability of gluon-gluon interaction using currently available forms of gluon distributions. We also study numerically how it changes with rapidity $y = \ln(1/x)$, mass number A of nuclei and running of the strong coupling constant $\alpha_S(Q^2)$.

6.2 Formalism

The density of gluon distribution in a nucleon in high density limit is given by the solution of non-linear evolution equation which resums the power of the function [20, 67]

$$\kappa_g(x, Q^2) = \frac{3\pi\alpha_S(Q^2)}{2Q^2R^2} xg(x, Q^2) \tag{6.1}$$

which represents the probability of gluon-gluon interaction inside the parton cascade, also denoted by the packing factor of partons in a parton cascade. Here R_N is the size of the target (nucleon/nuclei) which can also be interpreted as the correlation radius between two gluons in a target at $x \approx 1$ [67].

In case of nucleons, eq.(6.1) is written as

$$\kappa_{g_N}(x, Q^2) = \frac{3\pi\alpha_S(Q^2)}{2Q^2R_N^2} xg_N(x, Q^2) \tag{6.2}$$

In case of nuclei, $R_A = R_N \times A^{1/3}$ and $xg_A = A \times xg_N$ and hence this function takes the form

$$\kappa_{g_A}(x, Q^2) = A^{1/3} \times \kappa_{g_N}(x, Q^2) \tag{6.3}$$

Therefore, for the case of an interaction with nuclei, we can reach a hdQCD region at smaller parton density than in a nucleon [67].

There are three regions of κ:

1. If κ is very small ($\kappa \ll 1$), we have a low density QCD in which the parton cascade can be perfectly described by the DGLAP evolution equations.

2. if $\kappa \lesssim 1$, we are in the transition region between low and high density QCD . In this region we can still use pQCD, but have to take into account the interaction between partons inside the parton cascade. $\kappa = 1$ determines the saturation momentum scale $Q_S(x)$ [20, 67] for a given x.

3. if $\kappa \geq 1$, we reach the region of high parton density QCD [67].

With the introduction of our solution eq.(2.27) for gluon distribution function [70, 71], eqns.(6.1) and (6.3) for nucleon and nuclei become,

$$\begin{aligned}
\kappa_{G_N}(x, t) = {} & \frac{3\pi\alpha_S(Q^2)}{2Q^2R_N^2} G(\tau) \times \exp\left[\frac{(24+12k)}{(11+16k)} x \left(\frac{t}{t_0}\right)^{\frac{1}{\beta_0}(11+16k)}\right. \\
& + \frac{(66+96k)}{\beta_0^2} \left\{\ln\left(\frac{t_0}{t}\right)\right\}^2 + \ln\left\{x\left(\frac{t}{t_0}\right)^{\frac{1}{\beta_0}(11+16k)}\right\} \\
& \left. \times \ln\left(\frac{t_0}{t}\right)^{\frac{12}{\beta_0}} + \ln\left(\frac{t_0}{t}\right)^{\frac{1}{\beta_0}\left(\frac{2}{3}N_f+11\right)} - \frac{(24+12k)}{(11+16k)} x\right]
\end{aligned} \tag{6.4}$$

and

$$\kappa_{G_A}(x,t) = A^{1/3} \times \kappa_{G_N}(x,t) \tag{6.5}$$

where τ is given by eq.(2.21) in chapter 2.

A similar form of $\kappa_{G_N}(x,t)$ and $\kappa_{G_A}(x,t)$ can also be obtained by using the solution (36) of Ref. [62] in eqns.(6.1) and (6.3),

$$\begin{aligned}\kappa^{II}_{G_N}(x,t) &= \frac{3\pi\alpha_S(Q^2)}{2Q^2R_N^2}G(\tau)x^{-\{1-(t_0/t)^{12/\beta_0}\}}\left(\frac{t_0}{t}\right)^{2N_f/3\beta_0}\\ &\quad exp\left[-\frac{11}{12}\left\{1-\left(\frac{t_0}{t}\right)^{12/\beta_0}\right\}\right]\end{aligned} \tag{6.6}$$

and

$$\kappa^{II}_{G_A}(x,t) = A^{1/3} \times \kappa_{G_N}(x,t) \tag{6.7}$$

where,

$$\tau = \left[\left(-\ln\frac{1}{x}+\frac{11}{12}\right)\frac{t_0}{t}\right)^{12/\beta_0} - \frac{11}{12}\right] \tag{6.8}$$

Introduction of standard DLLA (double leading logarithmic approximation) result for gluon distribution [65] in eqns.(6.1) and (6.3) give,

$$\kappa^{DLLA}_{G_N}(x,t) = \frac{3\pi\alpha_S(Q^2)}{2Q^2R_N^2}G(x,t_0)\times\exp\left[\left\{\frac{48}{\beta_0}\ln\left(\frac{t}{t_0}\right)\ln\left(\frac{1}{x}\right)\right\}^{1/2}\right] \tag{6.9}$$

$$\kappa^{DLLA}_{G_A}(x,t) = A^{1/3} \times \kappa^{DLLA}_{G_N}(x,t) \tag{6.10}$$

provided the gluon distribution is not singular at $t = t_0$.

Similarly, introduction of AGL gluon distribution at running $\alpha_S(t)$ (AGL) [20] and fixed $\alpha_S(t)$ (AGL-II) in eqns.(6.1) and (6.3) give,

$$\kappa_{G_N}^{AGL}(x,t) = \frac{t}{1+t}\frac{N_C\alpha_S(Q^2)}{\pi}\ln\left(\frac{1}{x}\right) \quad (6.11)$$

$$\kappa_{G_A}^{AGL}(x,t) = A^{1/3}\kappa_{G_N}^{AGL}(x,t) \quad (6.12)$$

$$\kappa_{G_N}^{AGL-II}(x,t) = \frac{N_C\alpha_S(Q^2)}{\pi}\ln\left(\frac{1}{x}\right) \quad (6.13)$$

$$\kappa_{G_A}^{AGL-II}(x,t) = A^{1/3}\kappa_{G_N}^{AGL-II}(x,t) \quad (6.14)$$

The density of gluons in the transverse plane is defined as [67]

$$\rho_N = \frac{xg(x,t)}{\pi R_N^2} \quad (6.15)$$

6.3 Result and Discussion

For quantitative analysis, we use $\alpha_S(t) = \frac{4\pi}{\beta_0 t}$, $R_N^2 = 5\,GeV^{-2}$; A=1 (nucleon), A=40 (Ca-nucleus), A=64 (Cu-nucleus) and A=197 (Au-nucleus).

6.3.1 Nucleon

Figure 6.1 (a-b) represent variation of our predicted k_{G_N} with $y = \ln(1/x)$ for nucleon ($A = 1$). This shows that k_{G_N} increases with increase in y (decrease in x) at $Q^2 = 20\ GeV^2$. Figure 6.2 (a-b) represent variation of our predicted ρ_N with y for nucleon. Analysis shows that k_G increases with increase in y as well as Q^2. Our predicted result shows faster increase than the others. We record a few numerical values of k_{G_N} and ρ_N at $Q^2 = 20\ GeV^2$ in Table 6.1.

Fig.6.3 (a-b) represent variation k_{G_N} with $\alpha_S(t)$ for nucleon at a fixed x (0.01 and

Table 6.1: Numerical values of κ_{G_N} and ρ at $x = 10^{-3}$ and $Q^2 = 20\ GeV^2$.

Models	κ_{G_N}	ρ
κ_{G_N} : $Thiswork$	0.398	1.074
κ_{G_N} : $DLLA$	1.114	3.006
κ_{G_N} : AGL	2.289	7.634
κ_{G_N} : $AGL-II$	3.299	8.901

0.001). Table 6.2 records numerical values of $\alpha_S(t)$ at a few representative Q^2.

Table 6.2: Numerical values of $\alpha_S(t)$ at different Q^2.

$Q^2\ GeV^2$	$\alpha_S(t)$
10	0.331
20	0.287
30	0.266

6.3.2 Nuclei

Fig.6.4(a-c) represent variation k_{G_A} with $y = \ln(1/x)$ at a fixed $Q^2 = 20\ GeV^2$, for different nuclei ($A = 40$; Ca-nucleus, $A = 64$; Cu-nucleus and $A = 197$; Au-nucleus). We record a few numerical values of k_{G_A} in Table 6.3.

A comparison of Table 6.1 and Table 6.3 shows that for a given x, the gluon-gluon interaction probability k_G for nuclei is amplified compared to that for nucleon, which indicates that hdQCD is achieved in nuclei at even smaller kinematic range or parton density.

Table 6.3: Numerical values of κ_{G_A} for different A $(x = 10^{-3})$.

Models	$A = 40$	$A = 64$	$A = 197$
κ_{G_A} : *Thiswork*	1.365	1.597	3.323
κ_{G_A} : *DLLA*	3.816	4.463	6.492
κ_{G_A} : *AGL*	9.686	11.329	16.480
κ_{G_A} : *AGL − II*	11.294	13.210	19.216

Fig.6.5 (a-d) represent variation k_{G_A} with A at a fixed $x = 0.01$ and 0.001 $Q^2 = 10$ and 20 GeV^2 for different nuclei ($A = 40$, $A = 64$ and $A = 197$). Fig.6.6 (a-c) represent variation k_{G_A} with $\alpha_S(t)$ at a fixed x (0.001) for $A = 40$, $A = 64$ and $A = 197$.

The analysis overall shows that the gluon-gluon interaction probability k_{G_N} and k_{G_A} increases with increase in $y = \ln(1/x)$, A ($A = 1$, $A = 40$, $A = 64$ and $A = 197$) and $\alpha_S(t)$ both for nucleon and nuclei at fixed Q^2 and/or at fixed x; the nature of increments being different in different models.

6.3.3 Neutron Star

Neutron stars are very compact objects with typical radii of 10 to 12 km and masses of 1 to 2 solar mass giving rise to extreme matter density as high as 4 to 5 times the nuclear matter density. These are the densest form of matter so far being directly observed in the universe [120, 121, 122, 123].

The composition and properties of neutron stars are still theoretically uncertain [120]. The present limits on the radius and mass of the neutron stars are more model dependent [123]. Due to the poor predictive power of the models used to calculate the equation of state (too many free parameters that can be adjusted to reproduce the observational data and due to the intrinsic difficulties of astrophysical measurements, i.e. data with large error bars), no farm conclusions can be drawn yet concerning the occurrence of a quark matter core in neutron stars [121].

The analysis on gluon-gluon interaction probability $k_G(x,t)$ inside parton cascade (eq.6.4; fig.6.1a-b) and transverse gluon density $\rho_N(x,t)$ (eq.6.15; fig.6.2a-b) show that both $k_G(x,t)$ and $\rho_N(x,t)$ increase with increase in rapidity y (decrease in x, i.e., approaching hdQCD regime). These facts reveal that as density goes higher, partons still remain bound in the nucleons.

To explain other features of neutron star like its non-relativistic equation of state inspite of its high density is beyond of the scope of the present work.

6.4 Conclusion

In this chapter, we have studied the gluon-gluon interaction probability k_{G_N} and k_{G_A} in nucleon and nuclei with rapidity $y = \ln(1/x)$, mass number of nuclei A and the running coupling constant $\alpha_S(t)$. A comparative analysis of $k_{G_N}(x,t)$ and $k_{G_A}(x,t)$ is made on the basis of currently available models of gluon distribution function. Also we have studied some features of neutron stars as a special case.

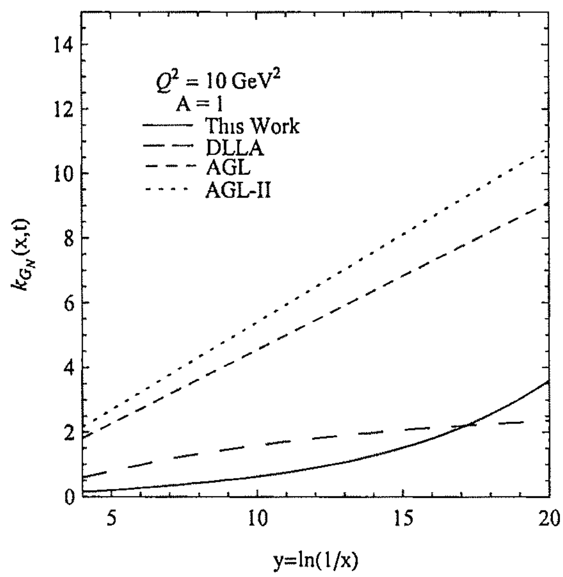

(a)

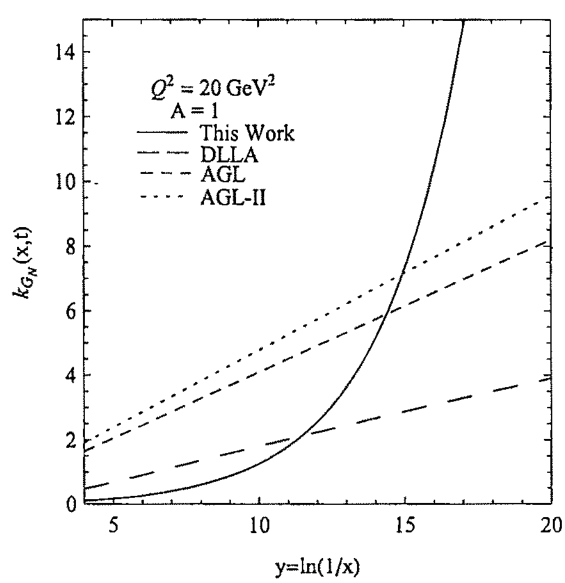

(b)

Figure 6.1: (a-b). Variation of predicted k_{G_N} with $y = \ln(1/x)$ for nucleon.

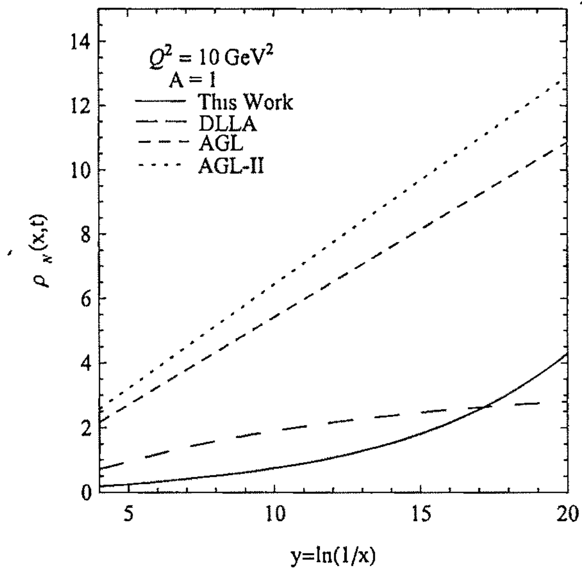

(a)

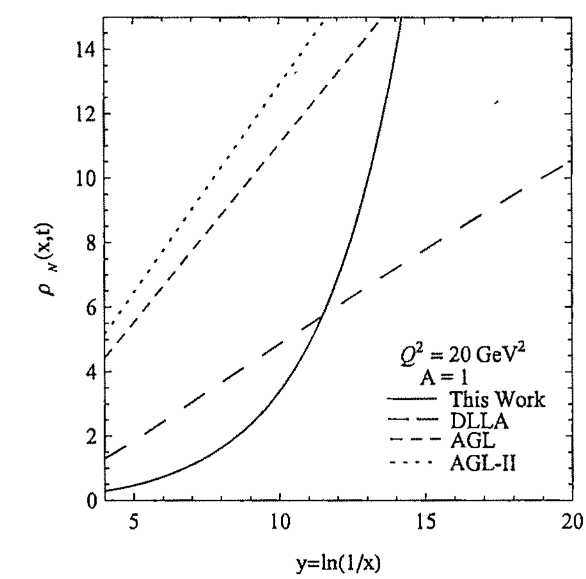

(b)

Figure 6.2: (a-b). Variation of predicted $\rho(x, t)$ with y for nucleon.

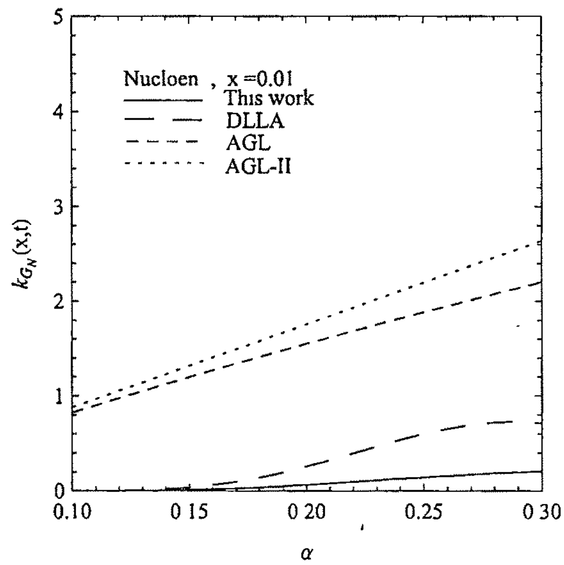

(a)

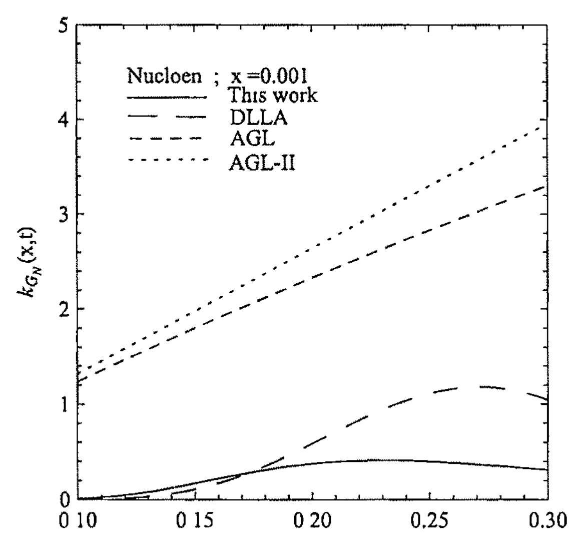

(b)

Figure 6.3: (a-b). Variation of predicted k_{G_N} with $\alpha_S(t)$ for nucleon.

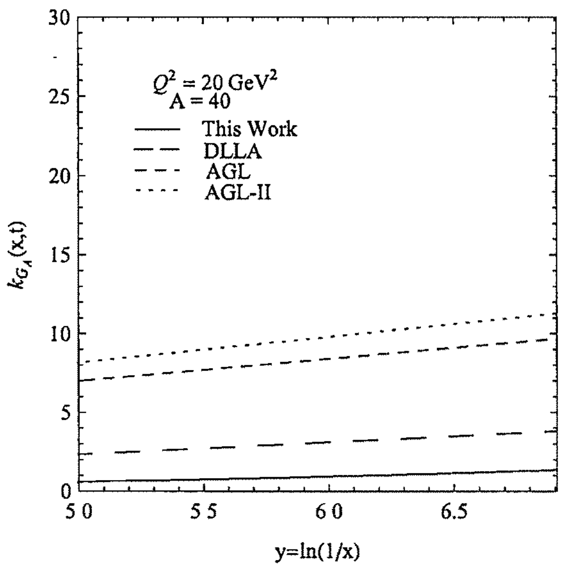

$Q^2 = 20\,\mathrm{GeV}^2$
A = 40
This Work
DLLA
AGL
AGL-II
$k_{G_A}(x,t)$
y=ln(1/x)

(a)

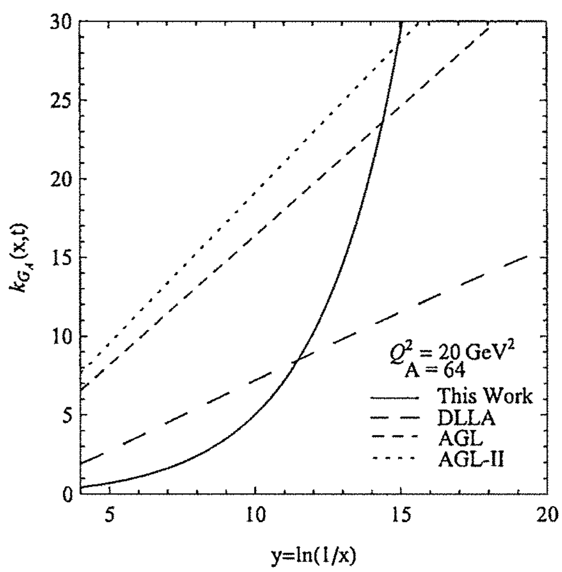

$Q^2 = 20\,\mathrm{GeV}^2$
A = 64
This Work
DLLA
AGL
AGL-II
$k_{G_A}(x,t)$
y=ln(1/x)

(b)

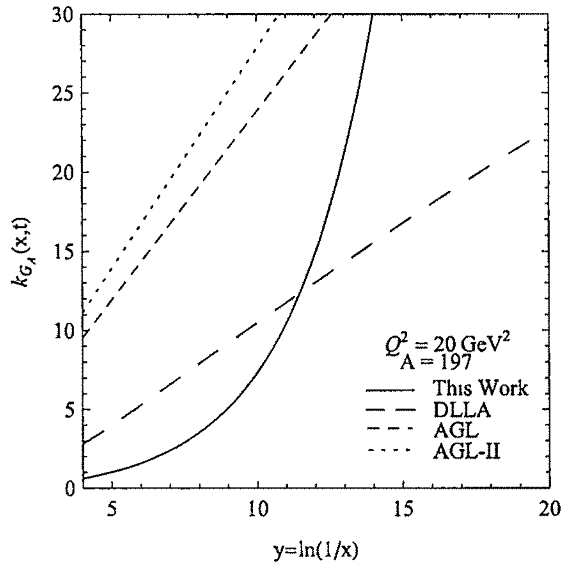

(c)

Figure 6.4: (a-c). Variation of predicted k_{G_A} with $y = \ln(1/x)$ for nuclei.

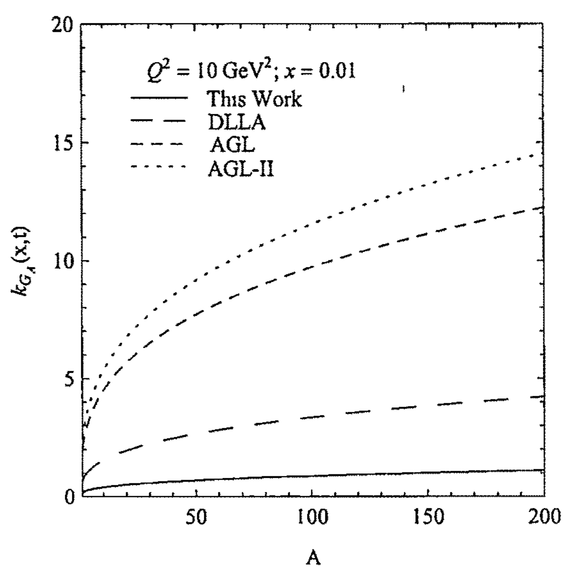

(a)

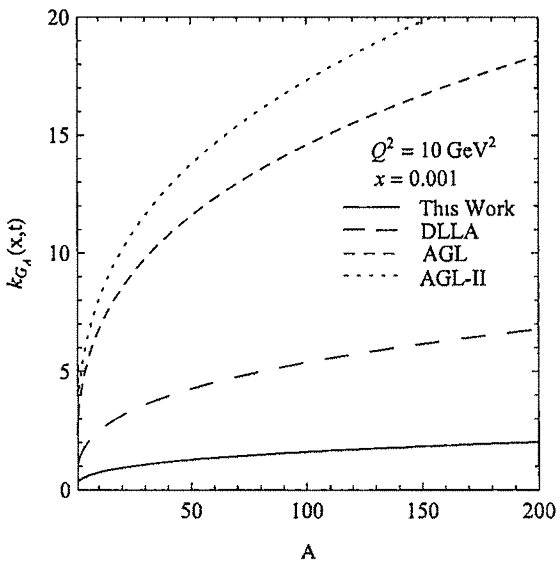
$Q^2 = 10\,\mathrm{GeV}^2$
$x = 0.001$
This Work
DLLA
AGL
AGL-II
$k_{G_A}(x,t)$
A
0
5
10
15
20
50
100
150
200

(b)

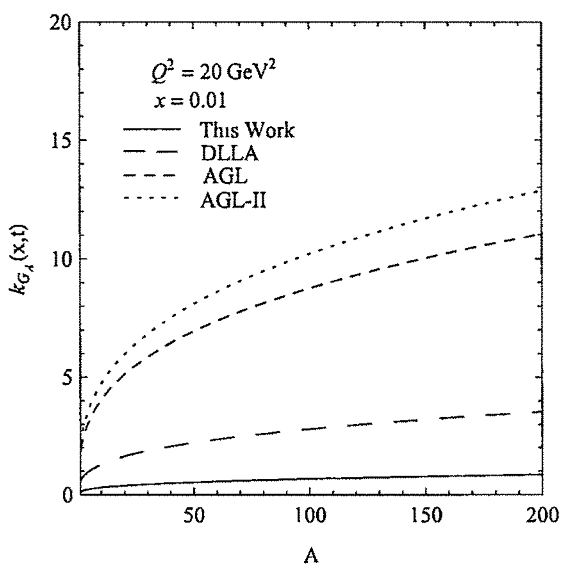
$Q^2 = 20\,\mathrm{GeV}^2$
$x = 0.01$
This Work
DLLA
AGL
AGL-II
$k_{G_A}(x,t)$
A
0
5
10
15
20
50
100
150
200

(c)

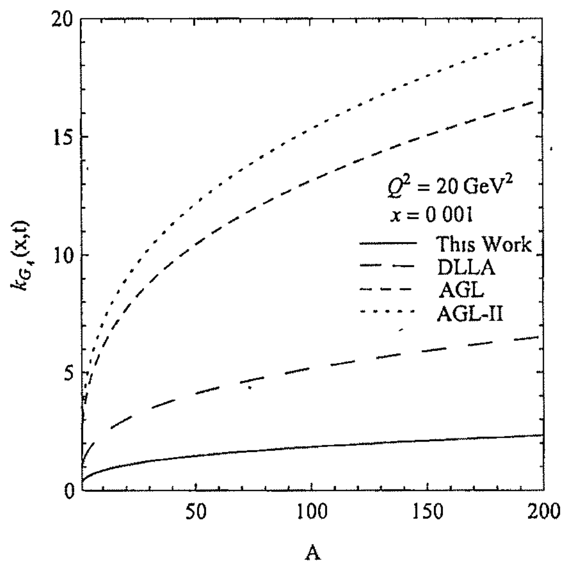

(d)

Figure 6.5: (a-d). Variation of predicted k_{G_A} with A for nuclei.

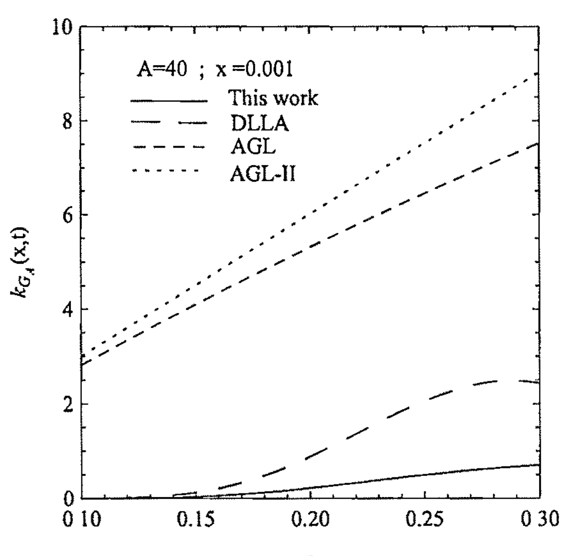

(a)

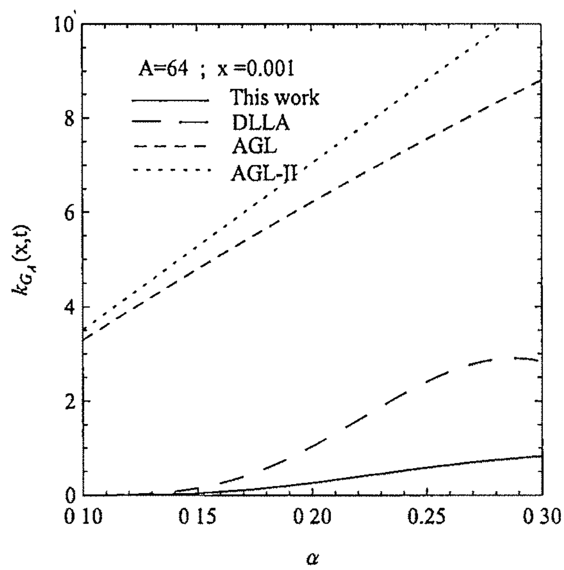

(b)

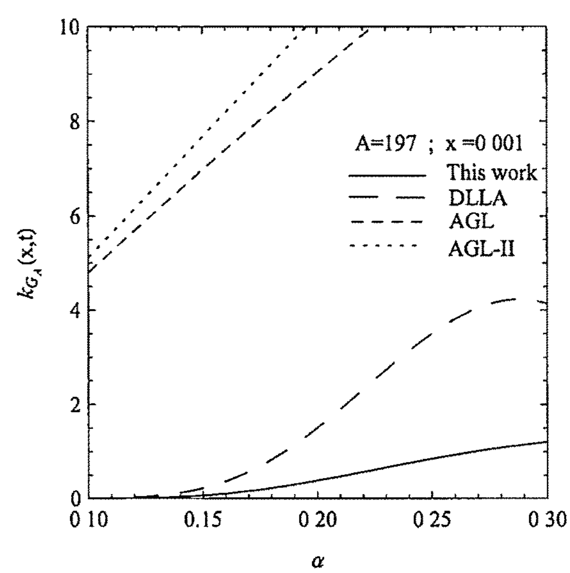

(c)

Figure 6.6: (a-c). Variation of predicted k_{G_A} with $\alpha_S(t)$ for nuclei.

Chapter 7

Conclusion and future scope

The present work (Thesis) devotes mainly to the higher order effects in structure functions and some aspects of high density QCD. The analysis is based on Dokshitzer, Gribov, Lipatov, Altarelli, Parisi (DGLAP) evolution equations [49, 50, 51, 52, 53] which are the basic tools to study the underlying dynamics of quarks and gluons.

Chapter 1 contains general introduction relevant to the present work. We have mentioned the important methods of solution of DGLAP evolution equations with brief outlines of the two used in this work.

In chapter 2, we solve DGLAP equations in LO [70] by using method of characteristics [42, 43] and obtain an analytical form of gluon distribution function $G(x, t)$ at small-x without any *ad-hoc* assumption of factorizability of x and t dependence of the gluon distribution function.

We compare our predicted result with MRST2001 LO exact results and with the parametrized experimental data from H1 2000 at different Q^2 values for $10^{-5} < x < 10^{-1}$. A comparison is also made with standard DLLA [65] result. The analysis shows that disagreement increases at lower Q^2 as wel as at higher Q^2 values. A good agreement of our predicted result with MRST2001LO exact results and H1 data within moderate x-

and Q^2-range is obtained.

In chapters 3 & 4, we have solved DGLAP equations for both the singlet structure and non-singlet structure functions in NLO and NNLO at small-x [72, 73] by using Lagrange's auxiliary method and obtain expressions for proton, neutron and deuteron structure functions corrected upto NLO and NNLO and analyse NMC data [74].

We have incorporated the NLO and NNLO effects to the proton, neutron and deuteron structure function $F_2^p(x,t)$, $F_2^n(x,t)$ and $F_2^d(x,t)$ in the more general approach [47, 46, 72, 73]. We compare our predicted result with MNC experiment data [74]. A good agreement of our predicted result with NMC experiment data is obtained.

In chapter 5, we obtain the expression of the tensor structure function $b_1^d(x,Q^2)$ of the deuteron in NLO and NNLO using the solutions of DGLAP equations for the singlet structure function $F_2^S(x,Q^2)$ obtained in chapters 3 & 4, and analyse HERMES experiment data [18].

HERMES has provided the first measurement of the deuteron tensor structure function b_1^d in the kinematic range $0.01 < x < 0.45$ and $0.5\ GeV^2 < Q^2 < 5\ GeV^2$. We analyse the predicted behaviour of the tensor structure function $b_1^d(x,t)$ in NLO and NNLO for both the average HERMES experimental and the theoretical asymmetry [98]. We have also checked the expected violation of QPM sum rule by the predicted result of b_1^d. The predicted behaviour of b_1^d is in good agreement with the experiment within the limits of uncertainties.

Chapter 6 deals with a quantitative study of gluon-gluon interaction probability $k_{G_N}(x,t)$ (which is also called packing factor) using currently available forms of gluon distributions.

Using the gluon distribution function obtained in chapter 2 as well as other forms of gluon distributions available in literature [70, 71, 65, 21], we obtain different expressions of κ_G for nucleon and nuclei and analyse the variation with rapidity $y = \ln(1/x)$, mass number A of nuclei and running coupling constant $\alpha_S(t)$.

Analysis shows that the gluon-gluon interaction probability k_G increases with increase in $y = \ln(1/x)$, A ($A = 1$, nucleon; $A = 40$, Ca-nucleus; $A = 64$, Cu-nucleus and $A = 197$, Au-nucleus) and $\alpha_S(t)$ both for nucleon and nuclei at fixed Q^2 and/or at fixed x.

Let us now conclude this chapter by mentioning a few topics for future research :

1. Analysis can be used to solve DGLAP equations for individual partons and hence PDFs for individual partons can be determined. Predicted results can also be compared with other experimental or parameterized data such as ALEKHIN, E665, HERA, RHIC, LHC etc.

2. The same analysis can be used for gluon distribution function in all available orders.

3. The entire analysis can be used to study polarized structure functions.

4. It is possible to analyse b_1^d using the solution of polarized DGLAP equations. Following the similar approaches, b_2^d can also be determined using Callen-Gross relation in both the polarized and unpolarized cases.

5. Study of unitarity or saturation correction in hdQCD processes needs modification to DGLAP evolution equations. The solution of this modified DGLAP evolution equations may possibly be dealt with the present approach followed in the thesis.

ADDENDA

List of Publications

A. Papers Published :

1. Tensor structure function $b_1^d(x,Q^2)$ of the deuteron at NLO and NNLO at small-x, (with D. K. Choudhury), *Euro. Phys. Journal C*, 72:2257 (2012).

2. An analysis of non-singlet structure function in next-to-next-to-leading order at small-x, (with D. K. Choudhury), *Indian Journal of Physics*, 85(2), 319-328 (2011).

3. An analysis of non-singlet structure function up to next-to-next-to-leading order at small-x , (with D. K. Choudhury), *International Journal of Pure & Applied Physics*, 6 : 3 (2010).

4. A numerical analysis of probability of gluon-gluon interaction $k_G(x,t)$ with improved solution of DGLAP equations (with D. K. Choudhury), *Assam University Journal of Science & Technology : Physical Sciences and Technology*, 6II : 112 (2010).

5. A Numerical Analysis of Variation of Gluon-Gluon Interaction Probability $k_{GA}(x,t)$ with nuclei A in High Density QCD, *Int. J. Phys. & App.*, 3(2) 189-192 (2011).

6. A Numerical Analysis of Variation of Transverse Gluon Density $\rho_N(x,t)$ with Rapidity y=ln(1/x) in High Density QCD, *Int. J. Phys. & App.*, 4 (2) 95-97 (2012).

B. Proceeding Paper Published :

1. Gluon distribution function and the method of characteristics , (with D. K. Choudhury), *Proceedings of the XVIII DAE-BRNS High Energy Physics Symposium*, edited by V. Singh, 18 : 112 (2008).

C. Paper Submitted :

1. An analysis of proton, neutron and deuteron structure function in next-to-next-to-leading order at small-x, (with D. K. Choudhury), submitted to *Indian Journal of Physics*.

D. Papers under Preparation :

1. A numerical analysis of gluon-gluon interaction probability and high density nuclear system such as neutron star.

Eur. Phys J C (2012) 72:2257
DOI 10 1140/epjc/s10052-012-2257-x

THE EUROPEAN PHYSICAL JOURNAL C

Regular Article - Theoretical Physics

Tensor structure function $b_1^d(x, Q^2)$ of the deuteron at NLO and NNLO at small-x

Saiful Islam[1,a], **D.K. Choudhury**[2]
[1]Department of Physics, R G.I., Assam, Guwahati, India
[2]Department of Physics, Gauhati University, Assam, Guwahati, India

Received 24 July 2012 / Revised 26 November 2012

Abstract The precision of the contemporary experimental data demands that the parton distribution functions (PDF's) should be corrected at least up to next-to-leading order (NLO) and preferably up to next-to-next-to-leading order (NNLO). A general form of tensor structure function $b_1^d(x, Q^2)$ of the deuteron at NLO and NNLO is obtained by using the solution of Dokshitzer, Gribov, Lipatov, Altarelli, Parisi (DGLAP) equation for singlet structure function at small-x Results are compared with HERA Experiment data.

1 Introduction

Deuteron, a spin-1 object, is described by eight structure functions [1], twice as many as required to describe e–p DIS. The tensor structure function $b_1^d(x, Q^2)$ of the deuteron is the most important one. It does not exist for spin-1/2 targets and vanishes in the absence of nuclear effects, i.e. if the deuteron simply consists of a proton and neutron at rest (a simple system of two particles without strong interactions to form a nucleus) [2, 3].

The expression of the tensor structure function $b_1^d(x, Q^2)$ of the deuteron within the Quark–Parton Model (QPM) is given by $b_1^d = \frac{1}{2}\sum_q e_q^2[2q_\uparrow^0 - (q_\downarrow^1 + q_\downarrow^{-1})]$, where $q_\uparrow^m$ ($q_\downarrow^m$) is the number density of quarks with spin-up (down) along the z-axis in a hadron (nucleus) with helicity m moving with infinite momentum along the z-axis. Reflection symmetry implies that $q_\uparrow^m = q_\downarrow^{-m}$. The sums run over quark and anti-quark flavors q with a charge e_q in units of the elementary charge e. Both structure functions and quark number densities depend on the Bjorken variable x and the square of the four-momentum transfer $-Q^2$ by the virtual photon.

The tensor structure function b_1^d describes the difference in the quark distributions between the helicity-0, $q^0 = (q_\uparrow^0 + q_\downarrow^0) = 2q_\uparrow^0$, and the averaged non-zero helicity, $q^1 = (q_\uparrow^1 + q_\downarrow^1) = (q_\uparrow^1 + q_\downarrow^{-1})$, states of the deuteron [1, 4, 5] Because b_1^d depends only on the spin averaged quark distributions $b_1^d = \frac{1}{2}\sum_q e_q^2[q^0 - q^1]$, its measurement does not require a polarized beam.

The deuteron, being a weakly bound state of spin-1/2 nucleons, b_1^d was initially predicted to be negligible at least at moderate and large-x [6, 7] following e–d DIS as single scattering. It was usually ignored in the extraction of polarization-dependent neutron structure functions g_1^n derived from deuteron and proton data, which is in general not a priori justified [2]. Later, it was realised that b_1^d could raise to values which significantly differ from zero as $x \to 0$, and its magnitude could reach about 1 % of the unpolarized structure function F_1^d, due to the same mechanism that leads to well-known effect of nuclear shadowing in unpolarized scattering [8]. This feature is described by coherent double-scattering models [3, 9–11].

2 Formalism

The tensor structure function $b_1^d(x, Q^2)$ of the deuteron is extracted from the tensor asymmetry factor A_{ZZ}^d using the relations [9, 12],

$$b_1^d(x, Q^2) = -\frac{3}{2}A_{ZZ}^d F_1^d(x, Q^2) \qquad (1)$$

$$F_1^d(x, Q^2) = \frac{(1 + \frac{Q^2}{\nu^2})}{2x(1 + R)} F_2^d(x, Q^2) \qquad (2)$$

No contribution from the hitherto unmeasured double spin-flip structure function Δ [13] is considered here, being kinematically suppressed for a longitudinally polarized target [14]. Here, $R = \sigma_L/\sigma_T$ is the ratio of longitudinal to transverse photo-absorption cross section [12] and $\nu = Q^2/2Mx$ is the virtual-photon energy. The polarization-averaged (unpolarized) structure functions $F_1^d(x, Q^2)$ and

[a] e-mail. s.phys res@gmail.com

Published online: 21 December 2012

$F_2^d(x, Q^2)$ of the deuteron describes the quark distributions averaged over the target spin states.

The structure function $F_2^d(x, Q^2)$ is related to the proton structure function $F_2^p(x, Q^2)$ and the neutron structure function $F_2^n(x, Q^2)$ by the relation

$$F_2^d(x, Q^2) = \frac{1}{2}F_2^p(x, Q^2)\left\{1 + \frac{F_2^n(x, Q^2)}{F_2^p(x, Q^2)}\right\} = \frac{1}{2}\left\{F_2^p(x, Q^2) + F_2^n(x, Q^2)\right\} \quad (3)$$

Experimentally, $F_2^d(x, Q^2)$ is calculated using the parameterizations of the precisely measured $F_2^p(x, Q^2)$ and the $F_2^n(x, Q^2)/F_2^p(x, Q^2)$ ratio [15, 16].

Also, $F_2^p(x, Q^2)$ and $F_2^n(x, Q^2)$ can be expressed in terms of the singlet and non-singlet structure functions $F_2^S(x, Q^2)$ and $F_2^{NS}(x, Q^2)$ as [17]

$$F_2^p(x, Q^2) = \frac{5}{18}F_2^S(x, Q^2) + \frac{5}{18}F_2^{NS}(x, Q^2) \quad (4)$$

$$F_2^n(x, Q^2) = \frac{5}{18}F_2^S(x, Q^2) - \frac{3}{18}F_2^{NS}(x, Q^2) \quad (5)$$

Using Eqs. (4) and (5) in Eq. (3),

$$F_2^d(x, Q^2) = \frac{5}{18}F_2^S(x, Q^2) \quad (6)$$

Using Eqs. (6) and (2) in Eq. (1),

$$b_1^d(x, Q^2) = -\frac{5}{24}A_{ZZ}^d\frac{(1 + \frac{Q^2}{\nu^2})}{2x(1 + R)}F_2^S(x, Q^2) \quad (7)$$

The solutions of DGLAP equations for the singlet structure function $F_2^S(x, Q^2)$ in NLO and NNLO at small-x have the form [18, 19]

$$F^S_{2\mathrm{NLO}}(x, t) = F^S_{2\mathrm{NLO}}(x, t_0)\left\{\frac{t^{m(1+\frac{b}{t})}}{t_0^{m(1+\frac{b}{t_0})}}\right\} \times e^{mb(\frac{1}{t}-\frac{1}{t_0})} \quad (8)$$

and

$$F^S_{2\mathrm{NNLO}}(x, t) = F^S_{2\mathrm{NNLO}}(x, t_0)\left\{\frac{t^{n(1+\frac{3b^2+b}{t})}}{t_0^{n(1+\frac{3b^2+b}{t_0})}}\right\} \times e^{n\{b^2(\frac{\ln^2(t)}{t}-\frac{\ln^2(t_0)}{t_0})+(4b^2+b-c)(\frac{1}{t}-\frac{1}{t_0})\}} \quad (9)$$

Using Eqs. (8) and (9) in Eq. (7), we obtain

$$b_1^d(x, t) = -\frac{5}{24}A_{ZZ}^d\frac{(1 + \frac{e^t\Lambda^2}{\nu^2})}{2x(1 + R)}F^S_{2\mathrm{NLO}}(x, t_0)\left\{\frac{t^{m(1+\frac{b}{t})}}{t_0^{m(1+\frac{b}{t_0})}}\right\} \times e^{mb(\frac{1}{t}-\frac{1}{t_0})} \quad (10)$$

and

$$b_1^d(x, t) = -\frac{5}{24}A_{ZZ}^d\frac{(1 + \frac{e^t\Lambda^2}{\nu^2})}{2x(1 + R)}F^S_{2\mathrm{NNLO}}(x, t_0)\left\{\frac{t^{n(1+\frac{3b^2+b}{t})}}{t_0^{n(1+\frac{3b^2+b}{t_0})}}\right\} \times e^{n\{b^2(\frac{\ln^2(t)}{t}-\frac{\ln^2(t_0)}{t_0})+(4b^2+b-c)(\frac{1}{t}-\frac{1}{t_0})\}} \quad (11)$$

where $t = \ln(\frac{Q^2}{\Lambda^2})$, $b = \frac{\beta_1}{\beta_0^2}$, $c = \frac{\beta_2}{\beta_0^3}$ and β_0, β_1, β_2 are the one-loop, two-loop and three-loop corrections to QCD β-function. Equations (10) and (11) are the expressions for $b_1^d(x, t)$ in NLO and NNLO.

3 Results and discussion

HERMES [2] has provided the first measurement of the deuteron tensor structure function b_1^d in the kinematic range $0.01 < x < 0.45$ and $0.5\ \mathrm{GeV}^2 < Q^2 < 5\ \mathrm{GeV}^2$. For quantitative analysis of b_1^d using Eqs. (10) and (11), we use MRST 2004 NLO and MRST 2006 NNLO inputs [20, 21] for the input distributions $F_2^S(x, t_0)$ with $Q_0^2 = 1\ \mathrm{GeV}^2$, $N_f = 4$ and $\Lambda = 0.323$ GeV, 0.235 GeV for NLO and NNLO, respectively. The value of R is taken 0.18 (SLAC) [22]

For comparison of b_1^d with HERMES experiment data [2], we have considered the x-range $0.032 < x < 0.248$ at the average $Q^2 = 2.037\ \mathrm{GeV}^2$, to exclude two extreme data points: ($x = 0.012$, $Q^2 = 0.5\ \mathrm{GeV}^2$) and ($x = 0.452$, $Q^2 = 4.69\ \mathrm{GeV}^2$); the first one being at a very low Q^2 (is less than Q_0^2) and the second one being at a large-x. However, the x-range of the experimental data points is not sufficiently small where our results based on small-x approximation are expected to hold very well. This relatively large-x values give negative best fit values of m and n which are in conformity with our earlier formulations [19, 23, 24] This analysis therefore explore if our results conform to data even at relatively large-x explored at HERMES experiment. Also we have considered the HERMES experiment average asymmetry $A_{ZZ}^{d(\mathrm{ex})} = 0.0074$ and a theoretical asymmetry $A_{ZZ}^{d(\mathrm{th})} = b_1^d/F_1^d = 0.01$ obtained by J. Edelmann, G. Piller and W. Weise in Ref. [9] following Glauber–Gribov multiple scattering theory for coherent double scattering of the e–d process

Figures 1(a–d) represent the behavior of the tensor structure function $b_1^d(x, t)$ with x. Figure 1(a) represents the variation of $b_1^d(x, t)$ with x in NLO and NNLO for experimental asymmetry $A_{ZZ}^{d(\mathrm{ex})} = 0.0074$ and the best-fit values $m = -1.061$ and $n = -1\ 025$. Estimated negative values of the exponent m and n presumably suggest that the x-range used in HERMES experiment do not correspond to sufficiently small-x region where such exponents are to be positive [23, 24]. Figure 1(b) represents the same for theoretical asymmetry $A_{ZZ}^{d(\mathrm{th})} = 0.01$. Figure 1(c) represents the variation $b_1^d(x, t)$ with x in NLO for $A_{ZZ}^{d(\mathrm{ex})} = 0.0074$ and $A_{ZZ}^{d(\mathrm{th})} = 0.01$. Figure 1(d) represents the same in NNLO.

The analysis shows that NNLO curves are more sensitive to the experimental data and also than the NLO curves at smaller-x specially, which is an expected general feature of higher order effects. Also, the analysis shows that both the experimental and theoretical asymmetries predict similar behavior; the theoretical asymmetry showing slightly smaller

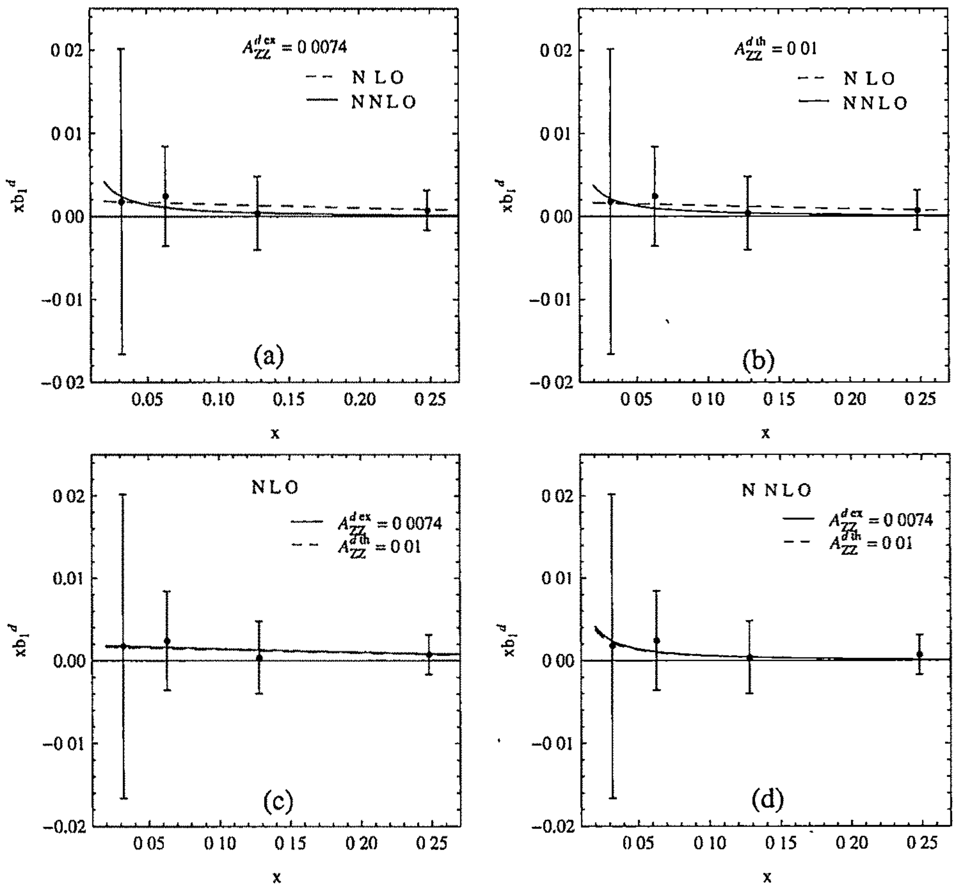

Fig. 1 Variations of the tensor structure function $b_1^d(x,t)$ with x

b_1^d values at smaller-x values. The curves are in good agreement with the HERMES data.

The violation of the QPM sum rule [25–27] for b_1^d is a signature of the mechanism that leads to the well-known effect of nuclear shadowing in unpolarized scattering. We have calculated the first moment of b_1^d at NLO and NNLO using Eqs. (10) and (11) and obtain non-zero values:

$$\int_{x\to 0}^{x=1} b_1^d(x,t)\,dx\Big|_{Q^2=\text{fixed}}^{\text{NLO,NNLO}} \neq 0$$

The integrand has a singularity at $x = 0$ and hence we have considered the lower limit as $x \to 0$. For example, in the x-limits $[10^{-10}, 1]$, at $Q^2 = 2.037\ \text{GeV}^2$, the integral give values 1.523×10^{-2} and 1.223×10^{-2} at NLO and NNLO, respectively. Similarly, in the x-range of our analysis, $[0.02, 0.30]$, at $Q^2 = 2.037\ \text{GeV}^2$, the integral give values 0.0139×10^{-2} and 0.0174×10^{-2} at NLO and NNLO, respectively. These calculations show that our results in Eqs. (10) and (11) also imply a violation of QPM sum rule.

Equation (3) is valid only when deuteron is a simple addition of proton and neutron which is true only in absence of binding effect. The use of this simplified assumption for $F_2^d(x,t)$ should therefore be justified only in the extreme limit of negligible binding effect between proton and neutron. This analysis explores how much this assumption for deuteron makes sense in its phenomenological study.

4 Conclusion

The asymmetry factor A^d_{ZZ} present in the expressions (10) and (11) for b_1^d includes the polarization-dependent part while the polarization-averaged contribution comes through the unpolarized singlet structure function F_2^S. The b_1^d measurement can be used to reduce the systematic uncertainty on the measurement of the polarized neutron structure function g_1^d.

The analysis predicts that b_1^d is non-vanishing, found to raise with decreasing x and also QPM sum rule is found to be violated. This can be interpreted to originate from the mechanism that leads to nuclear shadowing in unpolarized scattering which has been established in recent experiments at FNAL [28, 29] and CERN [30, 31]. Also the predicted behavior of b_1^d is in good agreement with the experiment within the limits of uncertainties.

References

1. P. Hoodbhoy et al., Nucl. Phys. B **312**, 571 (1989)

2 A Airapetian et al., Phys. Rev Lett. **95**, 242001 (2005)
3. K. Bora et al., Phys. Rev. D **57**, 6906 (1998)
4 A Pais, Phys Rev Lett. **19**, 544 (1967)
5 L L Frankfurt et al., Nucl. Phys. A **405**, 557 (1983)
6. H Khan et al, Phys Rev C **44**, 1219 (1991)
7. A Yu Umnikov, Phys. Lett. B **391**, 177 (1997)
8 J Ashman et al., Phys. Lett B **206**, 364 (1988)
9. J. Edelmann et al, Phys. Rev. C **57**, 3392 (1998)
10 H. Khan et al, Phys Lett. B **298**, 181 (1993)
11. J. Edelmann et al, Z. Phys. A **357**, 129 (1997)
12. L.W Whitlow et al, Phys. Lett. B **250**, 193 (1990)
13 R.L. Jaffe et al, Phys Lett B **223**, 218 (1989)
14 E Sather et al, Phys Rev D **42**, 1424 (1990)
15 H Abramowicz et al., arXiv hep-ph/9712415
16 P Amaudruz et al., Nucl Phys B **371**, 3 (1992)
17 W.B. Atwood, L F Abbott, R.M Barnett, Phys Rev. D **22**, 582 (1980)
18. D.K. Choudhury, S Islam, IJPAP **6**, 371 (2010)
19. D K Choudhury, S Islam, Indian J. Phys. **85**(2), 319 (2011)
20. A.D. Martin, R G Roberts, W. Stirling, R.S. Thorne, Phys Lett B **604**, 61 (2004)
21. A.D Martin, W Stirling, R.S. Thorne, G Watt, Phys Lett. B **652**, 292 (2007)
22 L.W. Whitlow et al, SLAC-PUB-5284
23. D.K. Choudhury, P K. Dhar, Indian J. Phys. **81**(2), 259 (2007)
24 D.K. Choudhury, P.K Dhar, Indian J Phys. **81**(8), 819 (2007)
25 N.N Nikolaev et al., Phys. Lett B **398**, 254 (1997)
26 L. Mankiewicz, Phys. Rev. D **40**, 255 (1989)
27 F E Close et al., Phys. Rev. D **42**, 2377 (1990)
28. M R Adams et al. (E665 Collab), Phys Rev. Lett. **75**, 1466 (1995)
29. M R. Adams et al. (E665 Collab.), Z. Phys C **67**, 403 (1995)
30. P. Amaudruz et al (NMC Collab.), Nucl. Phys B **441**, 3 (1995)
31 A Arneodo et al. (NMC Collab.), Nucl. Phys B **441**, 12 (1995)

Indian J Phys. **85** (2), 319-328 (2011)

An analysis of non-singlet structure function in next-to-next-to-leading order at small-x

D K Choudhury* and Saiful Islam

Department of Physics, Gauhati University,
Guwahati-781 014, Assam, India

E-mail dkc_phys@yahoo co in

Received 25 November 2009, accepted 15 March 2010

Abstract : A more general form of non-singlet structure function in Next-to-Next-to-leading order (NNLO) by solving Dokshitzer, Gribov, Lipatov, Altarelli, Parisi (DGLAP) equation at small-x is obtained. Results are compared with Fermi Lab Experiment E665 data

Keywords . Non-singlet structure function; DGLAP equation, small-x physics.

PACS Nos. · 12.38.-t, 12 38.Bx, 13.60 Hb

*Corresponding Author

International Journal of Pure and Applied Physics.
ISSN 0973-1776 Volume 6, Number 3 (2010), pp. 371–381

http://www.ripublication.com/ijpap.htm

An Analysis of Non-Singlet Structure Function upto next-to-next-to-Leading Order at Small-x

D.K. Choudhury and Saiful Islam

Department of Physics, Gauhati University, Assam, India
E-mail: saiful676@gmail.com

Abstract

We obtain a more general form of non-singlet structure function upto Next-to-Next-to-leading order (NNLO) by solving Dokshitzer, Gribov, Lipatov, Altarelli, Parisi (DGLAP) equation at small-x Results are compared with Fermi Lab Experiment E665 data.

AMS Subject Classification: 12.38.-t, 12.38.Bx, 13.60.Hb.
Keywords: Non-singlet structure function, NNLO effects, small-x physics.

Introduction

Precesion studies of some hadronic processes in the perturbative regime are going to be very important in order to confirm the validity of the mechanism of mass generation in the Standard Model at the new collider, the Large Hadron Collider (LHC). This program involves a rather complex analysis of the Quantum Chromodynamic (QCD) background, with the corresponding radiative corrections taken into account to higher orders.

Dokshitzer, Gribov, Lipatov, Altarelli, Parisi (DGLAP) evolution equations [1–5] are the basic tools to study the evolutions structure functions and hence the underlying dynamics quarks and gluons.

The higher order corrections to the evolution of PDF's is an immense field of work for researchers and of great interest for their useful applications in quantitative and reliable predictions of hard processes at present and future colliders. Such corrections are indirectly related to the predictions for W and Z production at LHC and Tevatron.

Studies of these corrections for specific processes have been performed by various groups and the highest level of precession so far achieved for the evolution of PDF's in purturbative QCD is next-to-next-to-leading order (NNLO) in α_s, the QCD coupling constant [6]. The quantification of the impact of these corrections requires the determination of hard scattering of the partonic cross-sections up to order α_s^3, with the matrix of the anomalous dimensions of the DGLAP kernals determined at the same perturbative order. Corrections beyond NNLO, i.e., higher twist corrections, like N^3LO, N^4LO etc., are not available yet in literature. This is because, increasing orders in α_s contain logarithms in Q^2, and order-by-order purturbation theory is not gauranteed to be more accurate here [7].

In some of our earlier communications [8–11], the DGLAP equations for non-singlet structure function have been solved in LO and NLO at small-x by using Lagrange's auxiliary method [12, 13]. In present paper, we incorporate NNLO effects in the formalism and analyse Fermi Lab μp Experiment E665 data [14].

Formalism

DGLAP equations for non-singlet structure function in LO, NLO and NNLO have the standard forms [1–5]:

$$\frac{\partial F_2^{NS}(x,t)}{\partial t} - \frac{\alpha_s(t)}{2\pi}\left[\frac{2}{3}\{3+4ln(1-x)\}F_2^{NS}(x,t) + I_1^{NS}(x,t)\right] = 0 \tag{2.1}$$

$$\begin{aligned}\frac{\partial F_2^{NS}(x,t)}{\partial t} &- \frac{\alpha_s(t)}{2\pi}\left[\frac{2}{3}\{3+4ln(1-x)\}F_2^{NS}(x,t) + I_1^{NS}(x,t)\right]\\ &-\left(\frac{\alpha_s(t)}{2\pi}\right)^2 I_1^{NS}(x,t) = 0\end{aligned} \tag{2.2}$$

$$\begin{aligned}\frac{\partial F_2^{NS}(x,t)}{\partial t} &- \frac{\alpha_s(t)}{2\pi}\left[\frac{2}{3}\{3+4ln(1-x)\}F_2^{NS}(x,t) + I_1^{NS}(x,t)\right]\\ &-\left(\frac{\alpha_s(t)}{2\pi}\right)^2 I_1^{NS}(x,t) - \left(\frac{\alpha_s(t)}{2\pi}\right)^3 I_2^{NS}(x,t) = 0\end{aligned} \tag{2.3}$$

where,

$$I_1^{NS}(x,t) = \frac{4}{3}\int_x^1 \frac{dz}{1-z}\left[(1+z^2)F_2^{NS}\left(\frac{x}{z},t\right) - 2F_2^{NS}(x,t)\right] \tag{2.4}$$

$$I_2^{NS}(x,t) = (x-1)F_2^{NS}(x,t)\int_0^1 f(z)dz + \int_x^1 f(z)F_2^{NS}\left(\frac{x}{z},t\right)dz \tag{2.5}$$

$$I_3^{NS}(x,t) = \int_x^1 \frac{dz}{z}\left[P_{NS}^{(2)}(x)F_2^{NS}\left(\frac{x}{z},t\right)\right] \tag{2.6}$$

Here, $t = \ln\left(\frac{Q^2}{\Lambda^2}\right)$, $\alpha_S(t) = \frac{4\pi}{\beta_0}$, $\beta_0 = 11 - \frac{2}{3}N_f$, Λ is the QCD cut-off parameter, N_f being the number of flavours. x is the Bjorken variable and Q^2 is the four momentum transfer in a deep inelastic scattering (DIS) process. Also,

$$\begin{aligned}
f(z) &= C_F^2[P_F(z) - P_A(z)] + \frac{1}{2}C - FC_A[P_G(z) + P_A(z)] \\
&\quad + C_F T_R N_f P_{N_f}(z) && (2.7) \\
P_F(z) &= -\frac{2(1+z^2)}{(1-z)} ln(z) ln(1-z) - \left(\frac{3}{1-z} + 2z\right) ln(z) \\
&\quad -\frac{1}{2}(1+z) ln(z) + \frac{40}{3}(1-z) && (2.8) \\
P_G(z) &= \frac{(1+z^2)}{(1-z)}\left(ln^2(z) + \frac{11}{3} ln(z) + \frac{67}{9} - \frac{\pi^2}{3}\right) \\
&\quad -2(1+z) ln(z) + \frac{40}{3}(1-z) && (2.9) \\
P_{N_f}(z) &= \frac{2}{3}\left[\frac{(1+z^2)}{(1-z)}\left(-ln(z) - \frac{5}{3}\right) - 2(1-z)\right] && (2.10) \\
P_A(z) &= \frac{2(1+z^2)}{(1-z)} \int_{(\frac{z}{1+z})}^{(\frac{1}{1+z})} \frac{dk}{k} ln\left(\frac{1-k}{k}\right) \\
&\quad +2(1+z) ln(z) + 4(1-z) && (2.11) \\
P_{NS}^{(2)}(x,t) &= N_f[[L_1(-163.9x^{-1} - 7.208x) + 151.49 + 44.51 \\
&\quad -43.12x^2 + 4.82x^3](1-x) + L_0 L_1(-173.1 + 46.18L_0) \\
&\quad +178.04L_0 + 6.892L_0^2 + \frac{40}{27}(L_0^4 - 2L_0^3)] && (2.12)
\end{aligned}$$

with $C_A = C_G = 3$, $L_0 = ln(x)$ and $L_1 = ln(1-x)$. The strong coupling constant $\alpha_s(t)$ is related to the β-function by the relation

$$\beta(\alpha_s) = \frac{\partial \alpha_s(t)}{\partial \ln Q^2} = -\frac{\beta_0}{4\pi}\alpha_s^2 - \frac{\beta_1}{16\pi^2}\alpha_s^3 - \frac{\beta_2}{64\pi^3}\alpha_s^4 + \cdots \quad (2.13)$$

where,

$$\begin{aligned}
\beta_0 &= \frac{11}{3}N_C - \frac{4}{3}T_f && (2.14) \\
\beta_1 &= \frac{34}{3}N_C^2 - \frac{10}{3}N_C N_f - 2C_F N_f && (2.15) \\
\beta_2 &= \frac{2857}{54}N_C^3 + 2C_F^2 T_f - \frac{205}{9}C_F N_C T_f + \frac{44}{9}C_F T_f^2 + \frac{158}{27}N_C T_f^2 && (2.16)
\end{aligned}$$

are the one-loop, two-loop and three-loop corrections to the QCD β-function. We set

$N_C = 3, C_F = \frac{N_C^2 - 1}{2N_C} = \frac{4}{3}$ and $T_f = \frac{1}{2}N_f$, with

$$\frac{\alpha(t)}{2\pi} = \frac{2}{\beta_0 t}\left[1 - \frac{\beta_1}{\beta_0^2}\frac{ln(t)}{t} + \frac{1}{\beta_0^3 t}\left\{\frac{\beta_1^2}{\beta_0}(ln^2(t) - ln(t) - 1) + \beta_2\right\} + O\left(\frac{1}{t^3}\right)\right] \tag{2.17}$$

The results used here are from direct x-space evolutions [15–17,22].

Now introducing the variable $u = 1 - z$, we note that [8, 11, 18]:

$$\frac{x}{z} = \frac{x}{1-u} = x\sum_{l=0}^{\infty} u^l = x + x\sum_{l=1}^{\infty} u^l \tag{2.18}$$

Since $x < z < 1$, so $0 < u < 1 - x$; hence the series is convergent for $|u| < 1$ and we can use Taylor's expansion of $F_2^{NS}\left(\frac{x}{z}, t\right)$ in approximated form [19,20,22] at small-x as:

$$F_2^{NS}\left(\frac{x}{z}, t\right) \approx F_2^{NS}(x,t) + x\sum_{l=1}^{\infty} u^l \frac{\partial F_2^{NS}(x,t)}{\partial x} \tag{2.19}$$

where terms containing x^2 and higher powers of x are neglected at small-x

Using eq (2.19), in eq. (2.4), (2.5), (2.6) and performing the u-integrations,

$$\frac{\partial F_2^{NS}(x,t)}{\partial t} - \frac{\alpha_s(t)}{2\pi}\left[A_1(x)F_2^{NS}(x,t) + A_2(x)\frac{\partial F_2^{NS}(x,t)}{\partial x}\right] = 0 \tag{2.20}$$

$$\frac{\partial F_2^{NS}(x,t)}{\partial t} - \frac{\alpha_s(t)}{2\pi}\left[A_1(x)F_2^{NS}(x,t) + A_2(x)\frac{\partial F_2^{NS}(x,t)}{\partial x}\right] - \left(\frac{\alpha_s(t)}{2\pi}\right)^2\left[B_1(x)F_2^{NS}(x,t) + B_2(x)\frac{\partial F_2^{NS}(x,t)}{\partial x}\right] = 0 \tag{2.21}$$

$$\frac{\partial F_2^{NS}(x,t)}{\partial t} - \frac{\alpha_s(t)}{2\pi}\left[A_1(x)F_2^{NS}(x,t) + A_2(x)\frac{\partial F_2^{NS}(x,t)}{\partial x}\right] - \left(\frac{\alpha_s(t)}{2\pi}\right)^2\left[B_1(x)F_2^{NS}(x,t) + B_2(x)\frac{\partial F_2^{NS}(x,t)}{\partial x}\right] - \left(\frac{\alpha_s(t)}{2\pi}\right)^3\left[C_1(x)F_2^{NS}(x,t) + C_2(x)\frac{\partial F_2^{NS}(x,t)}{\partial x}\right] = 0 \tag{2.22}$$

where,

$$A_1(x) = 2x + x^2 + 4ln(1-x) \tag{2.23}$$

$$A_2(x) = x - x^3 - 2xln(x) \tag{2.24}$$

$$B_1(x) = x\int_0^1 f(z)dz - \int_0^x f(z)dz + \frac{4}{3}N_f \int_x^1 F_{qq}(z)dz \tag{2.25}$$

$$B_2(x) = x\int_x^1 \left[f(z) + \frac{4}{3}N_f F_{qg}^S(z)\right]\frac{1-z}{z}dz \tag{2.26}$$

$$\begin{aligned} C_1(x) = {} & N_f \int_0^{1-x} \frac{dz}{1-z}\Big[\big\{ln(z)(-163.9(1-z)^{-1} - 7.208(1-z)) \\ & +151.49 + 44.51(1-z) - 43.12(1-z)^2 + 4.82(1-z)^3\big\}z \\ & +\big\{ln(z)ln(1-z)(-173.1 + 46.18ln(1-z)) + 178.04ln(1-z) \\ & +6.892ln^2(1-z) + \frac{40}{27}\left(ln^4(1-z) - 2ln^3(1-z)\right)\big\}\Big] \end{aligned} \tag{2.27}$$

$$\begin{aligned} C_2(x) = {} & N_f \int_0^{1-x} \frac{xdz}{(1-z)^2}\Big[\big\{ln(z)(-163.9(1-z)^{-1} - 7.208(1-z)) \\ & +151.49 + 44.51(1-z) - 43.12(1-z)^2 + 4.82(1-z)^3\big\}z \\ & +\big\{ln(z)ln(1-z)(-173.1 + 46.18ln(1-z)) + 178.04ln(1-z) \\ & +6.892ln^2(1-z) + \frac{40}{27}\left(ln^4(1-z) - 2ln^3(1-z)\right)\big\}\Big] \end{aligned} \tag{2.28}$$

Thus eq. (2.20), (2.21) and (2.22) take the forms,

$$\frac{\partial F_2^{NS}(x,t)}{\partial t} + L_1(x,t)\frac{\partial F_2^{NS}(x,t)}{\partial x} = M_1(x,t)F_2^{NS}(x,t) \tag{2.29}$$

$$\frac{\partial F_2^{NS}(x,t)}{\partial t} + L_2(x,t)\frac{\partial F_2^{NS}(x,t)}{\partial x} = M_2(x,t)F_2^{NS}(x,t) \tag{2.30}$$

$$\frac{\partial F_2^{NS}(x,t)}{\partial t} + L_3(x,t)\frac{\partial F_2^{NS}(x,t)}{\partial x} = M_3(x,t)F_2^{NS}(x,t) \tag{2.31}$$

where,

$$L_1(x,t) = \frac{2}{\beta_0 t}(A_2) \tag{2.32}$$

$$M_1(x,t) = \frac{2}{\beta_0 t}(A_1) \tag{2.33}$$

$$L_2(x,t) = \frac{2}{\beta_0 t}\left[1 - \frac{\beta_1}{\beta_0^2}\frac{ln(t)}{t}\right](A_2 + T_0 B_2) \tag{2.34}$$

$$M_2(x,t) = \frac{2}{\beta_0 t}\left[1-\frac{\beta_1}{\beta_0^2}\frac{ln(t)}{t}\right](A_1+T_0B_1) \tag{2.35}$$

$$L_3(x,t) = \frac{2}{\beta_0 t}\left[1-\frac{\beta_1}{\beta_0^2}\frac{ln(t)}{t}+\frac{1}{\beta_0^3 t}\left\{\frac{\beta_1^2}{\beta_0}(ln^2(t)-ln(t)-1)+\beta_2\right\}\right] \times(A_2+T_0B_2+T_1C_2) \tag{2.36}$$

$$M_3(x,t) = \frac{2}{\beta_0 t}\left[1-\frac{\beta_1}{\beta_0^2}\frac{ln(t)}{t}+\frac{1}{\beta_0^3 t}\left\{\frac{\beta_1^2}{\beta_0}(ln^2(t)-ln(t)-1)+\beta_2\right\}\right] \times(A_1+T_0B_1+T_1C_1) \tag{2.37}$$

Here, $T(t)=\frac{\alpha_s(t)}{2\pi}$. $T^2(t)$ and $T^3(t)$ are linearised through the ansatz. $T^2(t)=T_0T(t)$ and $T^3(t)=T_1T(t)$, where T_0 and T_1 are two suitable numerical parameters [8,21,22].

The general solution of eq. (2.29), which is frequently refered to as Lagrange's equation [12, 13], is obtained from the solutions of the equation

$$F(U_{LO},V_{LO})=0 \tag{2.38}$$

where, $F(U_{LO},V_{LO})$ is an arbitrary function. $U_{LO}(x,t,F_2^{NS})=C_1$ and $V_{LO}(x,t,F_2^{NS})=C_2$ are two independent solutions of equation

$$\frac{dx}{L_1(x,t)}=\frac{dt}{1}=\frac{dF_2^{NS}(x,t)}{M_1(x,t)F_2^{NS}(x,t)} \tag{2.39}$$

Solving eq. (2.39), we obtain

$$U_{LO}(x,t,F_2^{NS}) = t\times exp\left\{\frac{1}{a}N_1(x)\right\} \tag{2.40}$$

$$V_{LO}(x,t,F_2^{NS}) = F_2^{NS}(x,t)\times exp\left\{N_1'(x)\right\} \tag{2.41}$$

where,

$$N_1(x) = \int\frac{dx}{A_2(x)} \tag{2.42}$$

$$N_1'(x) = \int\frac{A_1(x)}{A_2(x)}dx \tag{2.43}$$

The most general form of eq. (2.38) is given by [8, 11],

$$V_{LO}=\alpha U_{LO}^{n_1}+\beta \tag{2.44}$$

where α and β are two arbitrary constants and n_1 is a real positive function of x and t which is to be determined through experimental parameterizations. For algebraic simplicity, we suppress its x and t-dependency.

From eq. (2.40), (2.41) and (2.44),

$$F_{2LO}^{NS}(x,t) = \frac{1}{exp\left\{N_1'(x)\right\}}\left[\alpha t^{n_1} \times exp\left\{\frac{1}{a}N_1(x)\right\} + \beta\right] \tag{2.45}$$

Using the initial condition [8–11],

$$F_2^{NS}(x,t)\big|_{x=1} = 0 \tag{2.46}$$

at any t for all orders, one gets,

$$\beta = -\alpha t^{n_1} \times exp\left\{\frac{1}{a}N_1(1)\right\} \tag{2.47}$$

Using eq. (2.47) in (2.45),

$$F_{2LO}^{NS}(x,t) = \frac{1}{exp\left\{N_1'(x)\right\}}\alpha t^{n_1}\left[exp\left\{\frac{1}{a}N_1(x)\right\} - exp\left\{\frac{1}{a}N_1(1)\right\}\right] \tag{2.48}$$

Defining the input function $F_{2LO}^{NS}(x,t_0)$ as,

$$F_{2LO}^{NS}(x,t_0) = \frac{1}{exp\left\{N_1'(x)\right\}}\alpha t_0^{n_1}\left[exp\left\{\frac{1}{a}N(x)\right\} - exp\left\{\frac{1}{a}N(1)\right\}\right] \tag{2.49}$$

we finally get,

$$F_{2LO}^{NS}(x,t) = F_{2LO}^{NS}(x,t_0)\left(\frac{t}{t_0}\right)^{n_1} \tag{2.50}$$

To get the solutions of eq. (2.30) and (2.31), we proceed in the same way and obtain,

$$U_{NLO}(x,t,F_2^{NS}) = t^{\left(1+\frac{b}{t}\right)}e^{\left(\frac{b}{t}\right)} \times exp\left\{\frac{1}{a}N_2(x)\right\} \tag{2.51}$$

$$V_{NLO}(x,t,F_2^{NS}) = F_2^{NS}(x,t) \times exp\left\{N_2'(x)\right\} \tag{2.52}$$

and

$$U_{NNLO}(x,t,F_2^{NS}) = t^{\left(1+\frac{3b^2+b}{t}\right)}e^{\left(\frac{4b^2+b^2\ln^2(t)+b-c}{t}\right)} \times exp\left\{\frac{1}{a}N_3(x)\right\} \tag{2.53}$$

$$V_{NNLO}(x,t,F_2^{NS}) = F_2^{NS}(x,t) \times exp\left\{N_3'(x)\right\} \tag{2.54}$$

where,

$$N_2(x) = \int \frac{dx}{A_2(x) + T_0 B_2(x)} \tag{2.55}$$

$$N_2'(x) = \int \frac{A_1(x) + T_0 B_1(x)}{A_2(x) + T_0 B_2(x)}dx \tag{2.56}$$

and

$$N_3(x) = \int \frac{dx}{A_2(x) + T_0 B_2(x) + T_1 C_2(x)} \tag{2.57}$$

$$N_3'(x) = \int \frac{A_1(x) + T_0 B_1(x) + T_1 C_1(x)}{A_2(x) + T_0 B_2(x) + T_1 C_2(x)} dx \tag{2.58}$$

Using the same most general form (eq. (2.44)) and the same initial condition (eq. (2.46)), we obtain,

$$\begin{aligned} F_{2NLO}^{NS}(x,t) &= \frac{1}{exp\left\{N_2'(x)\right\}} \alpha t^{n_2\left(1+\frac{b}{t}\right)} e^{n_2\left(\frac{b}{t}\right)} \\ &\times \left[exp\left\{\frac{1}{a} N_2(x)\right\} - exp\left\{\frac{1}{a} N_2(1)\right\} \right] \end{aligned} \tag{2.59}$$

$$\begin{aligned} F_{2NNLO}^{NS}(x,t) &= \frac{1}{exp\left\{N'(x)\right\}} \alpha t^{n_3\left(1+\frac{3b^2+b}{t}\right)} e^{n_3\left(\frac{4b^2+b^2 ln^2(t)+b-c}{t}\right)} \\ &\times \left[exp\left\{\frac{1}{a} N_3(x)\right\} - exp\left\{\frac{1}{a} N_3(1)\right\} \right] \end{aligned} \tag{2.60}$$

where n_2 and n_3 are other two real numbers to be determined through parameterizations.
Defining the input functions $F_{2NLO}^{NS}(x,t_0)$ and $F_{2NNLO}^{NS}(x,t_0)$ as,

$$\begin{aligned} F_{2NLO}^{NS}(x,t_0) &= \frac{1}{exp\left\{N_2'(x)\right\}} \alpha t_0^{n_2\left(1+\frac{b}{t_0}\right)} e^{n_2\left(\frac{b}{t_0}\right)} \\ &\times \left[exp\left\{\frac{1}{a} N_2(x)\right\} - exp\left\{\frac{1}{a} N_2(1)\right\} \right] \end{aligned} \tag{2.61}$$

$$\begin{aligned} F_{2NNLO}^{NS}(x.t_0) &= \frac{1}{exp\left\{N_3'(x)\right\}} \alpha t_0^{n_3\left(1+\frac{3b^2+b}{t_0}\right)} e^{n_3\left(\frac{4b^2+b^2 ln^2(t)+b-c}{t_0}\right)} \\ &\times \left[exp\left\{\frac{1}{a} N_3(x)\right\} - exp\left\{\frac{1}{a} N_3(1)\right\} \right] \end{aligned} \tag{2.62}$$

we finally get,

$$F_{2NLO}^{NS}(x,t) = F_{2NLO}^{NS}(x,t_0) \left\{ \frac{t^{n_2\left(1+\frac{b}{t}\right)}}{t_0^{n_2\left(1+\frac{b}{t_0}\right)}} \right\} \times e^{n_2 b\left(\frac{1}{t}-\frac{1}{t_0}\right)} \tag{2.63}$$

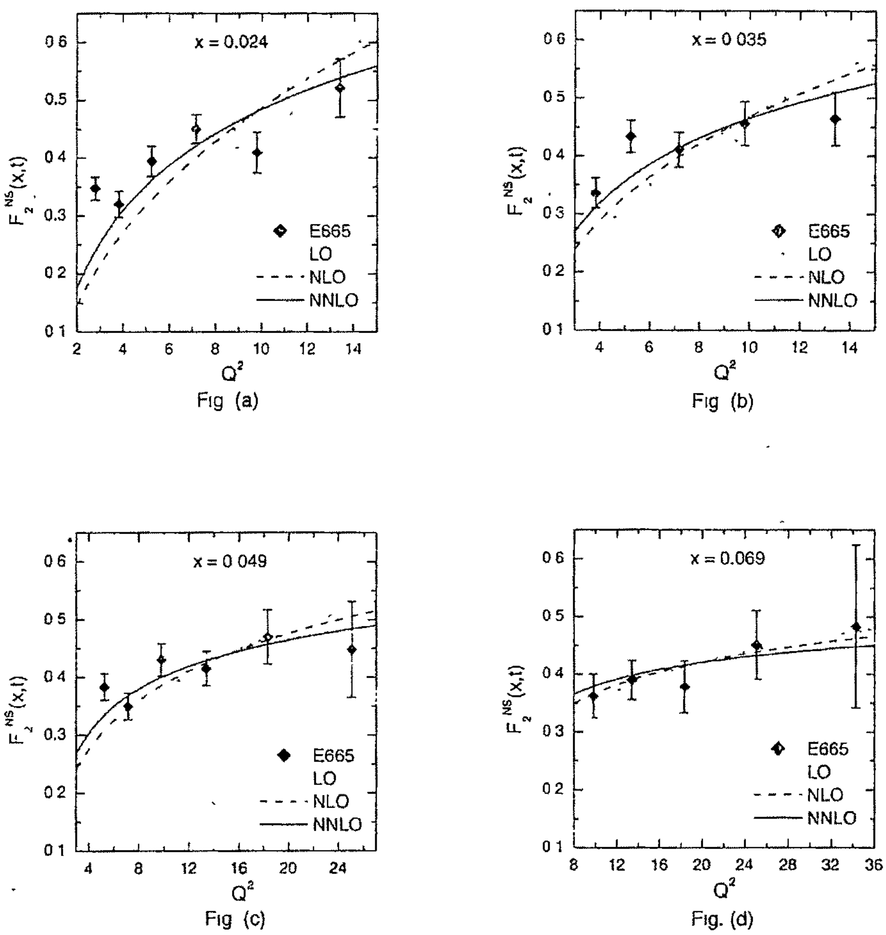

Figure 1: (a-d) Non-singlet structure function $F_2^{NS}(x,t)$ in LO, NLO and NNLO and its comparision to Fermi Lab μp experiment E665 data.

$$F^{NS}_{2NNLO}(x,t) = F^{NS}_{2NNLO}(x,t_0)\left\{\frac{t^{n_3\left(1+\frac{3b^2+b}{t}\right)}}{t_0^{n_3\left(1+\frac{3b^2+b}{t_0}\right)}}\right\} \times e^{n_3\left\{b^2\left(\frac{\ln^2(t)}{t}-\frac{\ln^2(t_0)}{t_0}\right)+(4b^2+b-c)\left(\frac{1}{t}-\frac{1}{t_0}\right)\right\}} \qquad (2.64)$$

Eq. (2.50), (2.63) and (2.64) represent the t-evolution of non-singlet structure function in LO, NLO and NNLO which are more general than that of ref. [22].

Results and Discussions

We have solved DGLAP evolution equation to incorporate the higher order effects (upto NNLO) to the non-singlet structure function $F_2^{NS}(x,t)$ in the more general approach [8, 11] shown in eq.(44). We compare our predicted result of t-evolution of $F_2^{NS}(x,t)$ with Fermi Lab μp experiment E665 data [14]. For quantitative analysis, we use MRST inputs for $F_2^{NS}(x,t_0)$ with $Q_0^2 = 1\ GeV^2$, $N_f = 4$ and $\Lambda = 0.220, 0.323, 0.235\ GeV$ for LO, NLO and NNLO respectively [23, 24].

Figures 1 (a-d), represent t-evolution of non-singlet structure function where our computed results for LO, NLO and NNLO from eq. (2.50), (2.63) and (2.64) are plotted against Q^2 at four different representative x-bins : $x = 0.024, 0.035, 0.049, 0.069$ in order to have a comparision among the LO, NLO and NNLO effects on non-singlet structure function. The figures represent best fit graphs for all the orders. The vertical error bars represent statistical uncertainties. The best fit values of n_1, n_2 and n_3 are found to be $n_1 = 2.390, 2.037, 1.481, 1.054$; $n_2 = 2.594, 2.134, 1.507, 1.014$ and $n_3 = 1.875, 1.578, 1.171, 0.814$ in the said x-bins. This indicates that n_1, n_2 and n_3 as defined in eq. (2.44) deviates significantly from unity and has x-dependence. Unlike the previous works [9, 10, 22], the present approach alone [8, 11] can acomodate such features of the experiment. A similar analysis for small-x H1 [25–31] and ZEUS [32–36] data of HERA ep collider is currently under study. A good agreement of our predicted result with E665 experimental data within moderate x and Q^2-range is obtained. This is so because DGLAP evolution equations hold well within this region of x and Q^2-range.

Acknowledgment

We thank P. K. Dhar for useful discussions.

References

[1] G. Altarelli and G. Parisi, *Nucl. Phys.*, **B126**, 289, 1977.

[2] V. N. Gribov and L. N. Lipatov, *Sov. J. Nucl. Phys.*, **15**, 438, 1972.

[3] L. N. Lipatov, *Sov. J. Nucl. Phys.*, **20**, 94, 1975.

[4] Yu. L. Dokshitzer, *Sov. Phys. JETP*, **46**, 641, 1977.

[5] L. F. Abbott, W. B. Atwood and R. M. Barnett, *Phys Rev.*, **D22**, 882, 1988.

[6] A. D. Martin, R. G. Roberts, W. Stirling and G Watt, *arXiv:hep-ph/0201127.*

[7] R. S. Thorne, *arXiv:hep-ph/0601245.*

[8] D K. Choudhury and P K. Dhar, *Indian J. Phys.*, **81(8)**, 819, 2007.

[9] D. K. Choudhury and A. Deshmukhya, *Indian J. Phys.*, **75A(2)**, 175, 2001.

[10] A. Deshmukhya and D. K. Choudhury, *Indian J. Phys.*, **75A(5)**, 573, 2001.

[11] D. K. Choudhury and P. K. Dhar, Indian J. Phys., **81(2)**, 259, 2007.

[12] I. N. Sneddon, *Elements of Partial Diffrential Equations*, (McGraw Hill, New York) p. 50, 1957.

[13] F. Ayres Jr., *Dyffrential Equations*, Schaums Outline Series (McGraw Hill, New York), 1988.

[14] M. R. Adams et al., (E665), *Phys. Rev.*, **D54**, 3006, 1996.

[15] S. Moch, J. A. M. Vermaseren and A. Vogt, *Nucl. Phys Proc. Suppl.*, **116**, 100, 2003.

[16] S. Moch, J. A. M. Vermaseren and A. Vogt, *Nucl. Phys.*, **B688**. 101, 2004.

[17] T. Gehrmann and E. Remiddi, *Comput. Phys. Commun.*, **141**, 296, 2001.

[18] D K. Choudhury, and P. K. Saharia, *Pramana-J. Phys.*, **58**, 593, 2002.

[19] W. Furmanski and R. Petronzio, *Z. Phys* , **C11**, 293, 1982.

[20] D. K Choudhury and P. K. Saharıah, *Pramana-J. Phys.*, **65**, 193, 2005.

[21] A. Deshmukhya and D. K. Choudhury, *Proc. of the 2nd Resional Conf. on Phys. Research in North-East, Guwahati, India*, 34 October, 2000.

[22] R. Baishya and J. K. Sarma, *Eur. Phys. J.*, **C60**, 585, 2009.

[23] A. D. Martin, R. G. Roberts, W. Stirling and R. S. thorne, *arXiv:hep-ph/0201127.*

[24] A. D. Martin, R. G. Roberts, W. Stirling and R. S. thorne, *arXiv:hep-ph/0110215.*

[25] H1 Collab.: S. Aid et al., *Phys. Lett.*, **B354**, 494, 1995.

[26] H1 Collab.: S. Aid et al., *Nucl. Phys.*, **B470**, 3, 1997.

[27] H1 Collab.: C. Adloff et al., *Nucl. Phys.*, **B497**, 3, 1997

[28] H1 Collab.: C. Adloff et al., *Phys. Lett.*, **B393**, 452, 1997.

[29] H1 Collab.: C. Adloff et al., *Euro. Phys. J.*, **C13**, 609, 2000.

[30] H1 Collab.: C. Adloff et al., *Euro. Phys. J.*, **C21**, 33, 2000.

[31] H1 Collab.: C. Adloff et al., *Phys. Lett.*, **B520**, 183, 2001.

[32] ZEUS Collab.. M. Derrick et al., *Phys. Lett.*, **B345**, 576, 1995.

[33] ZEUS Collab.: M. Derrick et al., *Z. Phys.*, **C69**, 607, 1996.

[34] ZEUS Collab.: M. Derrick et al., *Z. Phys.*, **C72**, 399, 1996.

[35] ZEUS Collab.: J. Breitweg et al., *Phys. Lett.*, **B407**, 432, 1997.

[36] ZEUS Collab.: S. Chekanov et al., *Euro. Phys. J.*, **C21**, 443, 2001.

Assam University Journal of Science &
Technology Physical Sciences and Technology
Vol 6 Number II
112-116 2010

A numerical analysis of Probability of Gluon-Gluon Interaction $k_G(x, Q^2)$ with improved solution of DGLAP equations

Saiful Islam and D. K. Choudhury*
Department of Physics, Gauhati University, Guwahati

Correspondence: *e-mail saiful676@gmail.com

Abstract

The application of method of characteristics in perturbative quantum chromo-dynamics (pQCD) is relatively new. In the present paper, we apply the method of characteristics to solve the DGLAP equation for gluon and obtain an expression for the probability of gluon-gluon interaction, $k_G(x,t)$. In the moderate Bjorken-x and Q^2-region the variation of the probability of gluon-gluon interaction $k_G(x,t)$ is in good agreement with exact results and parameterized experimental data.

Keywords : Gluon Distribution, Method of Characteristics, DGLAP Equation, Small-x physics

Introduction

Dokshitzer, Gribov, Lipatov, Altarelli, Parisi (DGLAP) evolution equations (Altarelli, et al., 1977) have been playing very important role in understanding the dynamics of evolutions of quark and gluons. Several approximate and numerical solutions of DGLAP evolution equations are available in literature (Deka and Choudhury, 1997), but their exact analytical solutions are not known (Hirai, et al., 1998). Because these evolution equations are partial differential equations (PDE), their ordinary solutions are not unique solutions, rather a range of solutions. Moreover, they are based on an *ad-hoc* assumption of factorizability of x and t dependence of the gluon momentum distribution $G(x,t)$. These limitations can be over come by the use of Method of Characteristics (Farlow, 1982).

The application of method of characteristics in perturbative quantum chromo-dynamics (pQCD), specially in the solution of DGLAP equations is relatively new. Some of these applications are available in recent literatures (Choudhury, et al., 2002, Baishya, et al., 2006) with considerable phenomenological success. In this paper, we solve DGLAP equations in leading order by using method of characteristics and obtain an analytical form of gluon-gluon interaction probability distribution at small-x which is free from the above mentioned limitations.

Formalism

The DGLAP equations for gluon distribution have the standard form

$$t\frac{\partial G(x,t)}{\partial t}=\frac{3\alpha_s(t)}{\pi}[\{(\frac{11}{12}-\frac{N_f}{18}+\ln(1-x)\}G(x,t)+\int_x^1 dz\frac{zG(\frac{x}{z},t)-G(x,t)}{(1-x)} \tag{1}$$

$$+\int_x^1 dz\{z(1-z)+\frac{(1-z)}{z}\}G(\frac{x}{z},t)+\frac{2}{9}\int_x^1\frac{1+(1-z)^2}{z}F_2^s(\frac{x}{z},t)]$$

where $t=\ln(\frac{Q^2}{\Lambda^2})$, $\alpha_s(t)=\frac{4\pi}{\beta_0}$, $\beta_0=11-\frac{2}{3}N_f$, N_f being the number of flavours.

The Probability of Gluon-Gluon Interaction, $k_G(x,t)$, is defined under AGL formalism as :

$$k_G(x,t)=\frac{\alpha_S N_C \pi}{2Q^2R^2}xG(x,t) \tag{2}$$

where, α_S is the coupling constant for strong interaction and N_C is the number of Colors.

To evaluate the integrals of eq.(1), we introduce a variable u as $u=1-z$ and note that :

$$\frac{x}{z}=\frac{x}{1-u}=x\sum_{l=0}^{\infty}u=x+x\sum_{l=1}^{\infty}u \tag{3}$$

Since $x<z<1$ so , hence the series is convergent for $|u|<1$ and we can use Taylor's expansion of and $G(x/z,t)$ in approximated form at small-x as

$$F_2^s(\frac{x}{z},t)\approx F_2^s(x,t)+x\sum_{l=1}^{\infty}u\frac{\partial F_2^s(x,t)}{\partial x} \tag{4}$$

$$G(\frac{x}{z},t)\approx G(x,t)+x\sum_{l=1}^{\infty}u\frac{\partial G(x,t)}{\partial x} \tag{5}$$

Since x is small, terms containing x^2 and higher powers of x are neglected. Using eq and in eq and performing the integrations w.r.t. z,

$$t\frac{\partial G(x,t)}{\partial t}=P(x)G(x,t)+Q(x)\frac{\partial G(x,t)}{\partial x}+R(x)F_2^s(x,t)+S(x)\frac{\partial F_2^s}{\partial x} \tag{6}$$

where at small-x,

$$P(x)=\frac{12}{\beta_0}\{\ln(\frac{1}{x})+2x-\frac{N_f}{18}-\frac{11}{12}\},\qquad Q(x)=\frac{11}{\beta_0}x$$
$$R(x)=\frac{12}{\beta_0}x \qquad\qquad S(x)=\frac{16}{\beta_0}x \tag{7}$$

A reasonable approximate relationship between $F_2^S(x,t)$ and $G(x,t)$, representing the relative strength of gluon to singlet distribution, can be taken as $F_2^S(x,t)=kG(x,t)$, where k is a suitable function of x or may be a constant. For simplicity and well adaptation to method of characteristics, k is considered here as a constant with $0<k<1$, since gluon distribution is always higher than singlet distributions at any Q^2. Using this relationship in eq.,

$$J(x)\frac{\partial G(x,t)}{\partial x}-t\frac{\partial G(x,t)}{\partial t}+H(x)G(x,t)=0 \tag{8}$$

where

$$H(x)=P(x)+kR(x) \quad\text{and}\quad J(x)=Q(x)+kS(x) \tag{9}$$

Eq (8) is a first order PDE, which can be solved by Method of Characteristics.

To use method of characteristics, let us introduce two variables S and τ as :

(10)

Use of eq (10) in eq (8) gives,

$$\frac{dG}{dS} + U(S,\tau)G(S,\tau) = 0 \tag{11}$$

which is an ODE in new coordinates (S,τ). Here, $U(S,\tau) = H(x)$. Solving eq.(10) with the boundary condition, at $S=0$, $t=t_0$ and $x=\tau$, we get the transformation equations as.

(12)

Expressing ODE (11) in terms of S and τ, integrating and transforming the resultant equation back to the original variables (x,t) with the help of transformation eq.(12), we get,

$$\begin{aligned} G(x,t) = G(x,t_0)\times\exp[&\frac{(24+12k)}{(11+16k)}x\left(\frac{t}{t_0}\right)^{\frac{1}{\beta_0}(11+16k)} \\ &+\frac{(66+96k)}{\beta_0^2}\{\ln(\frac{t_0}{t})\}^2+\ln\{x(\frac{t}{t_0})^{\frac{1}{\beta_0}(11+16k)}\}\ln(\frac{t_0}{t})^{\frac{12}{\beta_0}} \\ &+\ln(\frac{t_0}{t})^{\frac{1}{\beta_0}(\frac{2}{3}N_f+11)}-\frac{(24+12k)}{(11+16k)}x] \end{aligned} \tag{13}$$

where $G(x,t_0) = G(S,\tau) = G(\tau)$ is the input function obtained from the boundary condition, at $S=0$, $t=t_0$ and $x=\tau$. This $G(x,t)$ of eq.(1) is infect $xG(x,t)$ of eq.(2)

Using eq (13) in eq (2), finally we get,

$$\begin{aligned} k_G(x,Q^2) = \frac{\alpha_s N_c \pi}{2Q^2R^2}\times G(x,t_0)\times\exp[&\frac{(24+12k)}{(11+16k)}x\left(\frac{t}{t_0}\right)^{\frac{1}{\beta_0}(11+16k)} \\ &+\frac{(66+96k)}{\beta_0^2}\{\ln(\frac{t_0}{t})\}^2+\ln\{x(\frac{t}{t_0})^{\frac{1}{\beta_0}(11+16k)}\}\ln(\frac{t_0}{t})^{\frac{12}{\beta_0}} \\ &+\ln(\frac{t_0}{t})^{\frac{1}{\beta_0}(\frac{2}{3}N_f+11)}-\frac{(24+12k)}{(11+16k)}x] \end{aligned} \tag{14}$$

Equation (14) is our main result

Results and Discussions

We compare our predicted gluon-gluon interaction probability with MRST2004LO exact results and with the parameterized data from H12000 at different Q^2 values for $10^{-5} < x < 10^{-1}$. For Quantitative analysis, we have used MRST2001LO input and considered $Q^2_0 = 4\ Gev^2$, QCD cutoff parameter $\Lambda=220$ MeV $N_f=4$ and $N_c=3$ [19]. The Dependence of our prediction on the values of the arbitrary constant k have also been noted. The acceptable range of k is found to be $0 < k < 10^{-1}$. It is also observed that the predicted result is almost independent of k at k d" 10^{-2}.

The figures represent gluon-gluon interaction probability distribution $k_G(x,t)$ from our predicted result at different Q^2 = 10, 12, 14, 16, 20, 50 Gev^2 at k = 0.01. It is seen that disagreement of our predicted result with MRST2004LO exact results and H12000 parameterized data increases at lower Q^2 as well as at higher Q^2 values and also at very small-x regions. Comparisons show more suitability of our prediction at moderate Q^2-range. This is because standard DGLAP formalism holds well in moderate x- and Q^2-ranges.

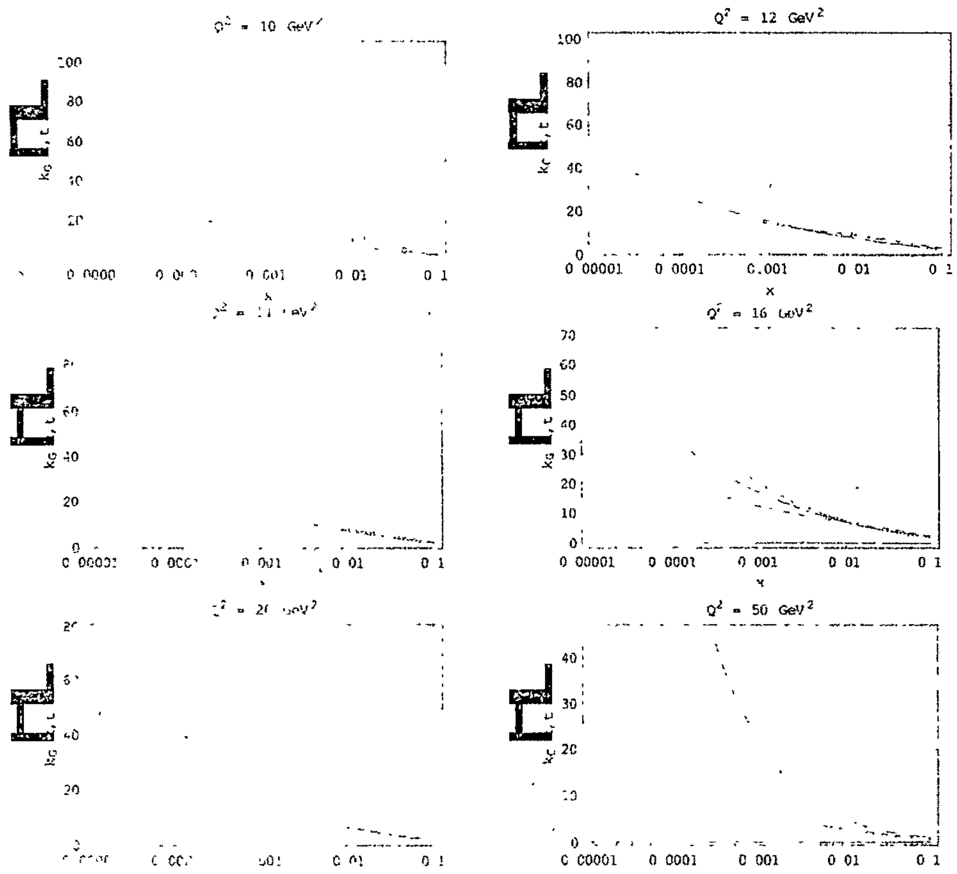

Figure: Predicted gluon-gluon interaction probability distribution $k_G(x,t)$ at different Q^2 values and its comparison with MRST2001LO exact results and with parameterized data from H12000. The continuous lines represent our prediction, dotted lines represent MRST2004LO exact results and the dashed lines represent H12000 parameterized data

Conclusion

In this paper, we have applied the method of characteristics to solve DGLAP equations for gluon distribution functions without any *ad-hoc* assumption of factorizability of x and t dependence of the gluon distribution $G(x,t)$ and obtained a form of probability of gluon-gluon interaction probability distribution $k_G(x,t)$. A good agreement of our predicted result with MRST2004LO exact results and parameter-ized data from H12000 is obtained.

References

G Altarelli and G Parisi Nucl Phys B126 289 (1977)

V N Gribov and L N Lipatov, Sov J Nucl. Phys 15 438 (1972)

Yu L Dokshitzer, Sov Phys JETP, 46, 641 (1977)

L F Abbott, W B Atwood and R M Barnett, Phys Rev D22 882 (1988)

R Deka and D K Choudhury, Z Phys. C75, 679 (1997)

D K Choudhury, R Deka and A Saikia, Euro Phys J C2 301 (1998)

D K Choudhury, and A Saikia, Pramana-J Phys 33 359 (1989)

A D Martin, R G Roberts W Stirling and R S thorne, hep-ph/0201127

M Hirai, S Kumano and Myiama, Comput. Phys. Commun 108, 38 (1998)

A. Cafarella et al , Nucl. Phys B748, 253 (2006)

W Furmanski and R Petronzio, Z. Phys. C11, 293 (1982)

D K. Choudhury et al Phys. Lett B403, 139 (1997)

D. K Choudhury, and P. K Saharia, Pramana-J. Phys. 58, 593 (2002)

R. Baishya and J K Sarma, Phys Rev. D74, 107702 (2006)

A DeRujula, et al , Nucl Phys Phys Rev D10, 1649 (1974)

S. J Farlow, Partial Differential Equations for Scientists and Engineers (John Willey, 1982) p.205

C Marquet and G Soyez, [arXiv hep-ph/0504080]

M B Gay Ducati, *Brazilian J Phys* 31, 2 (2001)

J Blumin, H. Botticher and A Guffanti, hep-ph/0407089

International Journal of Physics and Applications.
ISSN 0974-3103 Volume 3, Number 2 (2011), pp. 189-192

http://www.irphouse.com

A Numerical Analysis of Variation of Gluon-Gluon Interaction Probability $k_{GA}(x,t)$ with nuclei A in High Density QCD

Saiful Islam and D.K. Choudhury

Department of Physics, Gauhati University, Guwahati-781014, Assam, India
E-mail: s.phys.res@gmail.com

Abstract

We have studied the gluon-gluon interaction probability k_{GA} in nuclei with mass number of nuclei A. A comparative analysis of $k_{GA}(x,t)$ is made on the basis of currently available models of gluon distribution function.

Keywords: High density QCD; Gluon-gluon interaction probability; small-x physics.

PACS Nos.: 12.38.-t; 12.38.Bx; 13.60.Hb.

Introduction

Deep inelastic scattering (DIS) experiments along with high energy heavy ion collisions are furnishing crucial experimental inputs for achieving a more complete and deeper understanding of dense matter. Quantum chromodynamics (QCD) at high parton density i.e. hdQCD deals both with fundamental theoretical issues, such as unitarity of strong interactions at high energies, and with the challenge of describing experimental data coming at present from RHIC and LHC and expected exciting physics of forthcoming experiments. Over the past few years much theoretical effort has been devoted towards the understanding of the growth of the total scattering cross sections with energy [1].

While at small-x valence quarks are of little importance and the behavior of the sea is expected to follow that of the gluon distribution, which is not an observable quantity, is badly determined and represents one of the largest uncertainties in computation of cross sections both for moderate and large scales Q^2 [2]. In this situation and while waiting for new experimental data to come from lepton-ion, p-A or A-A colliders, the guidance from different theoretical models is of uttermost importance to perform safe extrapolations from the region where experimental data exist to those interesting for LHC studies [3] or physics beyond standard model.

With this aim, the present paper deals with a quantitative study of probability of gluon-gluon interaction using currently available forms of gluon distributions. We study numerically how it changes with mass number A of nuclei.

Formalism

The density of gluon distribution in a nucleon in high density limit is given by the solution of non-linear evolution equation which resums the power of the function [4, 5]:

$$k_g\left(x,Q^2\right)=\frac{3\pi\alpha_S\left(Q^2\right)}{2Q^2R^2}xg\left(x,Q^2\right) \tag{1}$$

which represents the probability of gluon-gluon interaction inside the parton cascade, also denoted by the packing factor of partons in a parton cascade. Here R_N is the size of the target (nucleon/nuclei) which can also be interpreted as the corelation radius between two glouns in a target at $x\approx 1$ [5]. In case of nucleons, eq.(1) is written as

$$k_{g_N}\left(x,Q^2\right)=\frac{3\pi\alpha_S\left(Q^2\right)}{2Q^2R^2}xg_N\left(x,Q^2\right) \tag{2}$$

In case of nuclei, $R_A = A^{1/3}\times R_N$ and $xg_A = A\times xg_N$ and hence this function takes the form

$$k_{g_A}\left(x,Q^2\right)=A^{1/3}\times k_{g_N}\left(x,Q^2\right) \tag{3}$$

Therefore, for the case of an interaction with nuclei, we can reach a hdQCD region at smaller parton density than in a nucleon [5]. With the introduction of our solution (22) of Ref. [6] or (13) of Ref. [7] for gluon distribution function, eq.(3) for nuclei becomes,

$$k_{G_A}\left(x,Q^2\right)=A^{1/3}\frac{3\pi\alpha_S\left(Q^2\right)}{2Q^2R^2}G(\tau)\exp\left[\begin{array}{l}\frac{(24+12k)}{(11+16k)}x\left(\frac{t}{t_0}\right)^{\frac{1}{\beta_0}(11+16k)}+\frac{(66+96k)}{\beta_0^2}\left\{\ln\left(\frac{t_0}{t}\right)\right\}^2\\ +\ln\left\{x\left(\frac{t}{t_0}\right)^{\frac{1}{\beta_0}(11+16k)}\right\}\ln\left(\frac{t_0}{t}\right)^{\frac{12}{\beta_0}}+\ln\left(\frac{t_0}{t}\right)^{\frac{1}{\beta_0}\left(\frac{2}{3}N_f+11\right)}\\ -\frac{(24+12k)}{(11+16k)}x\end{array}\right] \tag{4}$$

where τ is given by

$$\tau = x\left(\frac{t}{t_0}\right)^{\frac{1}{\beta_0}(11+16k)} \tag{5}$$

Introduction of standard DLLA (double leading logarithmic approximation) result for gluon distribution [8] in eq.(3) gives,

$$k_{G_A}^{DLLA}(x,t) = A^{1/3}\frac{3\pi\alpha_S(Q^2)}{2Q^2R^2}G(x,t_0)\exp\left[\left\{\frac{48}{\beta_0}\ln\left(\frac{t}{t_0}\right)-\ln\left(\frac{1}{x}\right)\right\}^{0.5}\right] \tag{6}$$

provided the gloun distribution is not singular at $t = t_0$.

Similarly, introduction of AGL [4] gluon distribution at running $\alpha_S(t)$ in eqns.(3) gives,

$$k_{G_A}^{AGL}(x,t) = A^{1/3}\frac{t}{1+t}\frac{2N_C Q^2 R_N^2}{3\pi^2}\ln\left(\frac{1}{x}\right) \tag{7}$$

Results and discussion

For quantitative analysis, we use $\alpha_S(t) = \dfrac{4\pi}{\beta_0 t}$, $R_N^2 = 5\ GeV^{-2}$; A=1 (nucleon), A=40 (Ca-nucleus), A=64 (Cu-nucleus) and A=197 (Au-nucleus).

Fig.1 represents variation k_{GA} with A at a fixed $x = 10^{-3}$ and Q^2=10 GeV^2. The analysis shows that the gluon-gluon interaction probability k_{GA} increases with increase in A at fixed Q^2 and/or at fixed x; the nature of increments being different in different models; i.e., gluon-gluon interaction probability is greater in heavier nuclei.

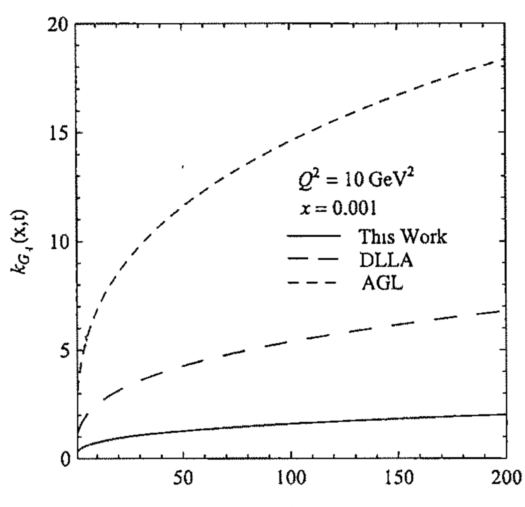

Figure 1: Variation of predicted k_{GA} with A for nuclei.

References

[1] M. B. Gay Ducati and V. P. Goncalves. hep-ph/0003098

[2] J. C. Collins D. E. Soper and G. Sterman. Adv. Ser. Direct. H E P, 5:1, (1988)

[3] N. Armesto and C. A. Salgado. arXiv:hep-ph/0301200

[4] M. B. Gay Ducati. Brazilian J. Phys., 31(2):115, (2001)

[5] Eugene Levin. arXiv:hep-ph/9806434, (1998)

[6] S. Islam and D. K. Choudhury. XVIII DAE-BRNS HEP Sym. vol 18, p112, (2008)

[7] D. K. Choudhury and S. Islam. Assam Univ. J. Sc. & Tech., 6(2):112, (2010).

[8] A. DeRujula S. L. Glashow and H. D. politzer. Phys. Rev., D10:1649, (1974).

International Journal of Physics and Applications.
ISSN 0974-3103 Volume 4, Number 2 (2012), pp. 95-97

http://www.irphouse.com

A Numerical Analysis of Variation of Transverse Gluon Density $\rho_N(x,t)$ with Rapidity $y=ln(1/x)$ in High Density QCD

Saiful Islam

Department of Physics, Royal Group of Institutions,
Guwahati-781035, Assam, India
E-mail: s.phys.res@gmail.com

Abstract

We have studied the variation of the transverse gluon density ρ_N in with $y=ln(1/x)$. A comparative analysis of ρ_N is made on the basis of different available models of gluon distribution function.

Keywords: Gluon density ; hdQCD ; small-x physics.

PACS Nos: 12.38.-t; 12.38.Bx; 13.60.Hb.

Introduction

Deep inelastic scattering (DIS) experiments along with high energy heavy ion collisions are furnishing crucial experimental inputs for achieving a more complete and deeper understanding of dense matter [1].

This short communication deals with a quantitative study of transverse gluon density using currently available forms of gluon distributions [4-8]. We study numerically how it changes with mass number A of nuclei.

Formalism

The density of gluons in the transverse plane is defined as [3] :

$$\rho_N\left(x,Q^2\right)=\frac{xg\left(x,Q^2\right)}{\pi R_N^2} \tag{1}$$

With the introduction of our solution eq.(13) of Ref. [5] or eq.(22) of Ref. [6] obtained in our earlier communications, eq. (1) becomes,

$$\rho_N(x,t)=\frac{G(x,t_0)}{\pi R_N^2}\exp\left[\begin{array}{l}\frac{(24+12k)}{(11+16k)}x\left(\frac{t}{t_0}\right)^{\frac{1}{\beta_0}(11+16k)}+\frac{(66+96k)}{\beta_0^2}\left\{\ln\left(\frac{t_0}{t}\right)\right\}^2\\ +\ln\left\{x\left(\frac{t}{t_0}\right)^{\frac{1}{\beta_0}(11+16k)}\right\}\ln\left(\frac{t_0}{t}\right)^{\frac{12}{\beta_0}}+\ln\left(\frac{t_0}{t}\right)^{\frac{1}{\beta_0}\left(\frac{2}{3}N_f+11\right)}-\frac{(24+12k)}{(11+16k)}x\end{array}\right] \quad (2)$$

where $t=\ln(Q^2/\Lambda^2)$, $\alpha_S(t)=4\pi/\beta_0$, $\beta_0=11-2N_f/3$, N_f being the number of flavours.

Introduction of standard DLLA (double leading logarithmic approximation) result for gluon distribution [7] in eqs.(1) gives,

$$\rho_N^{DLLA}(x,t)=\frac{G(x,t_0)}{\pi R_N^2}\exp\left[\left\{\frac{48}{\beta_0}\ln\left(\frac{t}{t_0}\right)-\ln\left(\frac{1}{x}\right)\right\}^{0.5}\right] \quad (3)$$

provided the gluon distribution is not singular at $t=t_0$.

Similarly, introduction of AGL gluon distribution at running $\alpha_S(t)$ (AGL) [8] in eq.(1) gives,

$$\rho_N^{AGL}(x,t)=\frac{t}{1+t}\frac{N_C\alpha_S(Q^2)}{\pi}\ln\left(\frac{1}{x}\right) \quad (4)$$

Results and Discussion

For quantitative analysis, we use $\alpha_S(t)=(4\pi)/(\beta_0 t)$, $R^2_N=5\ GeV^2$; mass no. $A=1$ (for nucleon) and MRST01LO [9] input. Fig.1(a-b), represent the variation transverse gluon density $\rho_N(x,t)$ with $y=\ln(1/x)$ at Q^2=10 GeV^2 and 20 GeV^2. The analysis shows that ρ_N increases with increase in y at fixed Q^2. It is also seen that ρ_N increases rapidly at higher Q^2 values. The nature of increments are different in different models.

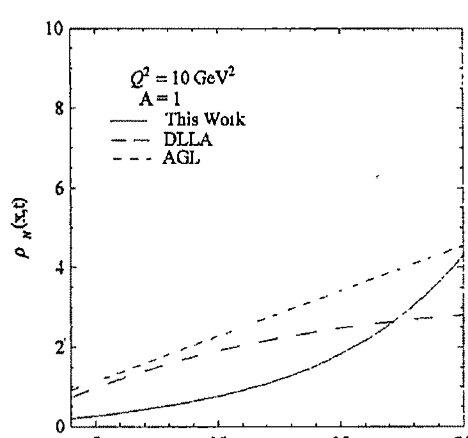

(a)

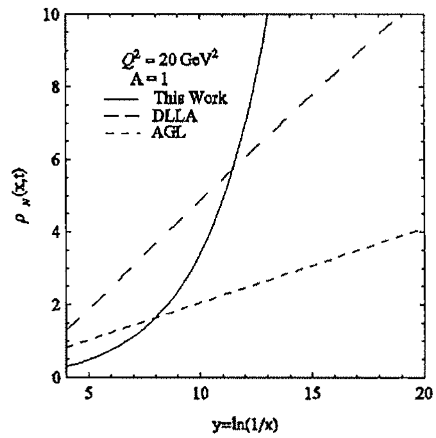

(b)

Figure 1 (a-b): Variation transverse gluon density $\rho_N(x,t)$ with y=ln(1/x) at $Q^2=10$ GeV^2 *and* 20 GeV^2.

References

[1] M. B. Gay Ducati and V. P. Goncalves. *arXiv: hep-ph/0003098* (2000)
[2] A. H. Mueller. *arXiv:hep-ph/9902302* (1999)
[3] Eugene Levin. *arXiv:hep-ph/9806434* (1998)
[4] S. Islam and D. K. Choudhury. *IJPA.* 3(2):189 (2011)
[5] D. K. Choudhury and S. Islam. *Assam Univ. J. Sc. & Tech.*, 6(2):112 (2010)
[6] S. Islam and D. K. Choudhury. *XVIII DAE-BRNS HEP Symp.* v18,p112(2008)
[7] A. DeRujula S. L. Glashow and H. D. politzer. *Phys. Rev.*, D10:1649 (1974)
[8] M. B. Gay Ducati. *Brazilian J. Phys.*, 31(2):115, (2001)
[9] A. D. Martin, *et. al. arXiv:hep- ph/0201127* (2002).

Gluon distribution function and the method of characteristics

Saiful Islam and D. K. Choudhury
Department of Physics, Gauhati University, Guwahati-781014, India
e-mail: saiful646@yahoo.co.in

The application of method of characteristics in perturbative quantum chromodynamics (pQCD) is relatively new. In the present paper, we solve Dokshitzer, Gribov, Lipatov, Altarelli, Parisi (DGLAP) equations by using this method and obtain an analytical form of gluon distribution function at small-x. Comparison with exact results as well as with data are reported.

INTRODUCTION

Dokshitzer, Gribov, Lipatov, Altarelli, Parisi (DGLAP) evolution equations [1–5] have been playing very important role in understanding the dynamics of evolutions of quark and gluons. Several approximate and numerical solutions of DGLAP evolution equations are available in literature [6–9], but their exact analytical solutions are not known [10, 11]. Because these evolution equations are partial differential quations (PDE), their ordinary solutions are not unique solutions, rather a range of solutions. These solutions were selected as the simplest ones with a single boundary condition on the non-perturbative x-distribution of the structure function at some $Q^2 = Q_0^2$. However complete solution of DGLAP equations with two diffrential variables generally needs two boundary conditions [18], one at $x \to 0$, $t \to \infty$ limit of double asymptotic scaling and the other at any fixed $Q^2 = Q_0^2$ Moreover, they are based on an ad-hoc assumption of factorizability of x and $t(= \ln \frac{Q^2}{\Lambda^2})$ dependence of the gluon momentum distribution G(x, t). These limitations can be over come by the use of Method of Characteristics [19, 20].

The method of characteristics is an important technique for solving initial value problems of first order PDE. In this method, the coordinates (x,t) are transferred to an appropriate new set of coordinates (S,τ) called characteristic coordinates so that the partial differential equation (PDE) reduces to ordinary differential equation (ODE) with respect to any one of the new variables. Thus the problem of solution of PDE reduces to that of ODE. This ODE can now be solved by standard methods. The last step is to plug in the values of S and τ in terms of x and t with the help of coordinate transformation equations to obtain the desired solution.

The application of method of characteristics in perturbative quantum chromodynamics (pQCD), specially in the solution of DGLAP equations is relatively new. Some of these applications are available in recent literatures [15–17] with considerable phenomenological success. In this paper, we solve DGLAP equations in leading order by using method of characteristics and obtain an analytical form of gluon distribution function at small-x which is free from the above mentioned limitations.

FORMALISM

DGLAP equations for gluon distribution have the standard form [1–5] :

$$t\frac{\partial G(x,t)}{\partial t} = \frac{3\alpha_s(t)}{\pi}\Big[\Big\{\frac{11}{12}-\frac{n_f}{18}+\ln(1-x)\Big\}G(x,t)+ \int_x^1 \frac{zG(\frac{x}{z},t)-G(x,t)}{1-x}dz + \int_x^1 \Big\{z(1-z)+\frac{(1-z)}{z}\Big\}G(\frac{x}{z},t) + \frac{2}{9}\int_x^1 \frac{1+(1-z)^2}{z}F_2^S(\frac{x}{z},t)\Big] \quad (1)$$

where $t=\ln(\frac{Q^2}{\Lambda^2})$, $\alpha_S(t)=\frac{4\pi}{\beta_0 t}$, $\beta_0=11-\frac{2}{3}n_f$, n_f being the number of flavours

To evaluate the integrals of eq.(1), we introduce a vari able u [8, 15] as :

$$u = 1 - z \quad (2)$$

Since $x < z < 1$, so $0 < u < 1 - x$ and hence x/z can be approximated at small-x as :

$$\frac{x}{z} = x(1-u)^{-1} \approx x(1+u) = x + xu \quad (3)$$

With the help of eq (3), Taylor's expansion of F_2^S ($\frac{x}{z}$, t) and G($\frac{x}{z}$, t) in approximated form [13, 14] at small-x can be given by :

$$F_2^S(\frac{x}{z},t) \approx F_2^S(x,t) + xu\frac{\partial F_2^S(x,t)}{\partial x} \quad (4)$$

$$G(\frac{x}{z},t) \approx G(x,t) + xu\frac{\partial G(x,t)}{\partial x} \quad (5)$$

Since x is small, terms containing x^2 and higher powersof x are neglected. Using eq.(4) and (5) in eq.(1) and performing the integrations w.r.t. z ,

$$t\frac{\partial G(x,t)}{\partial t} = P(x)G(x,t) + Q(x)\frac{\partial G(x,t)}{\partial x} + R(x)F_2^S(x,t) + S(x)\frac{\partial F_2^S(x,t)}{\partial x} \quad (6)$$

where, at small-x,

$$P(x) = \frac{12}{\beta_0}[\frac{\beta_0}{12}+\ln(\frac{1}{x})-\frac{1}{6}(11-12x)] \quad (7)$$

$$Q(x) = \frac{11}{\beta_0}x \quad (8)$$

$$R(x) = \frac{4}{3\beta_0}4\ln(\frac{1}{x})+(4x-3) \quad (9)$$

$$S(x) = -\frac{68}{9\beta_0}x \quad (10)$$

A reasonable approximate relationship between F_2^S (x, t) and G(x, t) representing the relative strength of gluon to singlet distribution can be taken as [8, 16] :

$$F_2^S(x,t) = kG(x,t) \quad (11)$$

where k is a suitable function of x or may be a constant. For simplicity and well adaptation to method of characteristics, k is considered here as a constant with 0 < k < 1 since gluon distribution is always higher than singlet distributions at any Q^2 Using eq.(11) in (6),

$$J(x)\frac{\partial G(x,t)}{\partial x} - t\frac{\partial G(x,t)}{\partial t} + H(x)G(x,t) = 0 \quad (12)$$

where

$$H(x) = P(x) + kR(x) \quad (13)$$

$$J(x) = Q(x) + kS(x) \quad (14)$$

Eq.(12) is a first order PDE, which can be solved by Method of Characteristics.

To use method of characteristics, let us introduce two variables S and as follows :

$$\frac{dx}{dS} = J(x) \quad (15)$$

$$\frac{dt}{dS} = -t \quad (16)$$

Use of eq.(15) and (16) in eq.(12) gives,

$$\frac{dG}{dS} + U(S,\tau)G(S,\tau) = 0 \quad (17)$$

which is an ODE in new coordinates (S,τ). Here, U(S,τ) = H(x). Explicitly,

$$U(S,\tau) = \frac{12}{\beta_0}\Big[\Big\{\frac{\beta_0}{12}+\ln(1-x)+ln(\frac{1}{x}) -\frac{1}{6}(1-x)(2x^2-x+11)\Big\} +\frac{k}{9}\Big\{4ln(\frac{1}{x})-(1-x)(3-x)\Big\}\Big] \quad (18)$$

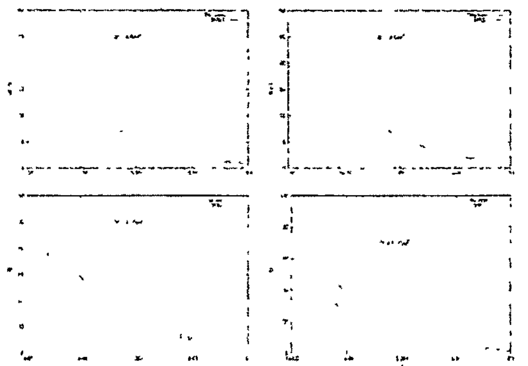

FIG 1. Gluon distribution from our predicted result and com- parison with MRST2001LO exact results at different Q2 = 8, 9, 10, and 11 Gev2.

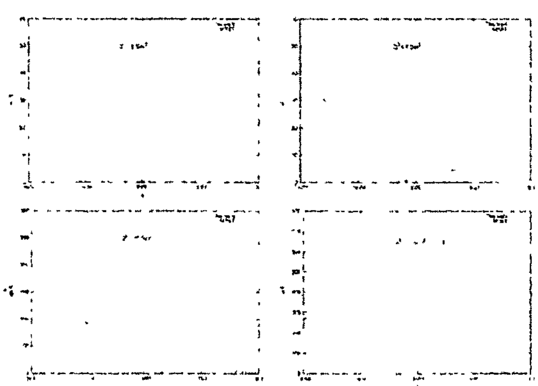

FIG 2. Gluon distribution from our predicted result and comparison with MRST2001LO exact results at different Q2 = 6, 7 and 15, 20 Gev2.

Solving eq. (15) and (16) with the boundary condition, at $S = 0$, $t = t_0$ and $x = \tau$, we get the transformation equations as :

$$S = \ln(\frac{t_0}{t}) \tag{19}$$

$$\tau = x(\frac{t}{t_0})^{\frac{1}{\beta_0}(11-\frac{68}{9}k)} \tag{20}$$

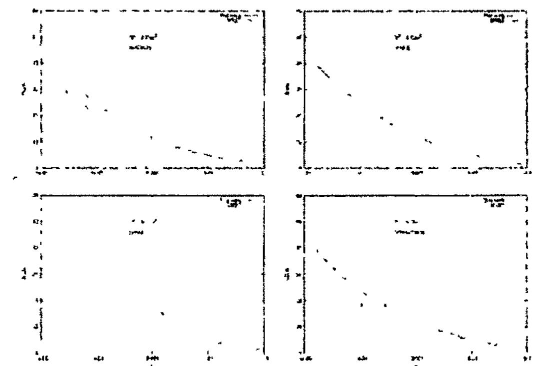

FIG 3: Dependance of the predicted gluon distribution on the values of the arbitrary constant k. The best fit value of k is found to be k = 0.0915586 at Q2 = 9Gev2.

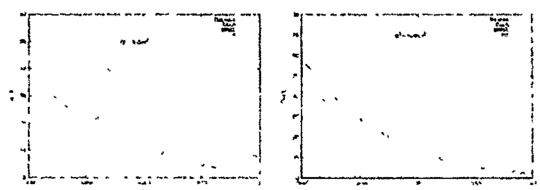

FIG 4. Predicted gluon distribution and comparison with MRST2001LO exact results, with data from H1 and with standard DLLA result

In terms of S and τ, the ODE (17) now becomes,

$$\frac{dG(S,\tau)}{G(S,\tau)} = -\frac{4}{\beta_0}\Big[(\frac{\beta_0}{4}-k-\frac{11}{2})+\frac{1}{\beta_0}(\frac{4k}{3}+3)(\frac{68k}{9}-11)S-(\frac{4k}{3}+3)\ln\tau + (\frac{4k}{3}+6)\tau\exp\Big\{\frac{1}{\beta_0}(11-\frac{68k}{9})S\Big\}\Big]dS \tag{21}$$

Integrating eq.(21) and transforming the resultant equaion back to the original variables (x, t) with the help oftransformation eq.(19) and (20), we get,

$$G(x,t) = G(x,t_0)\exp\Big[\frac{4(\frac{4k}{3}+6)}{11-\frac{68k}{9}}x(\frac{t}{t_0})^{\frac{1}{\beta_0}(11-\frac{68k}{9})} \Big\{1-\exp(\frac{(11-\frac{68k}{9})}{\beta_0})\ln(\frac{t_0}{t})\Big\} - \frac{4}{\beta_0}(\frac{\beta_0}{4}+k - \frac{11}{2})\ln(\frac{t_0}{t}) - \frac{1}{2\beta_0^2}(\frac{4k}{3}+3)(\frac{68k}{9}-11)$$

$$\left\{\ln(\frac{t_0}{t})\right\}^2+\frac{4}{\beta_0}\ln\left\{x(\frac{t_0}{t})^{\frac{1}{\beta_0}(11-\frac{88k}{9})}\right\}$$
$$(\frac{4k}{3}+3)\ln(\frac{t_0}{t})\Bigg] \quad (22)$$

where $G(x, t_0) = G(S,\tau) = G(\tau)$ is the input function obtained from the boundary condition, at $S = 0$, $t = t_0$ and $x = \tau$, Equation (22) is our main result.

Standard DLLA (double leading logarithmic approximation) result for gluon distribution [12] is given by

$$G(x\ t) = G(x,t_0)\exp\left[\left(\frac{48}{\beta_0}\ln(\frac{t}{t_0})\ln(\frac{1}{x})\right)^{0\ 5}\right] \quad (23)$$

provided the gloun distribution is not singular at $t = t_0$.

RESULTS AND DISCUSSIONS

In the present paper, we solve the LO (leading order) coupled DGLAP equations in the Bjorken x-space by applying the method of characteristics and obtain a form of gluon distribution valid to be at small-x For Quantitative analysis, we use MRST200$^{\prime}$ input [9] at $Q_0^2 = 4Gev^2$, QCD cutoff parameter $\Lambda = 220Mev$ and $n_f = 4$.

We compare our pridicted result with MRST2001LO exact results and with the parameterised data from H1 at diffrent Q^2 values for x-range. $10^{-5} < x < 10^{-1}$and k-range $0<k<10^{-1}$. It is observed that the predicted result is almost independent of k at $k \leq 10^{-2}$.A comparison is also made with standard DLLA result.

Fig.1 represents Gluon Distribution G(x, t) from our predicted result against x-values at fixed Q^2 values. Comparison is made with MRST2001LO exact results at different $Q^2 = 8, 9, 10, 11$ and 20 Gev^2 for the same x-range $10^{-5} < x < 10^{-1}$ and $k = 0.01$. A good agreement is obtained at Q^2 –range 8-11Gev^2. It is seen that disagreement increases at lower Q^2 as well as at higher Q^2 values Fig.2 represents Gluon Distribution G(x, t) from our predicted result and its comparison with MRST2001LO exact results at different Q^2 = 6, 7 and 15, 20 Gev^2. It is seen that disagreement increases at lower Q^2 as wel as at higher Q^2 values. Fig.3 represents Dependance of the predicted gluon distribution G (x, t) on the values of the arbitrary constant k. The acceptable range of k is found to be $0 < k < 10^{-1}$. The best fit value of k is found to be $k = 0.0915586$ through least-square method of curve fitting. It is also observed that the pre- dicted result is almost independent of k at k 10^{-2}. Fig.4 represents Predicted gluon distribution $G(x, t)$ and comparison with MRST2001LO exact results, with data from H1 and with standard DLLA result at $Q^2 = 9$ and 10 Gev^2 for the same x-range $10^{-5} < x < 10^{-1}$ and $k = 0.01$. Comparison shows more suitability of our predicted result over the standard DLLA result.

CONCLUSION

In this paper, we have applied the method of characteristics to solve the coupled DGLAP equations for gluon distribution functions without any ad-hoc assumption of factorizability of x and t dependence of the gluon momentum distribution G(x, t). A good agreement of our predicted result with MRST2001LO exact results and data within the kinematical range $10^{-5} < x < 10^{-1}$ and $8 < Q^2 < 12Gev^2$ for $0 < k < 10^{-1}$ is obtained.

However, we have not compared our results with data directly, since exact solutions like [9] reproduce the data correctly. A similar agreement of our result with data presumably needs a new fit of the input distributions and extra new parameters/functions. The same inputs as used [9] by us to compare our results with exact ones are not sufficient to reproduce the entire data for entire kinematical range as is evident from our analysis.

References

[1] G. Altarelli and G. Parisi, Nucl. Phys. **B126** 289 (1977)

[2] V. N. Gribov and L. N. Lipatov, Sov. J. Nucl. Phys. **15**,438 (1972)

[3] L. N. Lipatov, Sov. J. Nucl. Phys, **20**,94 (1975)

[4] Yu. L. Dokshitzer, Sov. Phys. JETP, **46**,641

(1977)
[5] L. F. Abbott, W. B. Atwood and R. M. Barnett, Phys. Rev. **D22** 882 (1988)
[6] R. Deka and D. K. Choudhury, Z. Phys. **C75**, 679 (1997)
[7] D. K. Choudhury, R. Deka and A. Saikia; Euro. Phys. J. **C2**, 301 (1998)
[8] D. K. Choudhury, and A. Saikia, Pramana-J. Phys. **33**, 359 (1989)
[9] A. D. Martin, R. G. Roberts, W. Stirling and R. S. thorne, hep-ph/ 0201127
[10] M. Hirai, S. Kumano and Myiama, Comput. Phys Com- mun. 108, 38 (1998)
[11] A. Cafarella et al., Nucl. Phys. **B748**, 253 (2006)
[12] A. DeRujula, S. L. Glashow, H. D. politzer, S. B Treiman, F. Wilzek and A. Zee, Nucl. Phys. Phys. Rev. **D10**, 1649 (1974)
[13] W. Furmanski and R. Petronzio, Z. Phys. **C11**, 293 (1982)
[14] D. K. Choudhury et al. Phys. Lett. **B403**, 139 (1997)
[15] D. K. Choudhury, and P. K. Saharia, Pramana-J. Phys. **58**, 593 (2002)
[16] R. Baishya and J. K. sarma, Phys. Rev. **D74**, 107702 (2006)
[17] D. K. Choudhury and P. K. Sahariah, hep-ph/ 0601059
[18] F. Ayres Jr., Diffrential Equations (McGraw Hill, Singapore, 1981) p.240
[19] S. J. Farlow, Partial Diffrential Equations for Scientists and Engineers (John Willey, 1982) p.205
[20] E. C. Zachmanoglou and W. D. Thoe, "Introduction to Partial Diffrential Equations with Applications". Williams Wilkins, (1976)